
# Dehydration of methanol and ethanol in the gas phase over heteropoly acid catalysts

Thesis submitted in accordance with the requirements of the University of Liverpool for the degree of Doctor in Philosophy by Walaa Alharbi

2017

# Abstract


## Dehydration of methanol and ethanol in the gas phase over heteropoly acid catalysts

PhD thesis by Walaa Alharbi

The aim of this thesis is to investigate heterogeneous catalysis for the dehydration of methanol and ethanol at a gas-solid interface over a wide range of solid Brønsted acid catalysts based on Keggin-type heteropoly acids (HPAs), focussing on the formation of dimethyl ether (DME) and diethyl ether (DEE), respectively.

The dehydration of methanol to dimethyl ether (DME) was studied over a wide range of bulk and supported HPAs and was compared with the reaction over HZSM-5 zeolites (Si/Al = 10−120). Turnover rates for these catalysts were measured under zero-order reaction conditions. The HPA catalysts were demonstrated to have much higher catalytic activities than the HZSM-5 zeolites. A good correlation between the turnover rates and catalyst acid strengths, represented by the initial enthalpies of ammonia adsorption, was established. This correlation holds for the HPA and HZSM-5 catalysts studied, which indicates that the methanol-to-DME dehydration occurs via the same (or a similar) mechanism with both HPA and HZSM-5 catalysts, and that the turnover rate of methanol dehydration for both catalysts is primarily determined by the strength of catalyst acid sites, regardless of the catalyst pore geometry.

Dehydration of ethanol was also studied over a wide range of solid Brønsted acid catalysts based on Keggin-type HPAs in a continuous flow fixed-bed reactor in the temperature range of 90-220 $^{o}$C. The catalysts included $H_3PW_{12}O_{40}$ (HPW) and $H_4SiW_{12}O_{40}$ (HSiW) supported on $SiO_2$, $TiO_2$, $Nb_2O_5$ and $ZrO_2$ with sub-monolayer HPA coverage, as well as bulk acidic Cs salts of HPW ($Cs_{2.5}H_{0.5}PW_{12}O_{40}$ and $Cs_{2.25}H_{0.75}PW_{12}O_{40}$) and the corresponding core-shell materials with the same total composition (15%HPW/$Cs_3PW_{12}O_{40}$ and 25%HPW/$Cs_3PW_{12}O_{40}$, respectively) comprising HPW supported on the neutral salt $Cs_3PW_{12}O_{40}$.

The ethanol-to-DEE reaction was found to be zero order in ethanol in the range of 1.5-10 kPa ethanol partial pressure. The acid strength of the catalysts was characterised by ammonia adsorption microcalorimetry. A fairly good correlation between the catalyst activity (turnover frequency) and the catalyst acid strength (initial enthalpy of ammonia adsorption) was established, which demonstrates that Brønsted acid sites play an important role in ethanol-to-DEE dehydration over HPA catalysts. The acid strength and the catalytic activity of core-shell catalysts HPW/$Cs_3PW_{12}O_{40}$ did not exceed those of the corresponding bulk Cs salts of HPW with the same total composition, which contradicts the claims in the literature of the superiority of the core-shell HPA catalysts.

## List of publications

The main results obtained in this thesis are disseminated in the following publications and conference presentations:

1. W. Alharbi, E. Brown, E. F. Kozhevnikova, I. V. Kozhevnikov, “Dehydration of ethanol over heteropoly acid catalysts in the gas phase”, J. Catal., 319 (2014) 174–181.
2. W. Alharbi, E. F. Kozhevnikova, I.V. Kozhevnikov, “Dehydration of methanol to dimethyl ether over heteropoly acid catalysts: the relationship between reaction rate and catalyst acid strength”, ACS Catal., 5 (2015) 7186−7193.
3. W. N. Alharbi, E. F. Kozhevnikova, I. V. Kozhevnikov, Poster day, University of Liverpool, Liverpool, United Kingdom, April, 2014 (poster).
4. W. N. Alharbi, E. F. Kozhevnikova, I. V. Kozhevnikov, 4th NORSC PG Symposium, Huddersfield University, Huddersfield, United Kingdom, October, 2014.
5. W. N. Alharbi, E. F. Kozhevnikova, I. V. Kozhevnikov, The 8th Saudi Students Conference, Imperial College London, London, United Kingdom, January, 2015.
6. W. N. Alharbi, E. F. Kozhevnikova, I. V. Kozhevnikov, Catalysis Fundamentals and Practice, University of Liverpool, Liverpool, United Kingdom, July, 2015.
7. W. N. Alharbi, E. F. Kozhevnikova, I. V. Kozhevnikov, The 9th Saudi Students Conference, University of Birmingham, Birmingham, United Kingdom, February, 2016.
8. W. N. Alharbi, E. F. Kozhevnikova, I. V. Kozhevnikov, The Royal Society of Chemistry, Burlington House, London, United Kingdom, April, 2016.

# Acknowledgements

First and foremost I would like to express my appreciation to Prof. Ivan V. Kozhevnikov for his guidance during my PhD. journey. Without his valuable assistance, this work would not have been completed.

I would also like to give a heartfelt, special thanks to Dr. Elena F. Kozhevnikova. She was not the only assistant in solving multiple technical problems during my PhD, but my mentor and friend. Her patience, flexibility, and faith in me during PhD journey enabled me to attend to life while also earning my PhD. She is motivating, encouraging, and enlightening. For this, I cannot thank her enough. I am forever grateful. Thank you Dr. Elena!

Special thanks should also be given to all members of the technical support team in the Chemistry Department and Kozhevenikov's group at the University of Liverpool.

I gratefully acknowledge the funding sources that made my PhD work possible. I was funded by the King Abdullah scholarship program for three years. My project was also supported by King Khalid University for last year of my PhD.

Last, but certainly not least, I must acknowledge with great and deep thanks to my mum, my husband, a special friend (Khadijah), my kids, and all my family. Through their love, patience, support and unwavering belief in me, I have been able to complete this long PhD journey. At the same time, they have also given me so many happy and beautiful memories throughout this journey. Thank you from all my heart and soul for your devotion, unconditional love, support, sense of humour, patience, optimism and advice; it was more valuable than you could ever imagine.

## List of Abbreviations

| | |
|---|---|
| HPA | Heteropoly acid |
| HPW | $H_3PW_{12}O_{40}$ |
| HSiW | $H_4SiW_{12}O_{40}$ |
| CsPW | Cesium salt (Cs2.5) of phosphotungstic acid ($H_3PW_{12}O_{40}$) |
| MeOH | Methanol |
| DME | Dimethyl ether |
| EtOH | Ethanol |
| DEE | Diethyl ether |
| BET | Brunauer-Emett-Teller method |
| TGA | Thermogravimetric analysis |
| IR | Infrared spectroscopy |
| XRD | X-ray diffraction |
| DSC | Differential scanning calorimetry |
| ICP | Inductively coupled plasma |
| GC | Gas chromatography |
| FTIR | Fourier transform infrared spectroscopy |
| TOF | Turnover frequency |

# Contents

# Chapter 1. Introduction

The focus in this chapter will be on heterogeneous catalysis and on the fundamental concepts that are required to understand how heterogeneous catalysis works. This chapter will also introduce heteropoly acids as acid catalysts and describe the dehydration of lower alcohols (methanol and ethanol).

## 1.1 Catalysis: the scope and definition

In 1812, Humphrey Davy and Gottlieb Kirchhoff first reported catalytic reactions. Davy studied the gas-phase oxidation of alcohol in air over platinum and Kirchhoff investigated the effect of acid catalysts in breaking down starch in a liquid phase.[1]

A catalyst can be defined as a substance that can enhance the rate of a chemical reaction without being used up. It provides an alternative reaction pathway with a reduced activation energy, as shown in **Figure 1.1**. Catalysts can be in different phases: gas, liquid or solid. Most frequently, however, they are liquids or solids.[1-2]

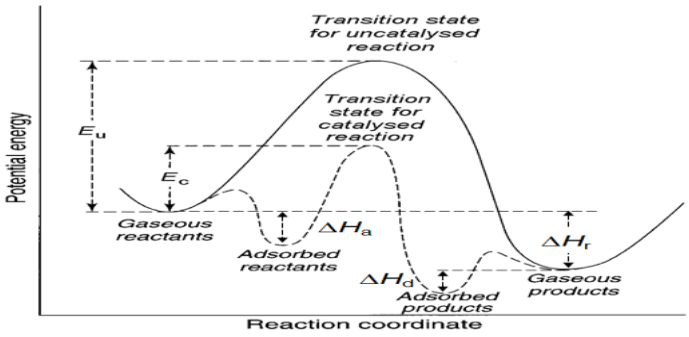


**Fig. 1.1.** Potential energy diagram for a reaction with and without a catalyst ($E_c$ is the activation energy of the catalysed reaction, $E_u$ the activation energy of uncatalysed reaction, $\Delta H_r$ the enthalpy of reaction, $\Delta H_a$ the enthalpy of reactant adsorption, and $\Delta H_d$ the enthalpy of product desorption).[1]

The economic benefits of catalysis are enormous, and catalysts are used in over 80% of the processes in the chemical, petrochemical and biochemical industries, as well as in the production of polymers.[3]

Traditionally, the area of catalysis has been divided into three main fields: homogeneous, heterogeneous and enzyme catalysis. Around 80% of all catalytic processes require heterogeneous catalysts, whereas 15% and 5% of catalytic processes involve homogeneous catalysts and biocatalysts, respectively.[4] In homogeneous catalysis, catalysts are present in the same phase as the starting materials and products, whereas in heterogeneous catalysis the catalysts are usually solids and the reactants and products are in the gas or liquid phase. Enzymes can operate in both homogeneous and heterogeneous systems. The characteristic features of homogeneous and heterogeneous catalysis are summarised in **Table 1.1**.[1, 5-7]

**Table 1.1.** *Comparison of homogeneous and heterogeneous catalysts.*

| **Homogeneous system** | **Heterogeneous system** |
|---|---|
| • Catalysts have a higher degree of dispersion since in theory each atom can be catalytically active.<br>• Exhibit a higher activity and selectivity.<br>• The mechanism is relatively well understood due to the well-defined reaction sites. Lower catalyst concentrations.<br>• Reaction temperatures are limited to between 50– 200 $^{o}$C.<br>• Lower thermal stability.<br>• Catalyst recycling is possible.<br>• Higher in catalyst losses and cost. | • Active sites are located on the surface since phase boundaries are present between the catalyst and the reactants.<br>• Exhibit a lower activity and selectivity.<br>• The mechanism is often obscure due to non-uniform distribution of active sites.<br>• The reaction temperature can often be higher than 250 $^{o}$C.<br>• Catalyst separation from reactants and products is easy.<br>• Higher thermal stability.<br>• Catalyst recycling is easy.<br>• Reduced in catalyst losses and cost. |

From the summary of the differences between homogeneous and heterogeneous catalysis, it can be concluded that both types of catalysis have their unique characteristics and properties. Heterogeneous systems have attracted much attention in a wide variety of organic reactions due to the ease of catalyst recovery and reuse. [1]

## 1.2 Heterogeneous catalysis

### 1.2.1 *Basic features of heterogeneous catalysis*

#### *1.2.1.1 Key steps of reactions on a porous solid catalyst*

**Figure 1.2** presents the steps in a heterogeneously catalysed reaction.[8-9] In general, reactions on a porous solid catalyst include the following seven steps: (1) external transfer of reactant from bulk fluid (gas or liquid) phase through the boundary layer to the outer surface of the catalyst granule (film diffusion), (2) internal (intraparticle) transfer of the reactant through the pores to active sites on the interior surface (pore diffusion), (3) adsorption of reactant, (4) chemical reaction on the surface of the catalyst, (5) desorption of product, (6) internal transfer of product through the pores to the external surface, and (7) external transfer of product through the boundary layer to the bulk fluid phase.

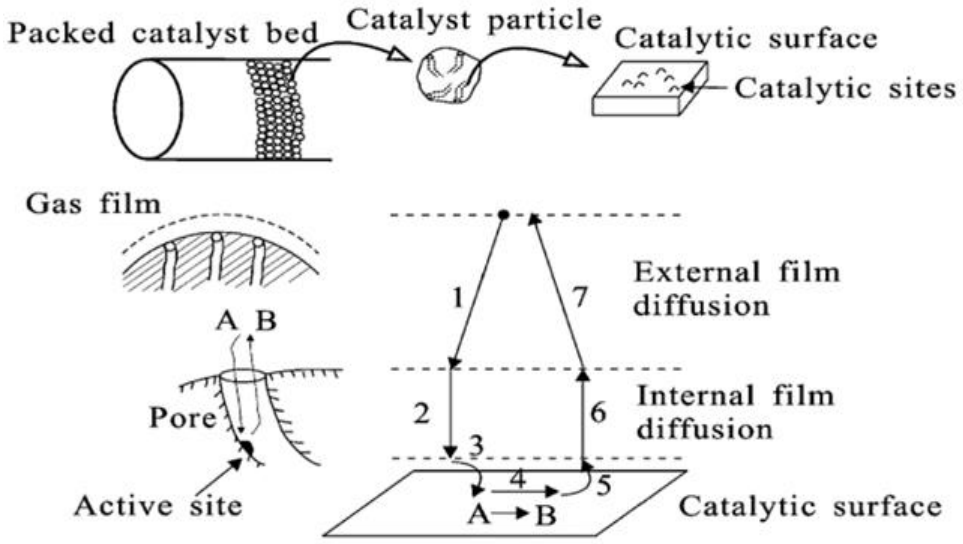


**Fig. 1.2.** Individual steps of a heterogeneous reaction in the gas phase over a solid porous catalyst.[10]

### *1.2.1.2 Adsorption*

Catalysis is essentially a chemical phenomenon, and thus it depends on the chemical nature of catalysts. For catalysis to occur, there must be a chemical interaction between the catalyst and the reactant, but this interaction must not change the chemical nature of the catalyst except at the surface.[11]

The surface free energy of solid catalysts is related to the number of unsaturated bonds in the surface atoms. Surfaces with lower coordination surface atoms have the highest surface free energy, the highest reactivity for adsorption, and the strongest binding for the adsorbate (high adsorption heat).[12] Furthermore, it is vital also to understand the concept of active sites since this is at the heart of heterogeneous catalysis. The active site can be introduced as an atom, or a group of atoms, in the catalyst involved in the catalytic reaction. This concept was first introduced by Taylor, who reported that structures of solid

surfaces are complex and non-uniform on an atomic scale and that atoms or ions with low coordination on the surface are capable of bonding reactant molecules and thus acting as active sites.[13, 14] Knowledge about these active sites is obtained by surface scientists from various characterisation techniques which will be discussed later.

Heterogeneous catalysis involves adsorption of reactant molecules on the catalyst surface. The degree of adsorption depends on the nature of the adsorbate and the adsorbent. Adsorption is classified into physisorption and chemisorption. **Table 1.2** summarises the main features of physical and chemical adsorption.[1, 14-15]

**Table 1.2.** *Comparisons between physisorption and chemisorption.*

| **Parameters** | **Physisorption** | **Chemisorption** |
|---|---|---|
| Type of bonding | Van der Waals forces, no electron transfer | Covalent bonding, electron transfer |
| Type of adsorbents | All solids | Some solids. |
| Type of adsorbates | Gases (intact molecules) | Gases dissociated into atoms, ions or radicals |
| Temperature | Close to the condensation temperature of the adsorbate | Wide range of temperatures and sometimes temperatures much higher than the condensation temperature |
| Heat of adsorption | $\Delta H$ around -10 kJ/mol, non-activated process | $\Delta H$ in range between -80 kJ/mol to -200 kJ/mol, may require activation energy |
| Rate of adsorption | Fast, reversible reaction | Reaction may be slow and irreversible |
| Surface coverage | Multilayers | Monolayer |

This comparison between physisorption and chemisorption implies that if the value of the heat of adsorption, or the activation energy of adsorption, is larger than the enthalpy of vaporisation, then the adsorption may be referred to as chemisorption. Sometimes, however, it is difficult to determine the type of adsorption since the heat of adsorption is often about 40-50 kJ/mol.[16] Other techniques that are useful in distinguishing between these two types of adsorption are electrical conductivity and IR spectroscopy.[17]

In order to study the phenomenon of adsorption experimentally, it is essential to generate clean surfaces using a vacuum system. The composition of the surface is determined by using specific techniques such as X-ray photoelectron spectroscopy (XPS). It is noticeable that the use of well-defined surfaces has tremendously expanded our understanding of heterogeneous catalysis in the last 20 years. For example, single crystals of most metals are now readily available.[18]

The adsorption isotherm is a quantitative relationship between the amount of adsorption and the pressure or concentration of the adsorbate above the surface at equilibrium. There are many types of adsorption isotherms. One of the early pioneers of this area of study and perhaps the most significant figure in the field of surface chemistry was Langmuir. Using clean metal filaments produced under a high vacuum, he developed the well-known Langmuir adsorption isotherm. This equation (equation 1.1) describes adsorption equilibrium between gas phase molecules (A) and the adsorption surface sites (M) at a constant temperature.[19] This can be represented by:

$$A_{(gas)} + M_{(surface)} \rightleftarrows AM_{(surface)}$$

The Langmuir adsorption isotherm can be expressed as follows:

$$\theta = \frac{bp}{1 + bp} \qquad (1.1)$$

Here, $\theta$ the relative number of sites of the surface which are covered with gaseous molecules (fractional coverage), $P$ is the partial pressure of $A$ and $b$ is the equilibrium constant for the distribution of adsorbate between the surface and the gas phase.[1]

### *1.2.1.3 The rate of catalytic reaction*

Kinetics is central to catalysis. It is kinetics that makes catalysis an exact science, and it is the essential tool for both the mechanistic studies of catalysis and the development of new catalytic processes. The measurement of the kinetic parameters of a catalysed reaction is important for several reasons. First, knowledge of the order of reaction with respect to reactants and products is essential for the definition of the mechanism of reactions. Secondly, the best design of the catalytic reactor, including the size and shape of the catalyst bed depends on information concerning the reaction orders as well as on the thermochemistry of the system. Finally, the effect of temperature on the rate can provide a useful clue to the nature of the slowest step in the total process. For heterogeneously catalysed reactions, the rate can be given by equation (1.2).[6, 20]

$$R = \frac{1}{W} \times \frac{dn}{dt} \qquad (1.2)$$

Here, $dn$ is the change in moles for reactant or product, $dt$ refers to time and $W$ is the catalyst weight.

The catalyst activity can also be expressed per unit surface area.[21] Alternatively, the rate can be given regarding the number of molecules reacted per active site per unit time. This is called turnover frequency (TOF) and is widely used in the academic literature on catalysis. Since the reaction does not take place across the entire surface but only at the active centres, the rate is more accurately expressed as the number of molecules formed (or reacted) per active site per unit time.[22]

In continuous flow fixed-bed reactor, the rate of catalytic reaction is given by equation (1.3).

$$R = \frac{XF}{W} \qquad (1.3)$$

Here, $X$ is the fractional conversion, $F$ is the molar flow rate of the substrate and $W$ is the catalyst weight. This equation is often applied under differential conditions at $X \leq 0.1$. The turnover rate (TOF) can then be calculated if the density of active sites in the catalyst is known.[1, 22]

### *1.2.1.4 Mechanism of heterogeneously catalysed reactions*

#### 1.2.1.4.1 Unimolecular reaction

After adsorption of the reactant molecules, the next step in a catalytic cycle is the surface reaction. For a unimolecular reaction, the following steps represent the conversion of *A* into products.

$$A \rightleftharpoons A_{ads} \xrightarrow[slow]{} X_{ads} \rightleftharpoons X$$

The chemical reaction on the surface is suggested to be the rate-limiting step; it is irreversible (one-way), and adsorption and desorption steps are at fast equilibrium. Accordingly, the rate of the overall reaction is given by the Langmuir equation (equation 1.4):

$$R = k\theta_A = \frac{k\ b_A p_A}{(1 + k\ b_a p_A)} \qquad (1.4)$$

Here, $\theta$ is the coverage of adsorbate of *A* on the surface (since *X* desorbs fast its coverage is assumed to be negligible), *k* is the rate constant, and $b_A$ is the adsorption equilibrium constant.

**Figure 1.3**, below, shows that the reactant pressure dependence of rate changes from the first order at low pressure to the zero order at high pressure as the surface becomes saturated with adsorbate and $\theta_A \approx 1$.[1, 11]

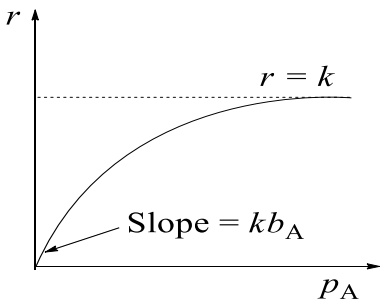


**Fig. 1.3**. The pressure dependence of the reaction rate for a system obeying Langmuir kinetics.[11]

### 1.2.1.4.2 Biomolecular reaction

For a reaction A + B ⟶ X, there are two different ways in which this reaction can occur at a surface: the Langmuir–Hinshelwood mechanism and the Eley–Rideal mechanism. These mechanisms can be identified by the dependency of the reaction rate on the reactant pressure.[11] **Figure 1.4** shows these two types.

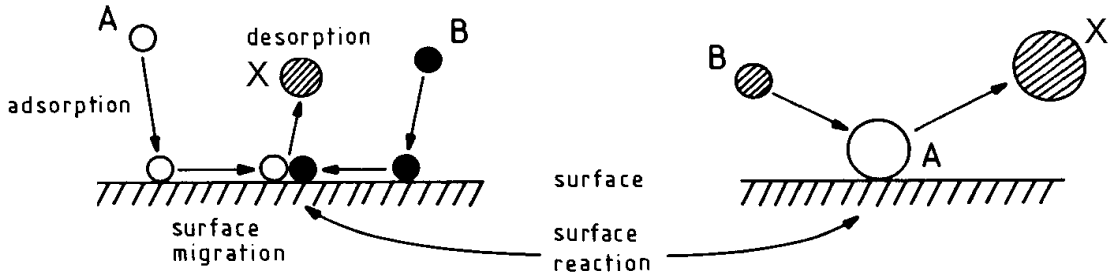


**Fig. 1.4**. The Langmuir–Hinshelwood mechanism (left) and the Eley–Rideal mechanism (right).[1]

In the Langmuir–Hinshelwood mechanism, both A and B adsorb fast on adjacent sites (via fast surface migration) and react in a rate-limiting step followed by fast desorption of products.

The rate of the overall reaction is given by the Langmuir-Hinshelwood equation (equation 1.5):

$$R = k\theta_A\theta_B = \frac{Kb_Ab_Bp_Ap_B}{(1 + b_Ap_A + b_Bp_b)^2} \qquad (1.5)$$

There are some consequences of this relationship. At low pressure, the equation is essentially first order in each reactant. When one reactant is weakly adsorbed, the terms involving that co-adsorbate are eliminated from the denominator, and the reaction becomes poisoned by a high coverage of the stronger binding adsorbate. If *B* is weakly adsorbed and *A* is very strongly adsorbed, then the rate can be represented by equation (1.6).[11]

$$R = \frac{kb_Bp_B}{b_Ap_A} \qquad (1.6)$$

A variant of this treatment yields the so-called Eley–Rideal equation for the situation where one species is not adsorbed at all. Here, *A* is adsorbed on the surface, where *B* reacts by impulsive collision with adsorbed *A* at the surface, hence the reaction is simple first order in *B* but Langmuir form in *A*.[11] The rate of the overall reaction is given by the Eley–Rideal equation (equation 1.7).

$$R = k\theta_A\, p_B = \frac{kb_Ap_Ap_B}{(1 + b_Ap_A)} \qquad (1.7)$$

The Langmuir–Hinshelwood mechanism is very common, whereas the Eley–Rideal mechanism is relatively rare.[1]

### 1.2.2 Effect of mass transfer in solid porous catalysts

Mass transfer limitations play a significant role in heterogeneous catalysis. The mass transport phenomenon occurs when the reactant molecules come into contact with the active sites, which usually located inside the solid catalyst pores, as represented in **Figure 1.2**.

Three process regimes are distinguished concerning the rate-limiting step: the kinetic regime (step 4 rate-limiting), the internal-diffusion regime (step 2 rate-limiting) and the external diffusion regime (step 1 rate-limiting).[1, 9]

Mass and heat transfer limitations within a solid porous catalyst can strongly affect reaction kinetics (reaction rate, order and activation energy). In such systems, concentration and temperature gradients exist that affect the course of the chemical reaction. There are two transport controlled regimes: internal diffusion and external diffusion. These are controlled by pore diffusion and film diffusion, respectively.

When a reaction proceeds in the internal-diffusion regime, its rate (per unit catalyst weight) decreases with increasing catalyst particle size due to an increase in diffusion distance. This is because mass transfer in catalyst pores occurs by diffusion and the rate of diffusion depends on the pore size. There are three types of diffusion in macro-, meso- and micropores: bulk or molecular diffusion, Knudsen diffusion and configurational diffusion, respectively.[22]

In the external diffusion regime, the reaction rate is limited by mass transport to the external surface of a catalyst through the boundary layer (film diffusion). The rate of film diffusion increases as the flow rate of the fluid phase increases. This is used to identify this regime.

Diffusion limitations can affect the activation energy of reaction ($E_a$ and $E$ are the apparent and true activation energies respectively), and this can also be used as diagnostic criteria for reaction regimes on solid porous catalysts. As can be seen in **Figure 1.5**, the apparent activation energy for an external diffusion regime is very low, $E_a \approx E_D$ (< 10 kJ/mol), as compared to the kinetic and internal-diffusion regimes, where $E_D$ is the diffusion activation energy.[1, 9]

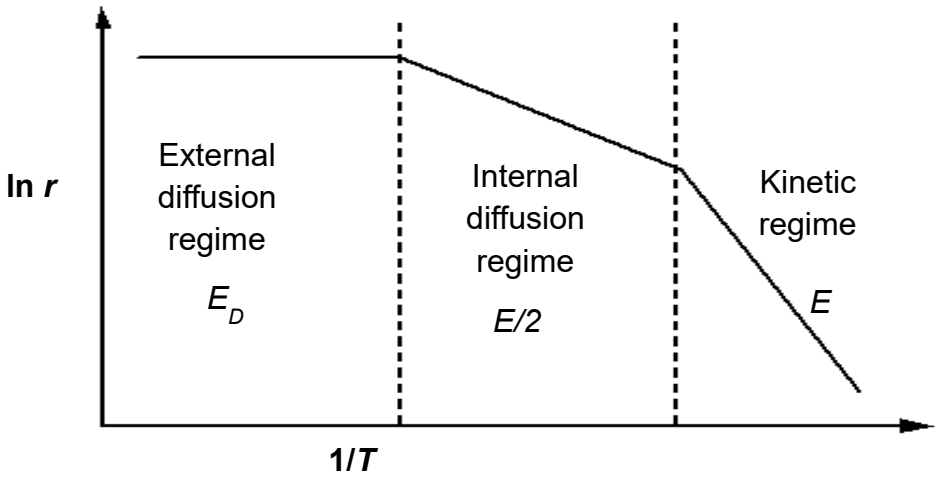


**Fig 1.5.** Diagnostic criteria for reaction regimes on solid porous catalysts by the activation energy.[1]

## 1.3 Catalysis by heteropoly acids

### 1.3.1 Introduction to heteropoly acids (HPA)

Heteropoly acids are comprised of heteropolyanions and protons as counter cations. Heteropolyanions are poloyoxometalate anions (nano-sized metal-oxygen cluster anions) having a general formula $[X_xM_mO_y]^{q-}$ ($x \leq m$), where X is a non-oxygen element in the inner part of polyanions (usually P, Si, As, Ge, etc.) called a heteroatom, and M is a

transition metal such as (Mo(VI), W(VI), V(V), Nb(V), Ta(V), and Ti(IV)) called an addendum atom.[23]

Heteropoly anions are formed by different mononuclear oxoanions that tend to polymerize by dehydration in an acidic aqueous solution at low pH to form a polyanion as presented in the following scheme:

$$23H^{+} + HPO_4^{-2} + 12WO_4^{-2} \longrightarrow [PW_{12}O_{40}]^{-3} + 12\ H_2O$$

The first heteropoly compound was discovered by Berzelius in 1826.[24] Catalysis by heteropoly acids (HPAs) has attracted much attention in the last few decades due to:

•Their unique catalytic properties such as acidity, solubility, thermal stability and redox potential.

•Their ability to operate efficiently under both heterogeneous and homogeneous conditions.

•Their compatibility with environmental and economic issues.

These unique physicochemical properties have been demonstrated both by successful large-scale applications and by promising laboratory results. Among the many applications of heteropoly compounds, catalysis is the most important. Presently, over 80% of patent applications for polyoxometalates involve catalysis.[25-27]

## 1.3.2 Structural hierarchy of solid heteropoly acids

Misono *et al*. introduced a special structural classification of solid heteropoly compounds that reflects the significance of the structural flexibility of these compounds. This is now widely applied in heterogeneous catalysis by polyoxometalates. Three structural levels have been distinguished and are defined as primary, secondary and tertiary structures.[28-29] This structural hierarchy is schematically illustrated in **Figure 1.6**.

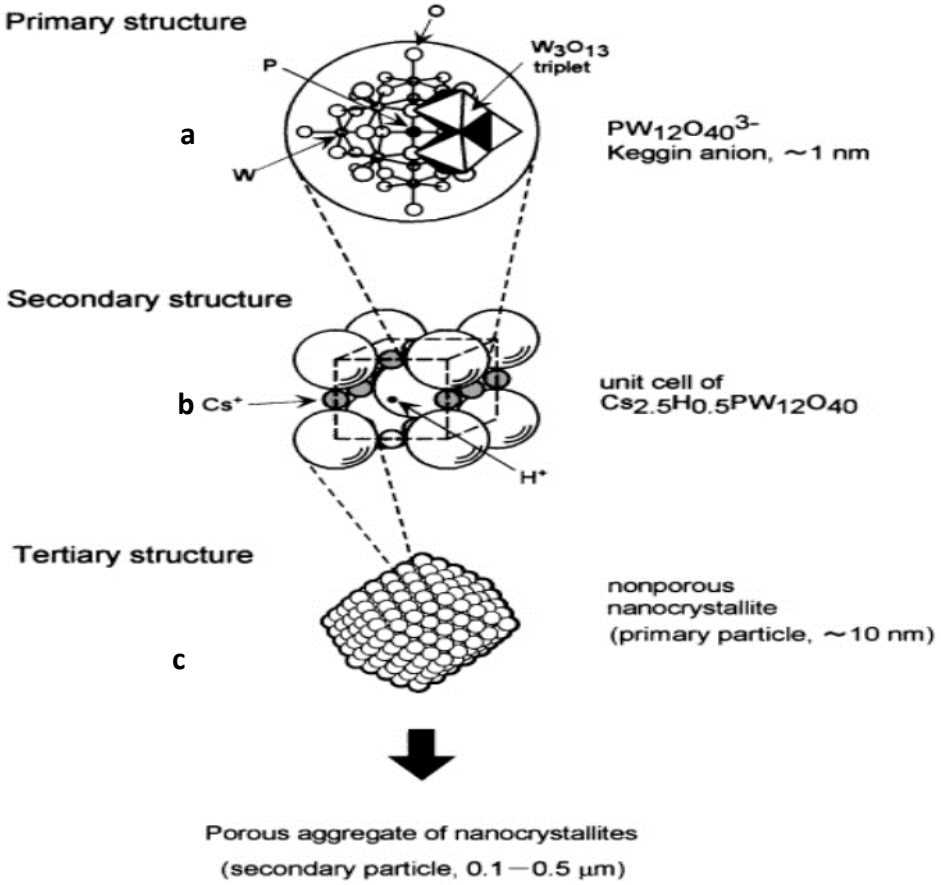


**Fig. 1.6.** Primary, secondary, and tertiary structures of a Keggin type heteropoly acid in a solid state: **(a)** primary structure (Keggin structure, $XM_{12}O_{40}$); **(b)** secondary structure for unit cell of ($Cs_{2.5}PW_{12}O_{40}$); **(c)** tertiary structure with porous aggregates [$Cs_{2.5}H_{0.5}PW_{12}O_{40}$].[30]

The primary structure is the heteropolyanion itself and has been classified according to the atomic ratio between the addendum atom (M) and the heteroatom (X). Several types of primary structures for heteropoly acids are known. **Table 1.3** summarises the three most important classes of heteropolyanions. Among these, the polyoxometalates with a Keggin structure are most important for catalysis due to their high stability and availability.[31-34]

**Table 1.3**. *The most common heteropolyanions*.

| **Name of structure of heteropoly ions** | **Chemical formula (M = W)** | **Heteroatom (X)** |
|---|---|---|
| Keggin | $[X_n^{+}M_{12}O_{40}]^{(8-n)-}$ | P (V) or As (V),<br>Si (IV) , Ge (IV) |
| Wells-Dawson | $[X_2M_{18}O_{62}]^{2x-16}$ | P (V) or As (V) |
| Anderson | $[X\ M_6O_{24}]^{n-}$ | Te (VI), Ni (IV), Pt (IV) |

The Keggin structure is presented in **Figure 1.7**. It can be seen that the primary structure of the polyanion consists of four types of oxygen: $X\text{-}O_a\text{-}(M)_3$, $M\text{-}O_b\text{-}M$ both connecting two $M_3O_{13}$ units by corner sharing; $M\text{-}O_c\text{-}M$ connecting two $M_3O_{13}$ units by edge-sharing; and $O_d$-M. These oxygens can be discriminated by $^{17}O$ nuclear magnetic resonance (NMR) and infrared spectroscopic techniques. The M-O and X-O bonds display infrared bands in the range of 600-1100 $cm^{-1}$.[23, 35]

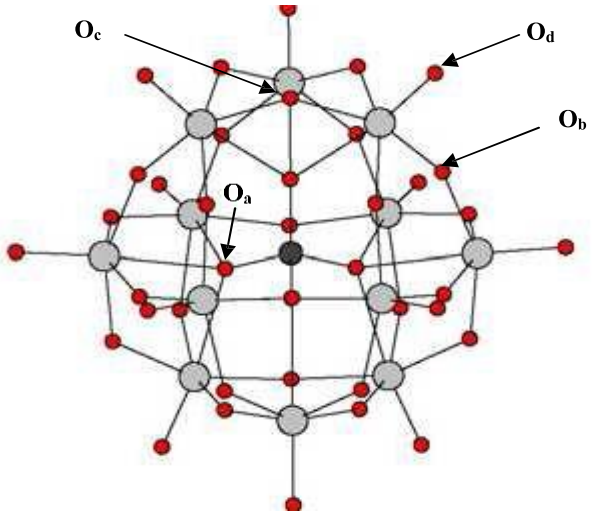


**Fig. 1.7**.The Keggin unit α-$XM_{12}O_{40}^{n}$.[28]

The secondary structure of heteropoly acids and their salts is formed from the coordination of polyanions (primary structure) with counter cations ($H^+$, $H_3O^+$, $H_5O_2^+$), hydration water of crystallization and other organic molecules. This structure strongly depends on the amount of hydration water.[36-37] These water molecules are easily removed from the solid by heating. A stable form contains six water molecules of hydration per Keggin unit. The protons of crystalline $H_3PW_{12}O_{40}.6H_2O$ are present as hydrated species $(H_5O_2)^+$ (**Figure 1.8**). Each $H_5O_2^+$ ion is bound to the terminal oxygen atoms in Keggin unit and links four neighbouring heteropolyanions. The acidic protons in $H_3PW_{12}O_{40}.6H_2O$ are located in the $H_5O_2^+$ bridges between lattice points, as shown in **Figure 1.8**. If n < 6, the acidic protons may be directly coordinated to oxygen atoms of the Keggin unit in $H_3O^+$ or remain in $H_5O_2^+$ bridges (**Figure 1.8**).[28, 30] The hydrated protons possess a higher mobility than non-hydrated protons and are responsible for the extremely high proton conductivity of crystalline heteropoly acid hydrates. The crystalline hexahydrate structure of $H_3PW_{12}O_{40}.6H_2O$ has been identified by single crystal X-ray diffraction and neutron diffraction techniques. The structure for anhydrous $H_3PW_{12}O_{40}$ and the cesium salt $Cs_3PW_{12}O_{40}$ has also been recorded to be the same. Furthermore, direct evidence of

the predominant protonation of the terminal oxygens in solid $H_3PW_{12}O_{40}$ and $H_4SiW_{12}O_{40}$ has been obtained by $^{17}O$ NMR by comparison of solution and solid-state spectra for these HPAs.[38-41]

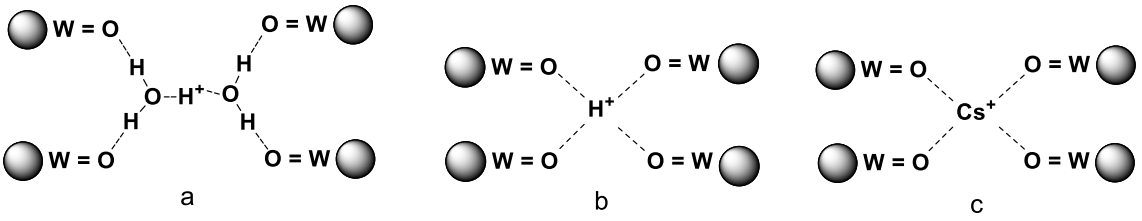


**Fig. 1.8.** Schematic structures: **(a)** bulk proton sites in crystalline hexahydrate $H_3PW_{12}O_{40}.6H_2O$ **(b)** bulk proton sites in anhydrous $H_3PW_{12}O_{40}$ and **(c)** $Cs^+$ location in $Cs_3PW_{12}O_{40}$.[28]

Besides the primary and secondary structures, there is a tertiary structure and higher-order structures which are suggested to influence the catalytic function of HPAs. The tertiary structure is the structure of solid HPAs as assembled (**Figure 1.6 (c)**). The sizes of the particles, pore structure, distribution of protons in the particle, etc., are the elements of the tertiary structure and play a major role in heterogeneous catalysis by HPAs.[28]

## 1.3.3 Properties of heteropoly acids

### *1.3.3.1 Acid properties of heteropoly acids*

The acid properties of heteropoly acids in aqueous solutions are well documented regarding their dissociation constants, and Hammett acidity functions.[26] Generally, heteropoly acids with a Keggin structure, such as $H_3PW_{12}O_{40}$ and $H_4SiW_{12}O_{40}$, are stronger Brønsted acids than the common mineral acids ($H_2SO_4$, HBr, HCl, $HNO_3$, and $HClO_4$). Their strong acidity can be attributed to the high mobility of the protons in the secondary structure of HPAs and the electrostatic interaction between protons and anions being much weaker in heteropoly acids than in mineral acids.[29]

HPAs as solid catalyst possess purely Brønsted acidity and are stronger acids than the conventional solid acids such as $SiO_2$-$Al_2O_3$, $H_3PO_4/SiO_2$, and zeolites. Their strength in respect to acidity refers to the dispersion of the negative charge over many atoms of the polyanion and also to the fact that the negative charge is less distributed over the outer surface of the polyanion owing to the double-bond character of the M=O bond, which polarizes the negative charge of $O_t$ to M.[42-44]

Okuhara *et al*. compared the acid strength of heteropoly acids and $SiO_2$-$Al_2O_3$ by thermal desorption of pyridine and found $H_3PW_{12}O_4$ to be stronger than $SiO_2$-$Al_2O_3$. Pyridine adsorbed on $SiO_2$-$Al_2O_3$ is fully desorbed at 300$^o$C, whereas pyridine adsorbed in $H_3PW_{12}O_4$ mostly remains on the surface at the same temperature.[29]

Heteropoly acids are soluble in polar solvents such as water, lower alcohols, ketones, ethers, and esters. In contrast, they are insoluble in non-polar solvents such as hydrocarbons. The acid strength of crystalline HPAs has been found to follow the same order in the solid state and solution. Usually, relative catalytic activities of HPAs are consistent with this order in both homogeneous and heterogeneous systems:

$$H_3PW_{12}O_{40} > H_4SiW_{12}O_{40} > H_3PMo_{12}O_{40} > H_4PMo_{12}VO_{40} > H_4SiMo_{12}O_{40}$$

Additionally, HPAs can generate carbocations from adsorbed olefins and arenes similar to other solid acids.[28-29, 45]

### *1.3.3.2 Thermal stability of heteropoly acids*

The stability of heteropoly compounds is an important factor for heterogeneous catalysis. Some solid heteropoly compounds are fairly stable and are thus applicable in reactions at moderately high temperatures (300–350 $^{o}$C). This stability may not be sufficient for catalyst regeneration, however, for example, burning coke that may form on the catalyst surface (500–550 $^{o}$C).[28]

The thermal decomposition of heteropoly compounds to form a mixture of oxides is a complex multistage process, and the catalyst activity may be permanently lost at an early stage of decomposition.[41]

The Keggin-type heteropoly compounds are the most stable among the various polyoxometalates. The decomposition temperature of the most typical Keggin heteropoly acids decreases in the following series:

$$H_3PW_{12}O_{40} > H_4SiW_{12}O_{40} > H_3PMo_{12}O_{40} > H_4SiMo_{12}O_{40}$$

465 $^{o}$C  445 $^{o}$C  375 $^{o}$C  350 $^{o}$C

Heteropoly salts are usually more stable than their parent acids. For instance, the acidic cesium salt $Cs_{2.5}H_{0.5}PW_{12}O_{40}$ is more stable than $H_3PW_{12}O_4$, with no decomposition of the salt being observed at 500 $^oC$.[28]

### *1.3.3.3 Modification of heteropoly acids*

Bulk Keggin HPAs exhibit higher catalytic activity in various reactions compared to conventional solid acid catalysts. Despite the advantages of Keggin HPAs (thermal stability and ease of synthesis), their catalytic application is limited since they have certain drawbacks such as their low specific surface area and high solubility in polar solvents.[46] These disadvantages can be overcome by the following methods, however: (1) exchange of the HPA's protons with different metal cations, and (2) supporting HPAs on suitable solid supports. These methods are outlined next.

#### 1.3.3.3.1 Metal-exchanged Keggin heteropoly acids

HPAs can be modified by exchanging their protons completely or partially with metal ions without affecting the primary structure.[29, 42] HPA salts with small cations ($Li^+$ or $Na^+$) behave like their parent acids and have high solubility in water and other polar organic solvents. In this case, the surface area is low (1-15 $m^2/g$). In contrast, HPA salts with large cations, such as $K^+$, $Cs^+$, exhibit a higher surface area (50-200 $m^2/g$), higher thermal stability and are insoluble in water, in contrast to their parent acids. These properties of HPA salts with large cations are beneficial for heterogeneous catalysis.[48–49]

On the other hand, the acid properties of heteropoly salts are complex since they are sensitive to counter cations, constituent elements of polyanions and the tertiary structure.[36]

Many studies have been carried out to determine the acid characteristics of the salts of HPAs using various techniques, including adsorption and thermal desorption of basic molecules, as well as NMR.[49-53]

According to the temperature programmed desorption (TPD) of ammonia and indicator tests, $Cs_{2.5}H_{0.5}PW_{12}O_{40}$ and $H_3PW_{12}O_{40}$ have similar acid strengths.[36] In the TPD of ammonia, $Cs_{2.5}H_{0.5}PW_{12}O_{40}$ gave a slightly broader peak than $H_3PW_{12}O_{40}$, showing a slight inhomogeneity of the acid strength.[54] Okuhara *et al*. studied the acid properties of $Cs_xH_{3-x}PW_{12}O_{40}$ and reported that as the Cs content increased from 0 to 2, the number of surface protons decreased at the beginning as the surface area was reduced. When the Cs content significantly increased and exceeded 2, however, the surface acidity increased, reaching its highest at x = 2.5. When x increased from 2.5 to 3.0, on the other hand, the number of surface protons decreased considerably since the formal concentration of protons became close to zero (**Figure 1.9**). The catalytic activity of $Cs_xH_{3-x}PW_{12}O_{40}$ in many reactions has been reported to correlate with their surface acidity.[29-30, 52]

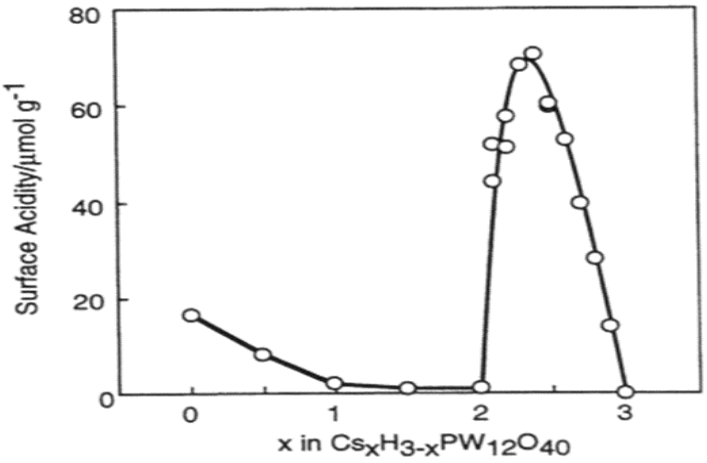


**Fig. 1.9.** The amount of surface protons (surface acidity) of $Cs_xH_{3-x}PW_{12}O_{40}$. [29]

### 1.3.3.3.2 Supported heteropoly acids

In this type of modification, the HPA is dispersed on acidic or neutral supports with a high surface area, such as silica, zirconia, niobia, titania, tin oxide, ceria, etc. The acidity and catalytic activity of supported HPAs depend on the nature of the carries, the HPA loading, condition of pre-treatment, etc.[55] Different types of interactions between HPAs and carries are suggested and summarised as follows:

- Hydrogen bonding, or adsorption types of interaction, may occur when the support is a hydrous metal oxide/metal oxide.[56- 57] An example is presented in **Figure 1.10**.

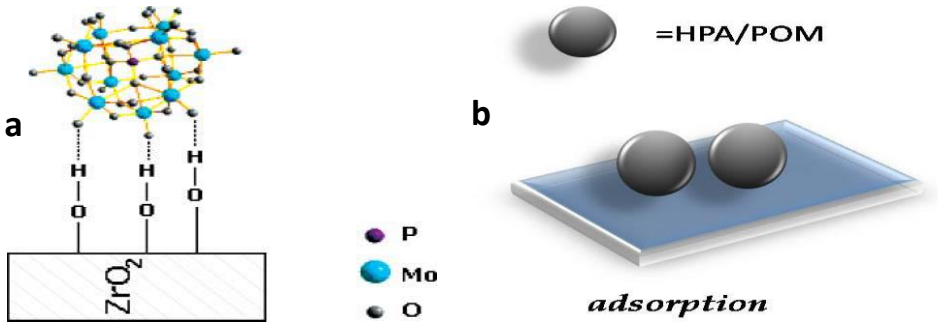


**Fig. 1.10. (a)** Interaction of $PMo_{11}$ with the surface of $ZrO_2$. [56] **(b)** Adsorption type reproduced from reference.[57]

- When the support is clay, intercalation is expected.[57] An example is presented in **Figure 1.11**.

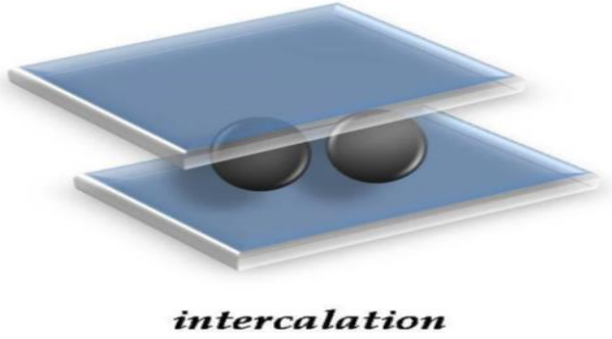


**Fig. 1.11.** Intercalation of HPA in clay type supports.[57]

- In the case of mesopores materials, encapsulation takes place, and a strong hydrogen bonding type of interaction can occur between the terminal oxygens of heteropolyanions and the silanol hydroxyl groups of mesopores materials.[57] **Figure 1.12** illustrates this kind of interaction.

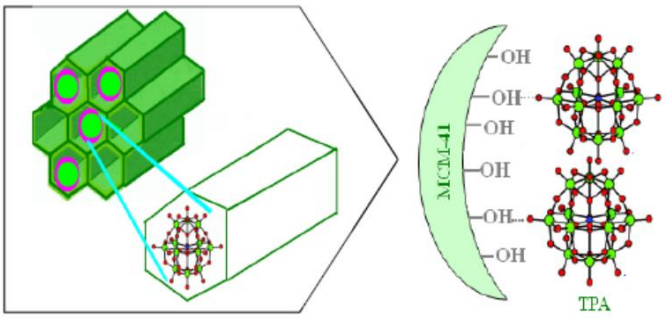


**Fig. 1.12.** Encapsulation of heteropolyanions into mesoporous supports.[57]

- Also, ion exchange and covalent bonding types of interactions are also possible, as seen in **Figure 1.13**.[57]

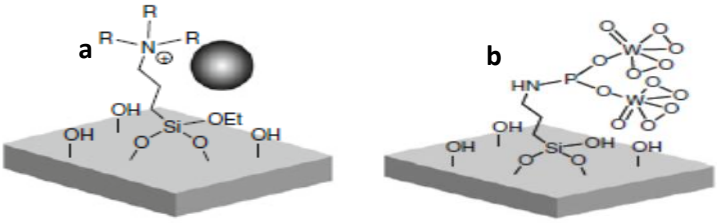


**Fig. 1.13. (a)** Ion exchange type and **(b)** covalent linkage type of interaction for supported HPA catalysts.[57]

The following benefits can be derived from supporting heteropoly acids:

- Thermal stability and surface area are increased.
- Higher catalytic activity and selectivity in some heterogeneous reactions.
- Easy separation from the reaction mixture and thus ease of reuse.[28, 58]

Several studies have been reported on immobilization of HPAs into different acidic supports such as $SiO_2$, and the physicochemical properties and catalytic applications of these have been evaluated.[59-60] It has been reported, for example, that the acid strength of bulk Keggin $H_3PW_{12}O_{40}$ decreased when it was supported on $SiO_2$. The effects of support on the acid strength of $H_3PW_{12}O_{40}$ catalysts is presented in **Table 1.4.** A reduction in acid strength can be observed in oxide supported HPAs, represented by enthalpy of ammonia adsorption.[61]

**Table 1.4.** *Effect of support on the acid strength of $H_3PW_{12}O_{40}$ catalysts*.

| **Catalyst** | **BET surface area** $m^2\ g^{-1}$ | $\Delta H_{NH3}$[a] **kJ mol$^{-1}$** |
|---|---|---|
| $H_3PW_{12}O_{40}$ | 2 | -195 |
| $C_{2.5}H_{0.5}PW_{12}O_{40}$ | 111 | -164 |
| 15% $H_3PW_{12}O_{40}/SiO_2$ | 229 | -154 |
| 15% $H_3PW_{12}O_{40}/TiO_2$ | 41 | -143 |
| 15% $H_3PW_{12}O_{40}/Nb_2O_5$ | 166 | -132 |
| 15% $H_3PW_{12}O_{40}/ZrO_2$ | 121 | -121 |

[a] Initial enthalpy of $NH_3$ adsorption

The use of neutral salts of heteropoly acids can be an alternative approach to improve the surface area and accessibility of surface protons. Matachowski *et al*. found that when a heteropoly acid is loaded onto a fully neutralised heteropoly salt, it is likely to undergo a self-assembly which arranges the catalysts into core shell particles.

These types of core shell catalysts are expected to have stronger proton sites than when using a more basic oxide support. This can be explained by the weak interaction between the heteropoly acid and its neutral salt.[62-64]

In addition, it is theorised that the core shell arrangement will increase the number of accessible protons for reactants and this factor make these particles more active for various catalytic reactions.[63] A diagram of these core shell particles is illustrated in **Figure 1.14.**

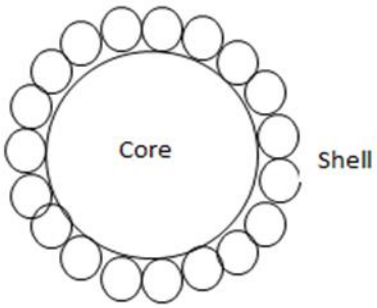


**Fig 1.14.** Cross-section of a core containing a neutral heteropoly salt and a shell containing the heteropoly acid itself.[64]

## 1.3.4 Types of heterogeneous catalysis by heteropoly acids

There are three different modes of catalysis by solid HPAs as demonstrated by Misono *et al.*: surface type, bulk type I (pseudo-liquid) and bulk type II (**Figure 1.15**).[28]

The surface type is a conventional acid or oxidation heterogeneous catalysis which takes place on the two-dimensional surface of solid catalysts (i.e., on the outer surface and pore walls). In this case, the reaction rate is proportional to the surface area. For acid catalysis, the rate correlates with the surface acidity of the catalyst.

Surface acid catalysis has been demonstrated for reactions over $Cs_xH_{3-x}PW_{12}O_{40}$ ($2 < x < 3$).[34]

Bulk type I catalysis is observed in reactions of polar substrates with solid bulk HPAs and soluble HPA salts (i.e., salts with small cations $Li^+$, $Na^+$, etc.) at relatively low temperatures. The reactant molecules are absorbed in the interstitial space between polyanions in the ionic crystal and react there. The products come out to the surface and are released to liquid or gas phases. In this case, the solid behaves like a concentrated solution (pseudo liquid phase), and the reaction field becomes three dimensional. The reaction rate is proportional to the volume of the catalyst.

Bulk type II catalysis is found in some oxidation reactions at high temperatures. In spite of the fact that the principal reaction may proceed on the surface, the whole bulk of the solid takes part in redox catalysis due to the rapid migration of redox carriers such as protons and electrons. The reaction rate is proportional to the volume of the catalyst.

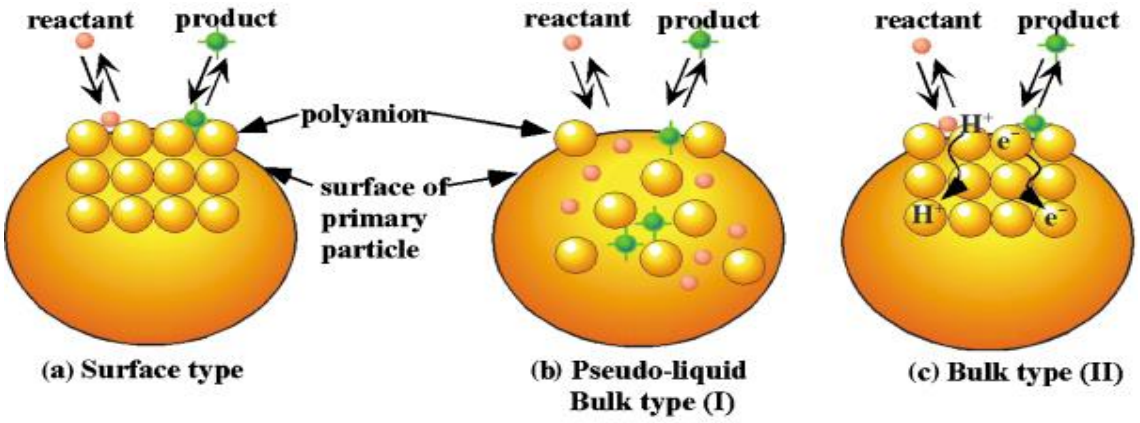


**Fig. 1.15**. The three types of catalysis by solid heteropoly compounds.[36]

The surface type and bulk type I mechanisms have been suggested for conversions of organic molecules over heteropoly acids.[29] For example, with bulk heteropoly acids at relatively low temperatures, small polar molecules (e.g. lower alcohols) possessing a high affinity to heteropoly acids may react via the bulk type I mechanism.[30] In the case of

supported heteropoly acids, on the other hand, reactions of polar substrates are more likely to occur via surface type catalysis.[28]

### 1.3.5 Application of HPAs in heterogeneous acid catalysis

HPAs have been applied in a wide range of reactions in heterogeneous systems.[36, 65-67]

Some reactions catalysed by solid acid catalysts based on HPA in the gas phase are mentioned below. More comprehensive accounts can be found in the following reviews. Misono *et al*. studied the effect of bulk solid heteropoly acids and their salts in the dehydration of alcohols. In particular, dehydration of isopropanol, as a standard test reaction, was carried out over different types of heteropoly acids and showed that $H_3PW_{12}O_{40}$ was much more active than $SiO_2$-$Al_2O_3$.[65] These reactions have also been studied using supported heteropoly acids. Silica-supported heteropoly acids with HPA loadings from about 20 to 50 wt%, or sometimes even higher, are preferred because of their high surface area. At lower loadings, the acidity of heteropoly acid decreases because of interaction with the support. Such catalysts are also quite sensitive to poisoning by impurities that may be present in the support or feed.[29]

Supported heteropoly acids have long been known as efficient catalysts for gas phase hydration of olefins such as ethylene and propylene to the corresponding alcohols.[68-69]

Heteropoly acids have also been applied for the skeletal isomerisation of linear alkanes.[60, 70] Bardin and Davis reported that the catalytic activity of bulk and silica-supported $H_3PW_{12}O_{40}$ in the isomerisation of n-butane and n-pentane at 200 $^oC$ decreased with increasing pre-treatment temperature, which suggests that the level of hydration is important. Catalyst deactivation was observed during this reaction, however, supposedly due to dehydration of the surface of the heteropoly acid.[60]

The conversion of methanol to hydrocarbons over heteropoly acids and their salts has been studied.[71- 74] Ono *et al*. applied $H_3PW_{12}O_{40}$, $H_4SiW_{12}O_{40}$ and their silver (I) and copper (II) salts for this reaction at 300 $^oC$, the main products being the $C_2$-$C_5$ aliphatic hydrocarbons. Cesium salts of heteropoly acids exhibited better selectivity to $C_2$-$C_4$ olefins, up to 64% for $Cs_{2.5}H_{0.5}PW_{12}O_{40}$.[72]

Recently Kozhevenikov's group have reported on the acidic and catalytic properties of heteropoly acids supported on $SiO_2$, $TiO_2$, $Nb_2O_5$, and $ZrO_2$.[61] These catalysts have been studied for the isomerization of α-pinene and longifolene and the dehydration of glycerol to acrolein.[75-77]

## 1.4 Zeolites

### 1.4.1 Properties of Zeolites

Zeolites are natural or synthetic inorganic macromolecular materials made from $SiO_4$ and $AlO_4$ tetrahedral building blocks linked by common oxygen atoms. The general formula of zeolites is $A^{m+}_{y/m}[SiO_2)_x \cdot (AlO_2)_y]$ $zH_2O$, where A is a cation with the charge m, (x+y) is the number of tetrahedra per crystallographic unit cell, and x/y is the so-called framework silica/alumina ratio, ($SiO_2/Al_2O_3$). According to Lowenstein's rule, the formation of two adjacent alumina tetrahedra that are linked through a common oxygen atom is forbidden. The negative charge localised on the $AlO_4^-$ tetrahedra is compensated for by an exchangeable cation such as $H^+$ and $Na^+$.[78]

Zeolites are highly porous crystalline compounds due to the extensive network of channels, channel intersections, and voids that make up the zeolite structure, which results

in high surface areas (400-800 $m^2/g$). The pores of zeolites are micropores (<2 nm in diameter) and strictly uniform. Consequently, the reaction rate on zeolite catalysts is usually limited by internal diffusion and strongly depends on molecule size. This results in shape selective catalysis, which is unique to zeolite catalysts. Three types of shape selectivity are distinguished:

- Reactant shape selectivity (when reactants with dimensions corresponding to the pore size can go inside to the active sites).
- Restricted transition state shape selectivity (in some cases, intermediate or transition states cannot be accommodated inside pores since the lack of space prohibits the reaction).
- Product shape selectivity (products with dimensions corresponding to the pore size can diffuse into the pores and leave through the channels).[79-82]

Zeolites are commonly synthesised with sodium acting as the charge balancing counter cation. For the majority of catalytic applications of zeolites the Brønsted acid form is required (i.e. the protonic form); this is readily produced by introducing ammonium ions followed by heat treatment. After the removal of ammonia, the protons remaining to counter the negative charge of the tetrahedral aluminium atoms react with oxygen in the lattice SiOAl groupings to generate a three coordinate Al next to a SiOH moiety; this mechanism is shown in Scheme 1.1.[82]

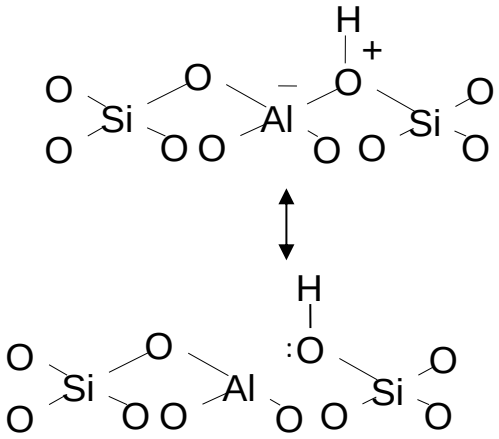


**Scheme 1.1.** Brønsted acid sites in zeolites.[82]

The hydroxyl groups with very acidic protons have been shown to be the source of the Brønsted acidity, and the Lewis acid sites are free vacancies on the framework aluminium created through dehydroxylation of the zeolite structure under heat treatment. Zeolite properties that have to be considered when evaluating the acidity of a zeolite in relation to a particular catalytic reaction include the total number of Brønsted and Lewis sites, their strength distributions, and their location. Each of these properties will have a significant influence on the effective acidity of an individual acid site in relation to a particular reaction. Basic molecules such as ammonia and pyridine are commonly used to probe the acid sites of zeolites in experimental techniques such as temperature programmed desorption (TPD), calorimetry, and Fourier transform infrared spectroscopy.[82-83]

Also, the structure and chemical composition of zeolites especially the ratio of Si/Al was found to affect the catalytic activity of Brønsted acid sites.[84] When the Si/Al ratio increases, the number of strong Brønsted sites also increases, whereas the total number of acid sites reduces since the aluminium atoms induce a higher degree of electron contribution than silicon. The strength of acid sites reduces when the number of

neighbouring aluminium atoms increases, while the catalytic activity of zeolites increases when the Si/Al ratio is increased.[85] The main source of the catalytic activity of zeolites has been related to Brønsted sites rather than Lewis sites.[81]

### 1.4.2 Application of zeolites in heterogeneous catalysis

There are many applications of zeolites due to their properties of strong acidity, thermal stability and shape selectivity, and their economic and environmental benefits. They have consequently been widely used as heterogeneous catalysts for the chemical and petrochemical industries. In industry, there are more than forty processes that apply zeolites as catalysts.[86- 87]

The most common industrial zeolites include the mordenite framework inverted (MFI), A and FAU types. There are two common MFI-type zeolites, silicalite-1 and ZSM-5. The difference between them is that Si/Al ratio in ZSM-5 is around 10-200, whereas in silicate-1 there is little or no aluminium content.[88]

The ZSM-5 zeolite has a two-dimensional channel network which consists of micropores with a size of 5−6 Å. The external surface of ZSM-5 crystals consists of pores with a solid framework between them (**Figure 1.16**). The general formula of a ZSM-5 zeolite is $Na_nAl_nSi_{96-n}O_{192}\cdot H_2O$, where n is smaller than 27, typically close to 3. $Na^+$ ions can be readily removed, however, to create Brønsted acid sites via ion-exchange and replacement by $H^+$.

The major contributor to the reactivity of HZSM-5 has been found to depend on the acidity introduced by aluminium in the silicate-alumina framework. Changes in acidity may, therefore, affect both reaction pathways and product distribution.[89]

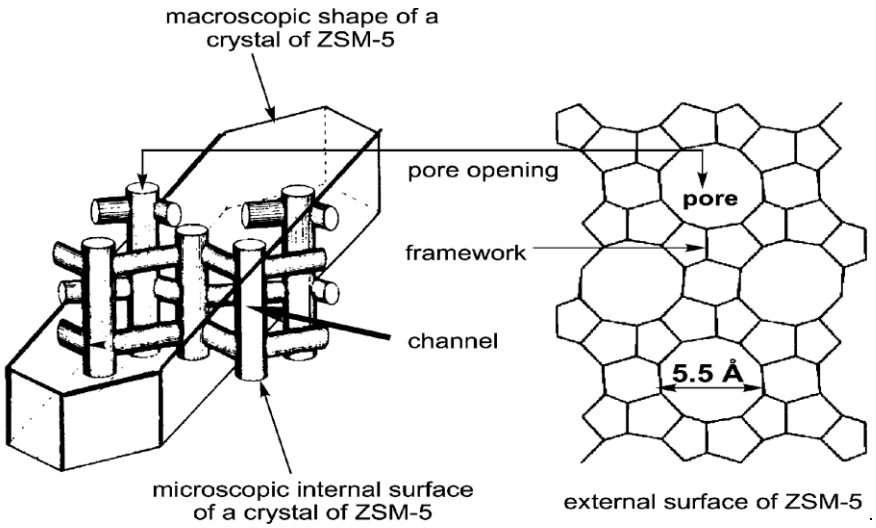


**Fig. 1.16.** Structure of ZSM-5 zeolite.[90]

The cracking of paraffin over ZSM-5 is one of the best known industrial reactions, wherein the ZSM-5 catalyst forms carbonium ions by protonation of paraffin such as n-hexane and n-butane to produce hydrogen gas, olefins, and paraffin at high temperatures.[91] Other examples of reactions catalysed by zeolites can be found in the references.[92-94]

Since the mass transport limitations of reactants and products are critical for reaction by zeolites, the pores can be changed to mesopores by decreasing the size of the zeolite crystals or by increasing the pore size to overcome diffusional limitations.[51, 52] Hartmann reports that mesoporous zeolites offer increased activity and resistance to deactivation.[51]

Zeolites have also been used as the catalysts for dehydration of lower alcohols such as methanol and ethanol, and this is discussed in the following sections.

## 1.5 Alcohol dehydration: scope and mechanism

Most primary and secondary alcohols undergo dehydration via the $E_2$ mechanism, while tertiary alcohols react via a two-step $E_1$ mechanism as a result of the higher stability of the carbenium ion. The $E_1$ mechanism requires strong acid sites and leads to olefin formation, while the $E_2$ mechanism, which occurs at both acid and base sites, leads to the formation of ether as well as olefins.[95]

The dehydration of simple alcohols over different types of Brønsted acids and some Lewis acid catalysts is one of the best-studied reactions in the field of heterogeneous acid catalysts.[96] Despite the many years of study, however, the mechanisms by which olefin and ether are formed are still not clear. Both intermolecular and intramolecular dehydration may occur during the dehydration of alcohols, depending on the reaction condition, the reactant and catalyst applied. The intermolecular dehydration of two alcohol molecules over alumina as a catalyst to produce ether was found to require a lower activation energy than the use of intramolecular dehydration to form alkenes. At low temperatures, therefore, the ether is the kinetically favoured product. Several studies have explored the mechanism of ether formation during dehydration of alcohols over alumina and found that the ether cannot be produced from secondary alcohol dehydration, except for isopropanol. It has also been reported that dehydration of primary alcohols to form ether occurred via the Langmuir-Hinshelwood mechanism. Deboer *et al*., however, reported that the formation of ether occurred via both the Elely-Rideal and Langmuir-Hinshelwood mechanisms.[97]

The mechanism proposed for alkene formation in the dehydration of isopropanol is shown in **Figure 1.17**.

It involves either surface Brønsted acid sites or Lewis acid sites, leading to hydrogen bonded or coordinated isopropanol species, respectively, followed by a concerted mechanism involving a hydrogen atom of a methyl group.[95, 98]

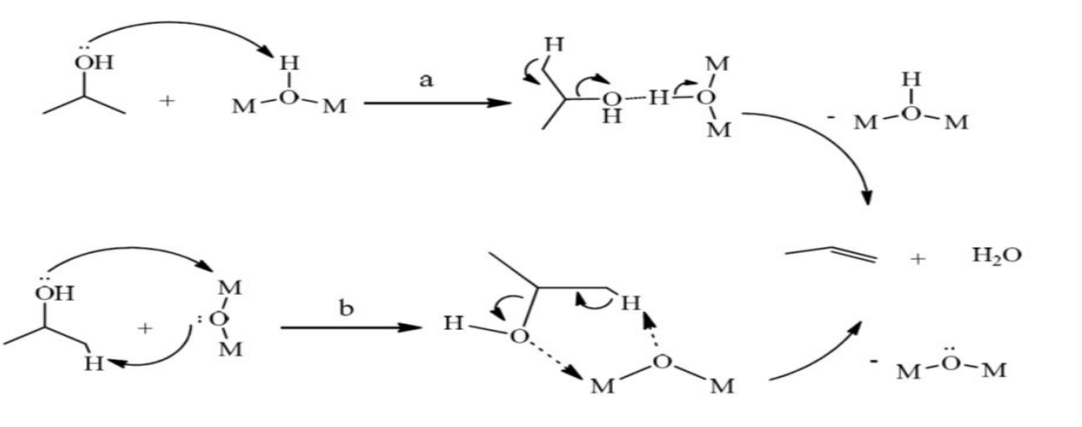


**Fig. 1.17.** Proposed mechanisms for propene formation: (a) involving surface Brønsted acid sites and (b) involving surface Lewis acid sites.[98]

The mechanisms proposed for diisopropyl ether formation are shown in **Figure 1.18**. Isopropyl ether is formed by an intermolecular dehydration which requires an acidic OH group.[95]

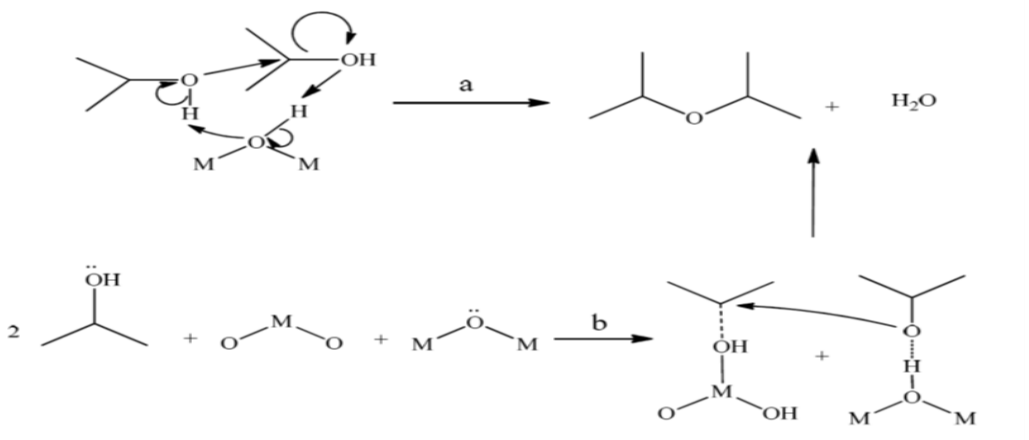


**Fig. 1.18.** Proposed mechanisms for ether formation (a) involving surface Brønsted acid sites and (b) involving surface Lewis acid sites.[98]

The dehydration of ethanol to yield ethene is suggested to occur through the $E_2$ elimination pathway (bimolecular elimination), which involves concerted cleavage of C–O, and C–H bonds in alcohol using a pair of acid and base catalyst sites. The formation of diethyl ether (DEE) may be represented by two different pathways, termed the associative pathway and the dissociative pathway (**Figure 1.19**), similar to the mechanism proposed for the formation of dimethyl ether from methanol. Both pathways are thought to take place at Brønsted acid sites. The associative (concerted) pathway, involves adsorption of two alcohol molecules, which react and form the ether directly. The dissociative (stepwise) pathway involves initial alcohol adsorption, followed by water elimination, leading to an adsorbed alkyl group and water. The alkyl group reacts with a second alcohol molecule to form the ether.[99]

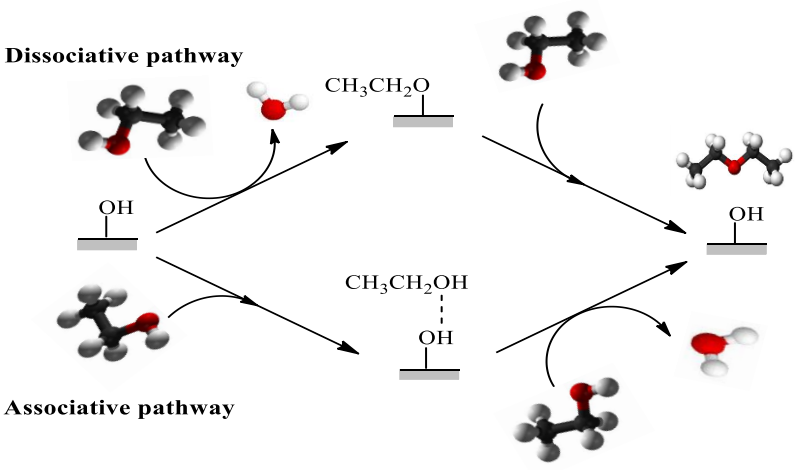


**Fig. 1.19.** Associative and dissociative pathways for the ethanol-to-DEE reaction.

## 1.6 Transformation of biomass into biodiesel

At the turn of the 19th century, fossil fuels were in abundant supply to satisfy the world's energy requirements. Growing energy costs, adverse environmental impacts, and decreasing supplies of fossil fuels have encouraged the investigation of sustainable materials that can be used as alternative fuels from renewable sources such as biomass.[100]

Biomass is a natural material derived from living, or recently lived organisms. It refers to plants or plant-derived materials. Biomass can be used as an energy source either directly via combustion or indirectly after converting it to different forms of biofuel. Conversion of biomass to biofuel can be achieved by thermal, chemical and biochemical methods. The most abundant form of biomass on the planet is lignocellulose, which is composed typically of cellulose, hemicellulose and an aromatic polymer lignin.[101-102]

**Figure 1.20** shows two methods that may be applied for the conversion of lignocellulose to biofuel. One includes pre-treatment and fermentation of biomass to yield bioethanol. Alternatively, lignocellulose may be converted to syngas ($H_2$ and CO) via gasification followed by Fischer-Tropsch synthesis to yield liquid hydrocarbons.[103]

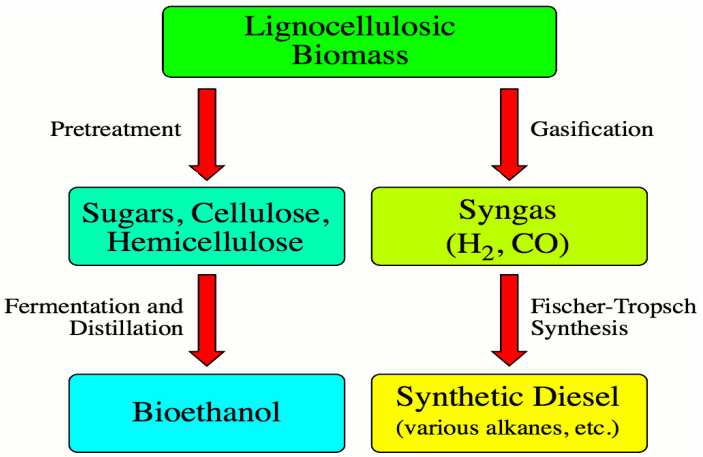


**Fig. 1.20.** Methods to produce ethanol and synthetic diesel from lignocellulosic biomass.[104]

Biofuels, such as alcohols and biodiesel, have been recommended as alternatives for internal combustion engines for vehicles. In particular, biodiesel has received much attention in recent years as a replacement for diesel fuel due to increased health and environmental concerns regarding the effects of diesel engine particulate and $NO_x$ emissions.[105]

Many investigations show that replacing diesel with biodiesel in diesel engines can lower the level of hydrocarbon (HC), carbon monoxide (CO) and particulate matter (PM) emissions, but that nitrogen oxide ($NO_x$) emissions may increase.[106] Nevertheless, biodiesel has some disadvantages, such as higher viscosity and pour point, and lower volatility compared with diesel. The poor cold flow properties of biodiesels have a direct impact on the operability of biodiesel blends in cold weather.[107] Lower alcohols and their ethers might be expected to improve the poor cold flow properties, however.[108]

Bioethanol is an oxygenated fuel that is used for internal combustion engines. It can be produced from any biomass feedstock containing carbohydrates, for example, corn, wheat, sugar-beets, potatoes, maize, and sugarcane. Biomethanol is the simplest and cheapest of the alcohols and can produce a range of polymers and fuels such as biohydrogen, bio-dimethyl ether (DME), methanol-to-gasoline (MTG). It can be formed

via gasifying organic materials. Both methanol and ethanol have higher octane numbers than petrol, which means that they are less likely to auto-ignite under pressure before the spark in internal combustion engines (knocking), and also gives a higher compression ratio for improved thermal efficiency and significantly more power than an equivalent petrol engine.[109-110]

Nevertheless, the major disadvantage of low carbon alcohols need to be considered in relation to petrol is that in cold weather, the high heat of vaporisation makes it difficult to start in methanol or ethanol engine.

Methanol and ethanol can be converted through a dehydration process into dimethyl ether and diethyl ether, respectively; either of which can be used as a transportation fuel.[108]

## 1.7 Production of ethers through dehydration of alcohols

Production of ethers by intermolecular dehydration of primary alcohols such as methanol and ethanol has attracted considerable attention in recent years. Dimethyl ether (DME) and diethyl ether (DEE) can be used as an alternative to diesel fuel or diesel fuel additives to reduce $NO_x$, $SO_x$ and particulate matter emissions.[100]

### 1.7.1 Liquid phase dehydration of alcohols

Dehydration of primary alcohols to produce ethers can be carried out in the liquid or gas phase. In the liquid-phase process, dehydration of primary alcohols was investigated over solid acid catalysts to produce dialkyl ethers with co-production of alkenes.[111-113] Water formed during alcohol dehydration is known to adsorb strongly on the solid acid catalyst,

however, inhibiting this reaction. Moreover, the solvent can have an impact on the performance of the catalysts.[114-115]

Much research has been done to optimize the ether production, as well as improve the stability of the catalyst.[116-118] Vanoye *et al*. found that the rate of dehydration of ethanol to diethyl ether over heterogeneous sulfonic-acid catalysts strongly depended on the solvent used.[119]

Recently, Khandan *et al*. investigated the dehydration of methanol to dimethyl ether in the liquid phase over zeolites ZSM-5, Y, Mordenite, Ferrierite, and Beta. The results showed that the Al-modified mordenite showed the highest activity in the production of dimethyl ether and the highest catalyst stability.[120]

Given the strong solvent effect and possible catalyst leaching, this thesis will be focused on alcohol dehydration in the gas phase. Particularly, it will be focused on the dehydration of methanol and ethanol to yield dimethyl ether and diethyl ether respectively, using HPA catalysts.

### 1.7.2 Dimethyl ether production through dehydration of methanol in gas phase

Dimethyl ether (DME) is an important feedstock for the chemical industry. Nowadays, it is produced commercially and used in a wide range of applications.[121] DME can also be used as a clean fuel alternative to liquefied petroleum gas (LPG), liquefied natural gas

(LNG), and also as a replacement for transportation diesel fuel. The advantages of using DME as fuel are as follows:

- DME has only C–H and C–O bonds, therefore, using DME as alternative fuel for diesel can reduce $CO_2$ and unburned hydrocarbon emissions.
- The DME has the lower latent heat of vaporisation. Therefore, the noise of the DME engine and NOx emissions may be less than for diesel engines.

These advantages have been confirmed by testing DME vehicles in Europe and North America, with one running for 750,000 miles.[122-123]

Two processes are used for DME production: an indirect and a direct process. In the indirect process, methanol is converted to DME in a catalytic dehydration reactor over a solid-acid catalyst. In the direct method, meanwhile, the synthesis gas is primarily converted to methanol over multifunctional catalysts, followed by dehydration to DME.[124]

Over the years, much of the research on methanol dehydration has focused on the methanol-to-gasoline (MTG) and methanol-to-olefin (MTO) and DME synthesis. The formation of DME is favourable at relatively low temperatures; whereas the MTG and MTO occur at higher temperatures. In addition to γ-alumina, acidic zeolites, especially MFI (HZSM-5) and heteropoly acids (HPAs) are among the most studied catalysts in methanol dehydration. These show significantly higher catalytic activities but, as yet, are less resistant to deactivation than γ-alumina.[125-132] A lot of effort has been made recently to modify these solid acid catalysts, and the summary of some important studies is provided below.

Woodhouse *et al*. patented methanol dehydration on pure $Al_2O_3$, or phosphoric acid modified $Al_2O_3$ catalysts. Water produced in the reaction process, however, blocked

active sites for methanol dehydration through competitive adsorption with methanol on the catalyst.[133-134]

Recently, Liu *et al*. have studied the dehydration of methanol to dimethyl ether over ɣ-$Al_2O_3$ modified with metal oxide ($Nb_2O_5$) in order to improve catalyst activity and stability.in the temperature range between 240 – 260 ºC. The modified catalyst exhibited a higher activity than the untreated ɣ-$Al_2O_3$.[135]

Sabour *et al*. investigated vapour phase dehydration of methanol at 250 – 400 ºC over Al-HMS catalysts compared to commercial γ-$Al_2O_3$. Al-HMS-5 and Al-HMS-10 each showed a high selectivity for DME. Among all the Al-HMS catalysts, Al-HMS-10 exhibited an optimum yield of 89% with 100% selectivity and excellent stability for methanol dehydration to DME.[136]

The strong acidity of ZSM-5 enhances the dehydration of DME to form undesired olefins and oligomers responsible for the formation of coke precursors. Lee *et al*. treated ZSM-5 samples with phosphorus compounds so as to modify their acidity and showed that the phosphorus loaded samples exhibited a significant improvement in catalytic properties compared to the phosphorus-free HZSM-5.[137]

Zhenga *et al*., meanwhile, investigated a series of zeolite composites with hierarchical porous structures and tunable acidities. In this study, the dehydration of methanol to DME showed that both the DME selectivity and the methanol conversion have a good linear dependence on the Lewis/Brönsted ratio: the conversion of methanol over the catalysts was decreased linearly with an increase in the Lewis/Brönsted ratio, although the selectivity of DME was increased linearly with an increase Lewis/Brönsted ratio. It was concluded that the hierarchy factor is a suitable tool to classify hierarchically structured materials with similar acidities and compositions in a diffusion controlled reaction (such

as isopropyl benzene cracking). For the acidity-controlled reactions such as the methanol conversion to DME, however, the hierarchy aspect may only play a negligible role.[138]

Supported HPA catalysts have been tested for DME synthesis by Ciftci *et al*., who synthesized tungstophosphoric acid (TPA) incorporated into mesoporous silicas. Two different preparations were used, one entailing a one-pot hydrothermal synthesis route and anther using wet impregnation of TPA into MCM-41. This was because TPA/MCM-41 showed higher surface area and higher activity regarding the dehydration of methanol than pure TPA. With this catalyst, DME yield passed through a maximum at about 200 $^{o}$C, above which point coke formation caused deactivation of the catalyst. The one-pot hydrothermal synthesis procedure, meanwhile, gave a better catalyst which did not lose any activity after repeated washing steps. This catalyst gave highly stable catalytic performance in the dehydration of methanol, with 100% DME selectivity in methanol dehydration at temperatures less than 300 $^{o}$C.[139]

Finally in this summary, the activity of silicotungstic acid (STA) impregnated onto aluminosilicate was studied by Varisli *et al*., with the STA impregnated catalyst showing a higher DME yield than the pure STA catalyst.[140]

### 1.7.3 Diethyl ether production through dehydration of ethanol in gas phase

In the last decade, dehydration of ethanol to diethyl ether (DEE) has attracted significant attention in the context of sustainable development. DEE is the thermodynamically favoured product since it is predominantly formed at lower temperatures, whereas the selectivity to ethene increases with increasing reaction temperature at the expense of DEE.

Diethyl ether has a high cetane number of 85-96 and higher energy density than ethanol. It has been reported as an oxygenated blending for diesel/biodiesel fuels and results in fewer $NO_x$ emissions compared to the diesel.[109]

Takahara *et al*. studied the activities of different solid acid catalysts, such as zeolites and silica–alumina, for the dehydration of ethanol to DEE and ethylene. Their results show that the catalyst activity for the conversion of ethanol can be correlated with the number of strong Brønsted acid sites in the catalyst.[141]

Zeolites such as FER, MFI, and MOR were investigated for the conversion of ethanol by Chiang and Bhan. They found that DEE formation was independent of partial ethanol pressure. Also, ethylene production was only observed on H-MOR among the three zeolites under investigation, which may relate to 8-MR side pockets protecting ethanol monomers from forming ethanol dimers. Furthermore, H-FER and H-MFI only catalysed bimolecular ethanol dehydration reactions. They also reported that the selectivity to ethylene and diethyl ether in ethanol conversion is determined by the stability of intermediates, the size of zeolite channels and the location of Brønsted acid sites. The size of the zeolite channels played an especially important role in the formation of diethyl ether since the pores of zeolite are large enough to accommodate ethanol dimers, leading to diethyl ether via a bimolecular pathway, since generating ethanol dimeric species is energetically more favourable than the generation of ethanol monomers. In zeolites with small channels, ethanol dehydration occurs via a unimolecular reaction pathway to yield ethylene.[142]

Varisli *et al*. investigated the dehydration of ethanol over three different heteropoly acid catalysts, tungstophosphoric acid (TPA), silicotungstic acid (STA) and molybdophosphoric acid (MPA) in a temperature range of 140 – 250 °C. At higher temperatures, very high selectivity for ethylene was obtained. Whereas at lower

temperatures, very high selectivity for diethyl ether was obtained. The presence of water vapour was shown to cause some reduction in catalyst activity. Among the three HPA catalysts, the activity trend was obtained as STA > TPA > MPA.[143]

Matachowski *et al*. investigated dehydration of ethanol in the gas phase over silver salt of tungstophosphoric acid ($Ag_3PW_{12}O_{40}\cdot 3H_2O$) at 100 – 220°C in nitrogen and air. It was found that relative humidity strongly affects the catalytic activity of the AgPW salt, as shown in **Figure 1.21**. The catalytic activity of $Ag_3PW_{12}O_{40}\cdot 3H_2O$ was stable in the conversion of ethanol to produce diethyl ether.[144]

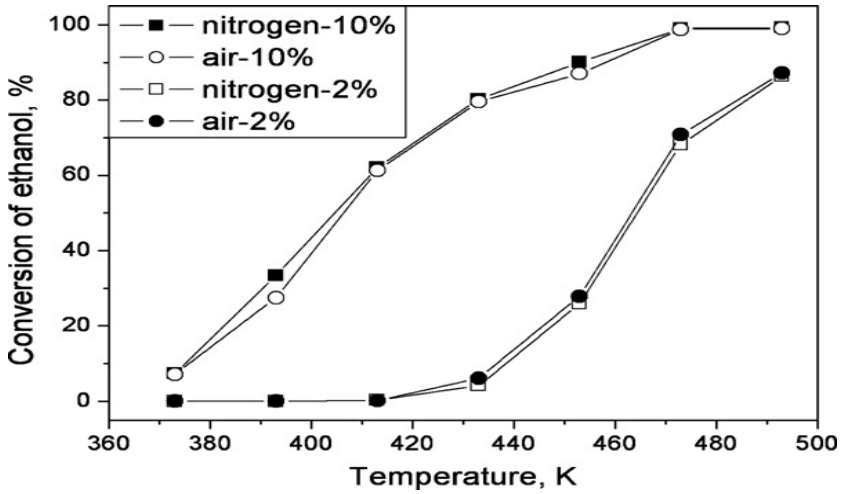


**Fig. 1.21**. Ethanol conversion on AgPW salt in nitrogen and air at various humidities.[144]

From the previous studies, it can be concluded that heterogeneous acid catalysts, in particular, HPAs, can carry out the dehydration of ethanol and methanol to produce ethers. However, improvements are still needed to overcome catalyst deactivation and improve reaction selectivity.

## 1.8 The scope and objectives of thesis

The processes that yield fuels and chemicals by conversion of fossil resources are essential to our modern life. The growing concern today, however, is with the future availability of fossil fuels and their associated environmental issues. While many chemical production processes have become environmentally friendly in the last few decades, the world's demand for fossil fuel has continued to grow and thus has led to a sharp increase in atmospheric carbon dioxide levels, resulting in global climate change.

Production of ethers by intermolecular dehydration of primary alcohols, such as methanol and ethanol, has attracted considerable attention in recent years. Dimethyl ether (DME) and diethyl ether (DEE) can be used as an alternative for diesel fuel or diesel fuel additives to reduce $NO_x$, $SO_x$ and particulate matter emissions.

Recently, heteropoly acids (HPAs) have attracted much interest as catalysts. They are revealing higher catalytic activities than conventional acid catalysts, offering significant economic and environmental advantages. In this context, the main aim of the study presented in this thesis is to investigate a wide range of Keggin type heteropoly acids as environmentally benign heterogeneous catalysts for dehydration of lower alcohols.

The main objectives of the thesis are:

- To modify heteropoly acids via exchange of protons of tungstophosphoric acid with different metal ions, such as Cs, or through being supported on high surface area acidic or neutral supports in order to improve their catalytic properties as efficient heterogeneous acid catalysts.
- To explore the formation of ether in dehydration of methanol and ethanol at a gas-solid interface.

- The primary goal is to examine the effect of catalyst acid strength on the reaction turnover rate to gain further evidence regarding the reaction mechanism for HPA acid catalysts.

This includes the preparation, characterisation and testing of a range of acidic solid materials such as bulk HPAs, $Cs_{2.5}H_{0.5}PW_{12}O_{40}$ and the acidic composites comprising $H_3PW_{12}O_{40}$ and $H_4SiW_{12}O_{40}$ supported on $Nb_2O_5$, $ZrO_2$, $SiO_2$ and $TiO_2$.

This is complemented by the characterisation of catalyst texture and the chemical environment of HPA on the catalyst surface by different techniques such as nitrogen adsorption, thermogravimetric analysis (TGA), infrared spectroscopy (IR) and X-ray diffraction (XRD). The acid strength of catalysts will be determined by ammonia adsorption microcalorimetry regarding the initial adsorption enthalpy.

## 1.9 Organisation of the thesis

Chapter 1 gives a general introduction to heterogeneous catalysis and the fundamental concepts that are required to understand how heterogeneous catalysis works. This chapter also introduces heteropoly acids as acid catalysts and describes the dehydration of lower alcohols (methanol and ethanol). Recent literature on the formation of dimethyl ether and diethyl ether through dehydration of methanol and ethanol is also reviewed.

Chapter 2 describes the preparation methods used for the synthesis of catalysts. The techniques used for catalyst characterisation along with the gas phase catalyst reaction testing procedures are also described.

Chapter 3 describes the results of catalyst characterisation and gives information about the structure and physicochemical properties of the prepared catalysts.

Chapter 4 describes the dehydration of methanol to dimethyl ether (DME) at a gas/solid interface over a wide range of bulk and supported Brønsted acid catalysts based on tungsten Keggin heteropoly acids (HPA) in comparison with the reaction over HZSM-5 zeolites (Si/Al = 10−120).

Chapter 5 deals with the dehydration of ethanol to DEE over a wide range of solid Brønsted acid catalysts based on Keggin-type heteropoly acids (HPAs) at a gas-solid interface in a continuous flow fixed-bed reactor in the temperature range of 90 – 220 $^{o}$C. The catalysts include $H_3PW_{12}O_{40}$ (HPW) and $H_4SiW_{12}O_{40}$ (HSiW) supported on $SiO_2$, $TiO_2$, $Nb_2O_5$ and $ZrO_2$ with sub-monolayer HPA coverage, as well as bulk acidic Cs salts of HPW ($Cs_{2.5}H_{0.5}PW_{12}O_{40}$ and $Cs_{2.25}H_{0.75}PW_{12}O_{40}$) and the corresponding core-shell materials with the same total composition (15%HPW/$Cs_3PW_{12}O_{40}$ and 25%HPW/$Cs_3PW_{12}O_{40}$, respectively) comprising HPW supported on the neutral salt $Cs_3PW_{12}O_{40}$.

Chapter 6 provides the main conclusions drawn from the findings of reaction studies and characterisation of the catalysts obtained in the present work.

## 1.10 References


1. J. M. Thomas, W. J. Thomas, Principles and Practice of Heterogeneous Catalysis, VCH, Weinheim, 1997.
2. J. Hagen, Industrial Catalysis: A Practical Approach, 2nd ed., Wiley-VCH, Weinheim, 2006.
3. O. Deutschmann, H. Knözinger, K. Kochloefl, K. Turek. Heterogeneous Catalysis and Solid Catalysts. Ullmann`s Encyclopedia of Industrial Chemistry, Electronic Release, 7th ed., Wiley-VCH Verlag GmbH & Co, Weinheim, 2009.
4. J. Concordia, J. Chem. Eng. Prog., 86 (1990) 50.
5. I. Fechete, Y. Wang, C. J. Védrine, Catal. Today, 189 (2012) 2.
6. J. K. Nørskov, F. Studt, F. Abild-Pedersen, T. Bligaard, Fundamental Concepts in Heterogeneous Catalysis, John Wiley & Sons, UK, 2014.
7. G. C. Bond, Heterogeneous catalysis: principles and applications, Clarendon Press, Wortley, 1974.
8. G. Ertl, Angew. Chem. Int. Ed. Engl., 29 (1990) 1219.
9. R. Klaewkla, M. Arend and W. F. Hoelderich, Mass Transfer-Advanced Aspects, In Tech, Germany, 2011.
10. C. H. Bartholomew, R. J. Farrauto, in Fundamentals of Industrial Catalytic Processes, Wiley-Interscience, Hoboken, 2006.
11. M. K. Bowker, The basis and applications of heterogeneous catalysis, Oxford University Press, Oxford, 1998.
12. G. Ertl, H. Knozinger, J. Weitkamp, Handbook of Heterogeneous Catalysis, Weinheim, VCH, 1997.

13. S. Lowell, J. E. Shields, M. A. Thomas, M. Thommes,Characterization of Porous Solids and Powders Surface Area, Porosity and Density, Kluwer Academic Publishers, Berlin, 2004.
14. I. Chorkendorff, J. W. Niemantsverdriet, Concepts of Modern Catalysis and Kinetics. Wiley-VCH, Weinheim, 2003.
15. B. Viswanathan, S. Sivasanker, A. V. Ramaswamy, Catalysis: Principles and applications, Norsa publishing house, New Delhi, 2002.
16. M. Beller, A. Renken, R. A. van Santen, Catalysis: from Principles to Applications, Wiley-VCH, Weinheim, 2012.
17. J. W. Niemantsverdriet, in Spectroscopy in Catalysis, Wiley-VCH Verlag GmbH & Co. KGaA, Weinheim, 2007.
18. A. Nilsson, L. G. M. Pettersson, J. K. Nørskov, Chemical Bonding at Surfaces and Interfaces. Elsevier, Amsterdam, 2008.
19. R. R. H Julian, Heterogeneous Catalysis Fundamentals and Applications, Elsevier B.V., Netherlands, 2012.
20. I. V. Kozhevnikov, A. Sinnema, R. J. J. Jansen, K. Pamin, H. Bekkum, Catal. Lett., 309 (1994) 241.
21. M. Boudart, Chem. Rev., 95 (1995) 661.
22. F. Lucio, Catal. Today, 52 (1999) 147.
23. J. F. Keggin, Nature, 131 (1933) 908.
24. J. J. Berzelius, Pogg. Ann. Phys. Chem., 6 (1826) 369.
25. I. V. Kozhevnikov, K. I. Matveev, Appl. Catal., 5 (1983) 135.
26. I. V. Kozhevnikov, Russ. Chem. Rev., 56 (1987) 811.
27. D. E. Katsoulis, Chem. Rev., 98 (1998) 359.

28. I. V. Kozhevnikov, Catalysts for Fine Chemicals. Catalysis by Polyoxometalates, Wiley, Chichester, 2002.
29. T. Okuhara, N. Mizuno, M. Misono, Adv. Catal., 41 (1996) 113.
30. M. Misono, Chem. Commun., 13 (2001) 1141.
31. D. S. Mansilla, M. R. Torviso, E. N. Alesso, P. G. Vazquez, C. V. Caceres, Appl. Catal. A: Gen., 375 (2010) 196.
32. G. A. Tsigdinos, C. J. Hallada, Inorg. Chem., 7 (1968) 437.
33. I. A. Weinstock, J. J. Cowan, E.M.G. Barbuzzi, H. Zeng, C.L. Hill, J. Am. Chem. Soc., 121 (1999) 4608.
34. M. Misono, K. Sakata, Y. Yoneda, W.Y. Lee, Proc. 7th Int. Congr. Catal. Tokyo (1980) 1047.
35. J. F. Keggin. Proc. Roy. Soc. A., 75 (1934) 144.
36. N. Mizuno, M. Misono, Chem. Rev., 98 (1998) 199.
37. I. V. Kozhevnikov, Chem. Rev., 98 (1998) 171.
38. I. V. Kozhevnikov, A. Sinnema, R. J. J. Jansen, H. V. Bekkum, Catal. Lett., 27 (1994) 187.
39. I. V. Kozhevnikov, A. Sinnema, H. V. Bekkum, Catal. Lett., 34 (1995) 213.
40. I. V. Kozhevnikov, A. Sinnema, H. V. Bekkum, M. Fournier, Catal., Lett. 41 (1996) 15.
41. G. M. Brown, M. R. Noe-Spirlet, W. R. Bushing, H. A. Levy, Acta Crystallogr. Sect. B., 33 (1977) 1038.
42. M. Misono, Catal. Rev. Sci. Eng., 29 (1987) 269.
43. M. Misono, Catal. Rev. Sci. Eng., 30 (1988) 339.
44. M. Misono, N. Mizuno, K. Katamura, A. Kasai, Y. Konishi, K. Sakata, T. Okuhara, Y. Yoneda, Bull. Chem. Soc. Jpn., 55 (1982) 400.

45. M. N. Timofeeva, A. V. Demidov, A. A. Davydov, I. V. Kozhevnikov, J. Mol. Catal., 79 (1993) 21.

46. J. E. Herrera, J. H. Kwak, J. Z. Hu, Y. Wang, C. H. F Peden, Top. Catal., 49 (2008) 259.

47. J. B. Moffat, J. Mol. Catal., 52 (1989) 169.

48. M. T. Pope, A. Muller, Angew. Chem. Int. Ed., 30 (1991) 34.

49. N. Essayem, R. Frety, G. Coudurier, J. C. Vedrine, J. Chem. Soc., Faraday. Trans., 93 (1997) 3243.

50. G. I. Kapustin, T. R. Brueva, A. L. Klyachko, M. N. Timofeeva, S. M. Kulikov, I. V. Kozhevnikov, Kinet. Catal., 31 (1990) 1017.

51. R. S. Drago, J. A. Dias, T. O. Maier, J. Am. Chem. Soc., 119 (1997) 7702.

52. N. Essayem, G. Coudurier, M. Fournier, J. C. Vedrine, Catal. Lett., 34 (1995) 223.

53. N. Essayem, Y. Y. Tong, H. Jobic, J. C. Vedrine, Appl. Catal. A., 194 (2000) 109.

54. T. Okuhara, T. Nishimura, H. Watanabe, M. Misono, J. Mol. Catal., 74 (1992) 247.

55. J. H. Clark, A. P. Kybett, D. J. Maequarrie, Supported reagents: preparation, analysis and application, VCH Inc. New York, 2000.

56. S. Pathan, A. Patel, Dalton. Trans., 40 (2011) 348.

57. N. Mizuno, K. Kamata, K. Yamaguchi, Top. Organomet. Chem., 37 (2011) 127.

58. N. Mizuno, K. Kamata, K. Yamaguchi, Liquid Phase Oxidations Catalyzed by Polyoxometalates. Taylor and Francis Group, New York, 2006.

59. Y. Izumi, R. Hasebe, K. Urabe, J. Catal., 84 (1983) 402.

60. B. B. Bardin, R.J. Davis, Appl. Catal. A., 200 (2000) 219.

61. A. M. Alsalme, P. V. Wiper, Y. Z. Khimyak, E. F. Kozhevnikova and I. V. Kozhevnikov, J. Catal., 276 (2010) 181.

62. L. Matachowski, A. Drelinkiewicz, D. Mucha, J. Kryściak-Czerwenka, R. Rachwalik, Appl. Catal. A., 469 (2014) 290.

63. P. Y. Gayraud, N. Essayem, J. C. Vedrine, Catal. Lett., 56 (1998) 35.

64. S. Kirsch, A. Doerk, E. Bartsch, H. Sillescu, K. Landfester, H. W. Spiess, W. Maechtle, Macromolecules., 32 (1999) 4508.

65. I. V. Kozhevnikov, Chem. Rev., 98 (1998) 171.

66. M. T. Pope, A. Mucler, Polyoxometalate Chemistry: From topology via self-assembly to applications Kluwer Academic, Netherlands, 2001.

67. M. T. Pope, A. Muller, Polyoxometalate Molecular Science, Kluwer Academic Publishers, Netherlands, 2003.

68. K. Weissermel, H. J. Arpe, Industrial Organic Chemistry, 3rd ed., VCH, Weinheim, 1997.

69. B. M. Andreev, G. K. Boreskov, S.G. Katalnikov, Khim. Prom., 6 (1961) 389.

70. K. Na, T. Okuhara, M. Misono, J. Catal., 170 (1997) 96.

71. J. B. Moffat, Metal – Oxygen Clusters: The Surface and Catalytic Properties of Heteropoly Oxometalates, Klumer Academic/ Plenum, New York, 2001.

72. T. Baba, Y. Ono, Appl. Catal., 8 (1983) 315.

73. H. Hayashi, J. B. Moffat, J. Catal., 83 (1983) 192.

74. T. Hibi, K. Takahashi, T. Okuhara, M. Misono, Y. Yoneda, Appl. Catal., 24 (1986) 69.

75. A. Alsalme, E. F. Kozhevnikova, I. V. Kozhevnikov, Appl. Catal. A: Gen., 390 (2010) 219.

76. K. A. da Silva Rocha, P. A. Robles-Dutenhefner, I. V. Kozhevnikov, E. V. Gusevskaya, Appl. Catal. A: Gen., 352 (2009) 188.

77. A. Alhanash, E. F. Kozhevnikova, I. V. Kozhevnikov, Appl. Catal. A: Gen., 378 (2010) 11.

78. J. Cejka, H. van Bekkum, A. Corma, F. Schueth, Introduction to Zeolite Molecular Sieves, Elsevier Science, Amsterdam, 2007.

79. B. Yilmaz and U. Müller, Top. Catal., 52 (2009) 888.

80. F. R. Ribeiro, F. Alvarez, C. Henriques, F. Lemos, J. M. Lopes, M. F. Ribeiro, J. Mol. Catal. A., 96 (1995) 245.

81. J. Weitkamp, Solid State Ionics, 131 (2000) 175.

82. D. W. Breck, Zeolite molecular sieves, J. Wiley and Sons, New York, 1974.

83. P. A. Jacobs, J. Martens, Stud. Surf. Sci. Catal., 58 (1991) 445.

84. V. R. Choudhary, D. B. Akolekar, J. Catal., 125 (1990) 143

85. B. Coq, J. Pardillos, F. Figueras, Appl. Catal., 62 (1990) 281.

86. B. Yilmaz, U. Muller, M. Feyen, H. Zhang, F.-S. Xiao, T. D. Baerdemaeker, B. Tijsebaert, P. Jacobs, D. De Vos, W. Zhang, X. Bao, H. Imai, T. Tatsumi, H. Gies, Chem. Comm., 48 (2012) 11549.

87. B. Yilmaz, U. Muller, B. Tijsebaert, D. D. Vos, B. Xie, F.S. Xiao, H. Gies, W. Zhang, X. Bao, H. Imai, T. Tatsumi, Chem. Comm., 47 (2011) 1812.

88. C. N. Satterfield, Heterogeneous Catalysis in Industrial Practice, Krieger, United States, 1996.

89. S. Kouva, J. Kanervo, F. Schüβler, R. Olindo, J. A. Lercher, Chem. Eng. Sci., 89 (2013) 40.

90. X. Lei, S. Jockusch, M. F. Ottaviani, N. J. Turro, Photobiol. Sci., 2 (2003) 1095.

91. B. C. Gates, Catalytic Chemistry, Wiley, Chichester, 1992.

92. H. V. Bekkum, E. M. Flanigen, P. A. Jacobs, J. C. Jansen, Introduction to Zeolite Science and Practice, 2nd ed., Elsevier, Amsterdam, 2001.

93. A. Corma, J. Catal., 216 (2003) 298.

94. C. H. Christensen, K. Johannsen, I. Schmidt, J. Am. Chem. Soc., 125 (2003) 13370.

95. Ali Alsalme, PhD Thesis, Department of Chemistry, University of Liverpool, UK, 2010.

96. P. Vazquez, L. Pizzio, C. Caceres, M. Blanco, H. Thomas, E. Alesso, L. Finkielsztein, B. Lantano, G. J. Aguirre, J. Mol. Catal. A: Chem., 161 (2000) 223.

97. S. Buchang, H. D. Burtron, J. Catal., 157 (1995) 359.

98. D. Haffad, A. Chambellan, J.C. Lavalley, J. Mol. Catal., A 168 (2001) 153.

99. W. Alharbi, E. Brown, E. F. Kozhevnikova., I.V Kozhevnikov, J. Catal. 319 (2014) 174.

100. S. Pariente, N. Tanchoux, F. Fajula, Green Chem., 11 (2009) 1256.

101. G. Guan, K. Kusakabe, N. Sakurai, K. Moriyama, Fuel, 88 (2009) 81.

102. Y. Zhang, M. A. Dube, D. D. McLean, M. Kates, Bioresour. Technol., 89 (2003) 1.

103. X. Zhang, M. Tu, M. G. Paice, Bioenergy Res., 4 (2011) 246.

104. C. Anton, H. Steinicke, Bioenergy-Chances and Limits, German Academy of Sciences Leopoldina, Halle (Saale), 2012.

105. A. K. Agarwal. Prog. Energ. Combust., 33 (2007) 233.

106. M. Zheng, M. C. Mulenga, G. T. Reader, M. Wang, D. S. K. Ting, J. Tjong, Fuel, 87 (2008) 714.

107. A. Sarin, R. Arora, N. P. Singh, R. Sarin, R. K. Malhotra , K. Kundu, Energ., 34 (2009) 2016.

108. G. Knothe, K. R. Steidley, Fuel, 84 (2005) 1059.

109. A. Corma, S. Iborra, A. Velty, Chem. Rev., 107 (2007) 2411.

110. C. Du, X. Zhao, D. Liu, C. S. K. Lin, K. Wilson, R. Luque, J. Clark, Handbook of Biofuels Production, Woodhead Publishing, Cambridge, 2016.

111. R. Bringué, J. Tejero, M. Iborra, J. F. Izquierdo, C. Fite, F. Cunill, Ind. Eng. Chem. Res., 46 (2007) 6865.
112. F. Cunill, J. Tejero, C. Fite, M. Iborra, J. F. Izquierdo, Ind. Eng. Chem. Res., 44 (2005) 318.
113. J. Tejero, C. Fite, M. Iborra, J. F. Izquierdo, R. Bringue, F. Cunill, Appl. Catal. A., 308 (2006) 223.
114. I. Hoek, T. A. Nijhuis, A. I. Stankiewicz, J. A. Moulijn, Appl. Catal. A., 266 (2004) 109.
115. S. Koujout, D. R. Brown, Catal. Lett., 98 (2004) 195.
116. Y. Fu, T. Hong, J. Chen, A. Auroux, J. Shen, Thermochim. Acta, 434 (2005) 22.
117. S. Jiang, Y. K. Hwang, S. H. Jhung, J. S. Chang, J. S. Hwang, T. X. Cai, Chem. Lett., 33 (2004) 1048.
118. S. D. Kim, S. C. Baek, Y. J. Lee, K. W. Jun, M. J. Kim, I. S. Yoo, Appl. Catal. A: Gen., 309 (2006) 139.
119. L. Vanoyea, M. L. Zanotaa, A. Desgranges, A. F. Reguillona, C. D. Bellefona, Appl. Catal. A: Gen., 394 (2011) 276.
120. D. N. Khandan, M. Kazemeini, M. Aghaziarati, Appl. Catal. A: Gen., 349 (2008) 6.
121. F. Raoof, M. Taghizadeh, A. Eliassi, F. Yaripour, Fuel, 87 (2008) 2967.
122. S. Wang, D. Mao, X. Guo, G. Wu, G. Lu, Catal. Comm., 10 (2009) 1367.
123. C. Arcoumanis, C. Bae, R. Crookes, E. Kinoshita, Fuel, 87 (2008) 1014.
124. S. Jiang, J. S. Hwang, T. Jin, T. Cai, W. Cho, Y. S. Baek, S. E. Park, Bull. Korean Chem. Soc., 25 (2004) 185.
125. Y. Fu, T. Hong, J. Chen, A. Auroux, J. Shen, Thermochim. Acta., 434 (2005) 22.
126. C. W. Seo, K. D. Jung, K. Y. Lee, K. S. Yoo, J. Ind. Eng. Chem., 15 (2009) 649.

127. M. Mollavali, F. Yaripour, F. S. Mohammadi, H. Atashi, Fuel Process. Technol., 90 (2009) 1093.
128. K. Lertjiamratn, P. Praserthdam, M. Arai, J. Panpranot, J. Appl. Catal. A., 378 (2010) 119.
129. R. T. Carr, M. Neurock, E. Iglesia, J. Catal., 278 (2011) 78.
130. P. G. Moses, J. K Nørskov, ACS Catal., 3 (2013) 735.
131. R. M. Ladera, J. L. G. Fierro, M. Ojeda, S. Rojas, J. Catal., 312 (2014) 195.
132. A. L. Jones, R. T. Carr, S. I. Zones, E. Iglesia, J. Catal., 312 (2014) 58.
133. J. C. Woodhouse, US patent, 2014408 (1935).
134. M. Xu, J. H. Lunsford, D. W. Goodman, Appl. Catal. A: Gen., 149 (1997) 289.
135. D. Liu, C. Yao, J. Zhang, D. Fang, D. Chen, Fuel, 90 (2011) 1738.
136. B. Sabour, M. H. Peyrovi, T. Hamoule, M. Rashidzadeh, J. Inst. Eng. Chem., 18 (2012) 986.
137. Y. Lee, J. M. Kim, J. W. Bae, C. Shin, K. Jun, Fuel, 88 (2009) 1915.
138. J. Zhenga, Q. Zenga, Y. Yia, Y. Wanga, J. Maa, B. Qinb, X. Zhangb, W. Sunb, R. Li, Catal. Today, 168 (2011) 124.
139. A. Ciftci, D. Varisli, K. C. Tokay, N. A. Sezgi, T. Dogu, Chem. Eng. J., 208 (2012) 85.
140. D. Varisli, K. C. Tokay, A. Ciftci, T. Dogu, G. Dogu, Turk. J. Chem., 33 (2009) 355.
141. I. Takahara, M. Saito, M. Inaba, K. Muruta, Catal. Lett., 105 (2005) 249.
142. H. Chiang, A. Bhan, J. Catal., 271 (2010) 251.
143. D. Varisil, T. Dogu, J. Dogu, Chem. Eng. Sci., 62 (2007) 5349.
144. L. Matachowski, M. Zimowska, D. Mucha, T. Machej, Appl. Catal. B: Environ., 124 (2012) 448.

# Chapter 2. Experimental

This chapter consists of three parts. The first part describes the preparation of heteropoly acid catalysts. The second part represents techniques used for characterization of these catalysts. The third part describes the experimental setup and the reaction procedure for methanol and ethanol dehydration in the gas phase.

## 2.1 Chemicals and solvents

Alcohols, other chemicals, and catalysts were purchased from Sigma-Aldrich and used as supplied without further purification. Cesium carbonate (99.9%), $H_3PW_{12}O_{40}$ (HPW) (>99.9%), $Nb_2O_5$ (>99.5%), $ZrO_2$ (>99.0%), $TiO_2$ (>98.0%), ammonia aqueous solution (30%), ethanol (99.9%), $ZrOCl_2.8H_2O$ (98.0%), silica Aerosil 300 ($S_{BET}$, 300 $m^2g^{-1}$) and $NbCl_5$ (99%) were utilized for preparation of catalysts. Bulk HPW, $H_4SiW_{12}O_{40}$ (HSiW) (99.9%), $H_3PMo_{12}O_{40}$ (HPMo) (99.9%) were used as commercial catalysts. Zeolites $NH_4^+$-ZSM-5 (Si/Al = 10, 17, 30, 43 and 120 as determined by ICP-AES analysis) were from Zeolyst International, and they were converted into the $H^+$ forms by air calcination at 500 $^oC$ for 6 h. Methanol (99.9%), ethanol (≥99.8%) and iso-propanol (99.0%) were used as reactants for the dehydration reaction.

## 2.2 Catalyst preparation

### 2.2.1 Preparation of cesium salts $Cs_xH_{3-x}PW_{12}O_{40}$

The cesium salts $Cs_nH_{3-n}PW_{12}O_{40}$ (n = 2.25, 2.5 and 3) were prepared according to the literature procedure.[1] $Cs_{2.5}H_{.5}PW_{12}O_{40}$ and $Cs_{2.25}H_{0.75}PW_{12}O_{40}$ were prepared by adding dropwise the required amount of an aqueous solution of cesium carbonate (0.47 M) to aqueous solution of $H_3PW_{12}O_{40}$ (0.75 M) at room temperature with stirring.

The precipitate obtained was aged in an aqueous slurry for 48 h at room temperature and dried in a rotary evaporator at 45 $^oC$/3 kPa and after that in an oven at 150 $^oC/10^{-3}$ kPa for 1.5 h. The preparation of $Cs_{2.5}PW_{12}O_{40}$ and $Cs_{2.25}PW_{12}O_{40}$ was carried out according to stoichiometric equations (2.1) and (2.2).

$$5\ Cs_2CO_3 + 4\ H_3PW_{12}O_{40} \rightarrow 4\ Cs_{2.5}H_{0.5}PW_{12}O_{40} + 5\ H_2O + 5\ CO_2 \quad \textbf{(2.1)}$$

$$9\ Cs_2CO_3 + 8\ H_3PW_{12}O_{40} \rightarrow 8\ Cs_{2.25}H_{0.75}PW_{12}O_{40} + 9\ H_2O + 9\ CO_2 \quad \textbf{(2.2)}$$

The neutral cesium salt $Cs_3PW_{12}O_{40}$ was prepared similarly using solutions of the same concentration as for $Cs_{2.5}PW$ and $Cs_{2.25}PW$ (equation 2.3).

$$3\ Cs_2CO_3 + 2\ H_3PW_{12}O_{40} \rightarrow 2\ Cs_3PW_{12}O_{40} + 3\ CO_2 + 3\ H_2O \quad \textbf{(2.3)}$$

The precipitate obtained was aged in the aqueous mixture for 48 h at room temperature and dried in a rotary evaporator at 45 °C/3 kPa and after that in an oven at 150 °C/0.1 kPa for 1.5 h.

The cesium salts $Cs_{2.5}PW$ and $Cs_{2.25}PW$ were then calcined for 90 minutes under vacuum at 150 °C. The $Cs_3PW_{12}O_{40}$ was calcined at 300 °C for 3 hours under air. The HPA catalysts prepared were ground and sieved to 45-180 μm particle size. BET and TGA were performed on the catalysts thus made.

### 2.2.2 Preparation of supported HPW catalysts

Preparation of catalysts and supports and catalyst characterisation techniques have been described elsewhere.[2, 3]

Catalyst supports P25 titania (anatase/rutile = 3:1), and Aerosil 300 silica were from Degussa. $ZrO_2$ and $Nb_2O_5$ oxides were prepared in the lab and are described in the following sections.

In general, supported HPA catalysts were prepared by wet impregnation of oxide supports with an aqueous HPA solution and calcined at 150 °C/ $10^{-3}$ kPa for 1.5 h under vacuum.

Supported 15 wt% HPW on $Nb_2O_5$, $ZrO_2$ and $TiO_2$ were prepared by wet impregnation. An aqueous solution of HPW (0.88 g) was mixed with 5 g of oxide support to form a slurry with a minimal amount of aqueous phase then the slurry was aged for 24 h with stirring at room temperature followed by drying in a rotary evaporator at 45 °C under vacuum (3 kPa). The catalysts were ground in a mortar. Finally, the catalysts were calcined at 150°C for 1.5 h under vacuum (0.1 kPa).[1]

Catalysts containing 5, 10, 15 and 20 wt% HPA (either $H_3PW_{12}O_{40}$ or $H_4SiW_{12}O_{40}$) on silica were prepared by stirring a suspension of Aerosil 300 silica in aqueous solution, containing a certain amount of heteropoly acids and left overnight at room temperature

for ageing followed by drying at 45 °C/3 kPa using a rotary evaporator. Finally, the catalyst was dried at 150 °C/0.1 kPa under vacuum for 1.5 h.[3-4]

### 2.2.3 Preparation of $Nb_2O_5$

$Nb_2O_5$ with a surface area of 183 $m^2/g$ was prepared as described in the literature.[5] $NbCl_5$ powder (12 g) was dissolved in 24 ml of ethanol and slowly added to 600 ml of 0.18 M $NH_3$ aqueous solution to afford a white precipitate of niobic acid $Nb_2O_5.nH_2O$. The hydrogel was aged with stirring overnight and then filtered through a Buchner funnel.

The white precipitate was washed with distilled water many times to remove chloride ions. The filtrate was tested for remaining $Cl^-$ by adding a small amount of $AgNO_3$ solution. In the presence of chloride ions, the filtrate turned turbid due to the formation of AgCl (equation 2.4).

$$AgNO_{3\,(aq)} + Cl^-_{\,(aq)} \rightarrow AgCl_{\,(s)} + NO_3^-_{\,(aq)} \qquad \textbf{(2.4)}$$

This test was carried out together with a blank test, where distilled water was used instead of the filtrate. The white precipitate was washed with distilled water until the filtrate was clear ($[Cl^-] < 10^{-8}$ mol/l in washings). Finally, the precipitate was dried in an oven at 100 °C for 24 hours then calcinated at 400 °C /3 h/air.[2, 6]

## 2.2.4 Preparation of $ZrO_2$

$$ZrOCl_2 + 2NH_4OH \rightarrow ZrO_2 + 2NH_4Cl + H_2O \quad \textbf{(2.5)}$$

Equation 2.5 describes the method of preparation $ZrO_2$. To an aqueous solution of 15 g (0.046 mol) of $ZrOCl_2.8H_2O$ (MW 322.2) in 200 ml of $H_2O$ was added dropwise ca. 10 ml of 30% aqueous ammonia using a burette at room temperature with intense stirring until a pH of 10 was reached (pH paper). A white precipitate of hydrous zirconium oxide was formed.[2, 6] The hydrogel formed was aged at room temperature overnight with stirring then filtered through a filter paper using a Buchner funnel and washed with distilled water until chloride free (test with 0.02 M $AgNO_3$). After that the oxide was dried in an oven at 110 °C for 24 h then calcined at 400 °C /3 h/air.[1]

## 2.2.5 Preparation of core-shell catalysts

The core-shell catalysts 15%HPW/$Cs_3PW_{12}O_{40}$ and 25%HPW/$Cs_3PW_{12}O_{40}$ were prepared by wet impregnation of $Cs_3PW_{12}O_{40}$ powder with the required amount of HPW aqueous solution, followed by drying in a rotary evaporator at 45 °C /3 kPa and after that in an oven at 150 °C/$10^{-3}$ kPa for 1.5 h. The $Cs_3PW_{12}O_{40}$ support was calcined at 300 °C under air for 3 h to harden its structure.[7]

## 2.3 Catalyst characterisation techniques

### 2.3.1 Surface area and porosity

Adsorption measurements have a wide range of applications, with the most significant being the measurement of catalyst surface area and porosity.

The activity of a catalyst is accurately expressed as the rate of reaction per unit area of the active surface, and this can be used as a basis to compare between different catalysts. Thus, catalysts with a high surface area are preferred for some reactions. The total surface areas of porous solids are much higher than the area of the external surface as a result of the contribution of the pore walls. Typically, heterogeneous catalysts have a specific surface area between 1 and 1000 $m^2/g$ while their external surface area is in the range of 0.01-10 $m^2/g$.[8-9]

The pores are divided into three classes according to their size: microspores (size < 2 nm), mesopores (2 nm < size < 50 nm) and macrospores (size > 50 nm).[10-11] It is known that the pores can have different kinds of shape: they can have a uniform shape across their entire length, ink-bottle shaped or funnel shaped. Also, pores can be closed, open at only one end (blind), or open at both ends (through). Each pore can also be isolated, or connected to other pores to form a porous network (**Figure 2.1**).

Morphological parameters are vital to understanding catalytic behaviour in the reaction atmosphere. Firstly, the catalytic process occurs on the surface of the catalyst; secondly, to reach the surface, the reactants must be distributed across the porous catalysts and the products have to leave the surfaces of the catalyst; thirdly, mass transfer occurs inside the particles, influenced by pore size (molecular diffusion in micropores, Knudsen diffusion in mesopores and bulk diffusion in macropores); finally, carbonaceous deposition can also cause deactivation phenomena for micro and mesoporous materials.[12-14]

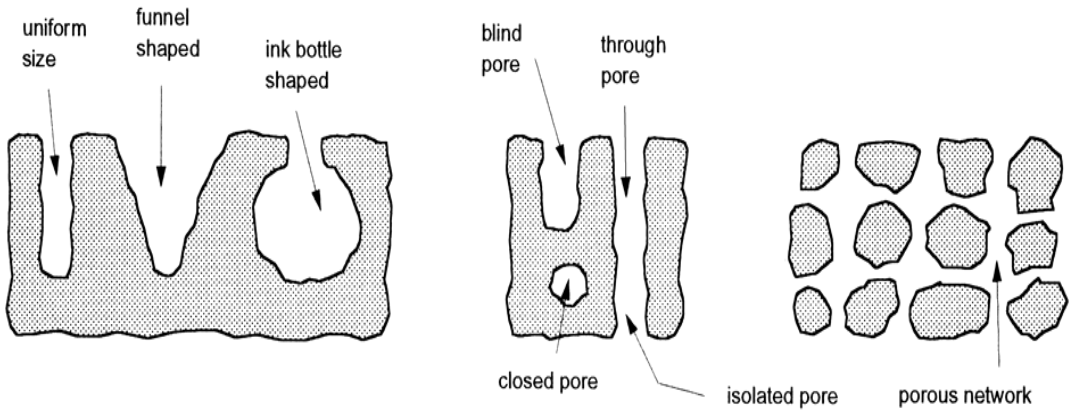


**Fig. 2.1.** Types and shapes of pores.[15]

The physical adsorption of inert gasses such as nitrogen is utilized to determine the surface area of catalysts.[16-19] The total surface area of catalysts is calculated using the Brunauer-Emmett-Teller (BET) equation, which was developed in 1938, based on the physical adsorption of inert gases, such as nitrogen. The BET isotherm is an extension of the Langmuir isotherm which takes into account multilayered adsorption.[20-21] The monolayer volume ($V_m$) and surface area are determined using equations (2.6) and (2.7), respectively. In equation 2.6: $P$ is the equilibrium pressure, $P_0$ is the saturation pressure, $C$ is a BET constant, $V$ is the volume of gas adsorbed at constant $P$ and $V_m$ is the volume of gas adsorbed corresponding to the monolayer.

$$\frac{P}{V(P_0 - P)} = \frac{1}{V_m C} + \frac{C-1}{V_m C} \times \frac{P}{P_0} \qquad (\mathbf{2.6})$$

$P/V(P_0 - P)$ is plotted versus $P/P_0$, and in the range of $P/P_0$ between 0.05 and 0.35, where a linear relationship exists, $V_m$, the volume of the monolayer, can be deduced from the gradient.

At low $P$, i.e., $P/P_0 < 0.05$ adsorption is underestimated and at high P, i.e., $P/P_0 > 0.35$ the method overestimates adsorption due to multilayer adsorption.[22] Consequently, the value of $V_m$ can be calculated, which is then converted to the surface area (S) using equation 2.7:

$$S = V_{\mathrm{m}} \times \frac{N_{\mathrm{A}}}{V_{\mathrm{A}}} \times A \qquad (\mathbf{2.7})$$

Here $A$ is the cross-sectional area of the nitrogen molecule (0.162 $nm^2$), $N_A$ is the Avogadro number (6.022 $\times 10^{23}$ $mol^{-1}$), and $V_A$ is the molar volume of $N_2$ (22.4 L/mol at standard conditions). The specific surface area is calculated by dividing the area obtained by the weight of the catalyst used in the measurement.

The main disadvantage of using the Brunauer-Emmett-Teller (BET) method appears in the case of microporous catalysts as the monolayer volume calculated by BET equation corresponds to the micropores volume added to the monolayer volume on the external surface of microporous solids.[23-24]

In 1965, the t-plot method was developed by de Boer and coworkers. It can be used to determine the total surface area and volume of microporous materials. However, the total surface area cannot be measured in ultra-microporous materials (pore size < 0.7 nm) such as zeolites. The small ratio of pore size/adsorbate molecular size and the strong interaction of adsorbate with pore wall makes the adsorption very different from that given on open surfaces.

Kripton and Argon adsorption at 77 K can be applied to determine low surface areas ($< 1\ m^2\ g^{-1}$).[25-26]

Our experiments were conducted on a Micromeritics ASAP 2010 adsorption apparatus. Typically, 0.10 - 0.15 g sample was packed into the sample tube and degassed at 250 °C for 4-6 h to reach a vacuum of $10^{-3}$ Torr. After outgassing, the sample was allowed to cool to room temperature, and the tube was then immersed in liquid nitrogen. Finally, the gas pressure was allowed to reach equilibrium before subsequent dosing, and then a series of 55 successive nitrogen doses were applied to obtain an adsorption isotherm. At the end of the analysis, the sample was weighed, and this weight was used for calculation of surface area and pore volume.

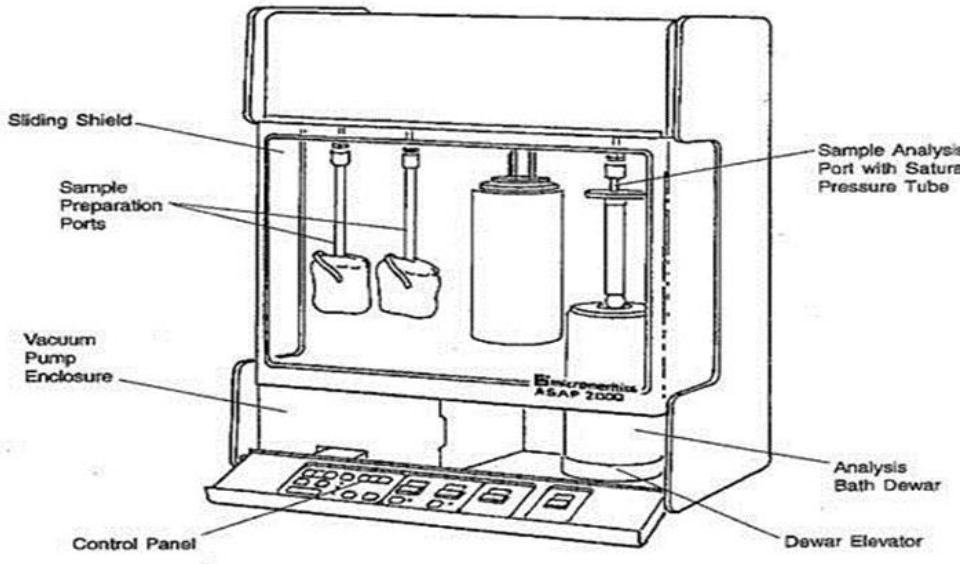


**Fig. 2.2.** The Micromeritics ASAP 2010 instrument.[27]

### 2.3.2 Thermogravimetric analysis (TGA)

The TGA technique is used to measure the change in the weight of a substance as the temperature rises. The change of the weight of the sample may occur due to a physical change or chemical reactions, for example, loss of water or other volatile materials. The TGA is utilized to rank materials in order of their thermal stability by comparing their loss of weight versus temperature. Other TGA applications include the determination of moisture and coke percentage as well as the oxidation temperature of samples.[28]

Balance with a programmed furnace is the basic instrumental requirement for TGA analysis, and the results are recorded as the thermogravimetric curve. **Figure 2.3** shows the schematic diagram of a TGA apparatus. Typical TGA curves display the changes in sample weight as a function of temperature or time. **Figure 2.4** shows a typical thermogravimetric curve for $H_3PW_{12}O_{40}$.

In this study, a Perkin Elmer TGA 7 instrument was used to determine the water content in materials applied in catalyst synthesis. The technique was also employed to evaluate the thermal stability of the catalysts under study.

1. Standard quartz hang down wire link.
2. Platinum hangdown wire kit.
3. Platinum stirrup kit.
4. Platinum sample pan kit.
5. Balance tare weight.
6. O-Ring.
7. Extension Tube.
8. Sample thermocouple.
9. Furnace tube
10. Flexible PTFE tubing.

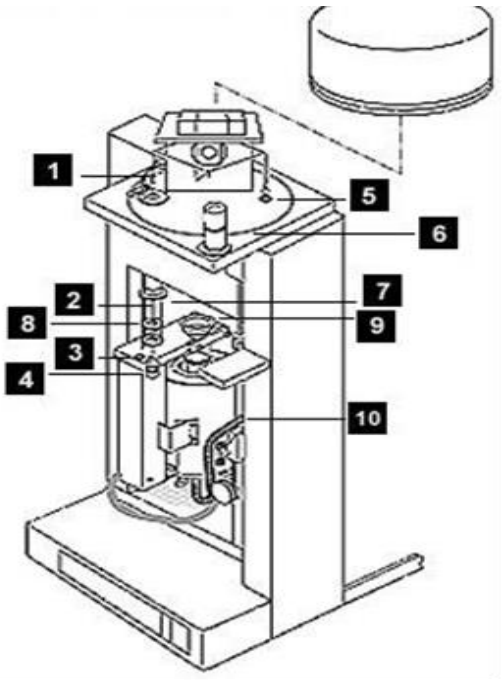


**Fig. 2.3.** Schematic diagram of A Perkin Elmer TGA 7 instrument.[29]

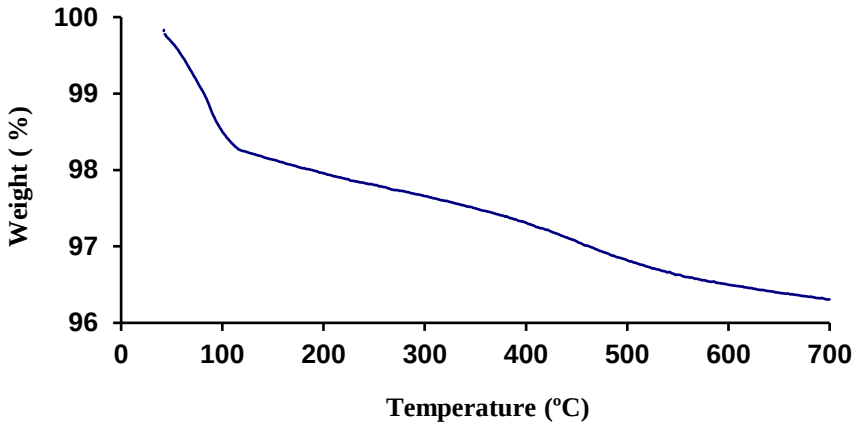


**Fig. 2.4.** TGA analysis for $H_3PW_{12}O_{40}$ after pretreatment under vacuum at 150 °C/0.5 Torr for 1.5 h.

### 2.3.3 C H N Analysis

Combustion analysis is a valuable tool for the determination of C, N and H content in catalyst samples.[30] The catalytic activity can be reduced when coke deposits on its surface.[31] Carbon and hydrogen analysis was applied in this study to measure the C and H content in spent catalysts and performed by Mr. S. G. Apter on a Thermo Flash EA 1112 series analyzer at ~2000 ºC.

### 2.3.4 Inductively coupled plasma atomic emission spectroscopy (ICP-AES)

Inductively Coupled Plasma - Atomic Emission Spectrometry (ICP-AES) is an emission spectroscopy method that uses gases such as argon to form a plasma at high temperatures between 6000 and 8000 °C that is used for atomization and excitation of sample.[30]

The high temperature of argon plasma is capable of emitting energy from atoms. The fundamental principles of this procedure are that each element emits energy at wavelengths specific to its atomic character. Although each element emits energy at multiple wavelengths, in the ICP-AES technique, it is most common to select a single wavelength (or a very few) for a given element. The intensity of the energy emitted at the chosen wavelength is proportional to the amount (concentration) of that element in the sample being analyzed. Thus, by determining which wavelengths are emitted from a sample and by determining their intensities, the analyst can qualitatively and quantitatively find the elements from the given sample relative to a reference standard.[31] The ICP-AES instrument is shown in **Figure 2.5**.

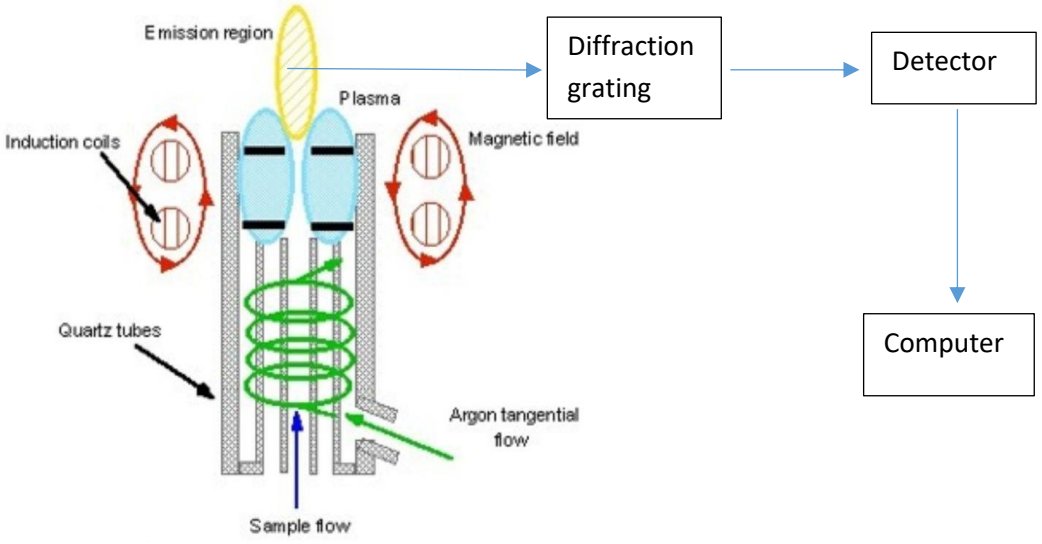


**Fig. 2.5**. The diagram of the basic design of the ICP-AES instrument.

In this work, ICP-AES was used to determine the ratio of Si/Al in zeolites $NH_4^+$-ZSM-5. Before analysis, a 50 mg sample of catalyst was dissolved in an appropriate solution. In this case, it was dissolved in 10 ml of 10% KOH and gently heated at 40 °C for some time. The solution then was diluted using distilled water in a standard flask and was submitted for analysis. ICP spectroscopy was carried out on a Spectro Ciros emission spectrometer available in the Department of Chemistry.

## 2.3.5 Fourier transform infrared spectroscopy (FTIR)

Infrared spectroscopy undoubtedly is one of the most important characterisation techniques in catalysis research. This method can be used for obtaining information about the structural framework of materials.[33-34] It can be applied for investigating the presence of Lewis (L) and Brønsted (B) active sites on the surface of catalysts. The L or B nature of acid sites can be determined by FTIR of adsorbed pyridine.[2, 35]

In Fourier transform, infrared spectroscopy, IR radiation provided from a laser source capable of covering the whole field of IR frequencies is passed through a sample. When infrared radiation reaches the surface of the sample, one or several processes can occur such as absorption, reflection from the surface, or it can enter the sample then be scattered.[36]

To improve the throughput of a spectrum, the sample with high absorption can be diluted with a diffusely scattering background such as KBr, which lowers absorption.

The diffuse reflectance technique (DRIFT) is mostly suitable for powders or fibres. The design employs flat reflectors and an alignment mirror which is utilized to focus diffusely scattered light (**Figure 2.6**).

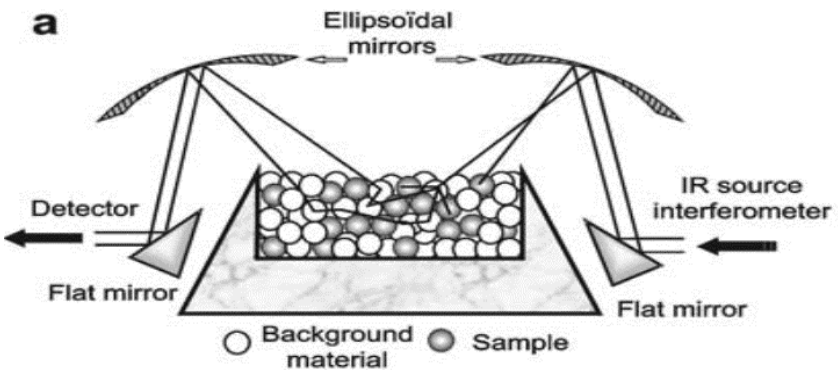


**Fig. 2.6.** Diagram of the diffuse reflectance infrared Fourier transform (DRIFT) accessory.[36]

In this study, diffuse reflectance infrared Fourier transform (DRIFT) spectroscopy was utilized to examine the state of bulk HPAs and supported HPW on $Nb_2O_5$, $ZrO_2$, $TiO_2$, $SiO_2$, as well as bulk salts $Cs_nH_{3-n}PW$, and core-shell catalysts HPW/$Cs_3PW$. Furthermore, it was also used to determine the nature of acid sites (Brønsted and Lewis) by adsorption of pyridine.

The structural framework of HPAs was also investigated by DRIFT spectroscopy. The samples were prepared by drying a small amount of catalyst at 150 °C / 0.01 kPa for 1 h under vacuum. After that 0.005 g of the catalyst was diluted with 0.045 g of dried KBr powder (10 wt%) and ground thoroughly to create a diffusely scattering matrix that lowers absorption and hence increases the throughput of the beam, enhancing the resolution for analysis. The region between 1200 $cm^{-1}$ to 500 $cm^{-1}$ gives information on the primary structure of the heteropoly compounds.[36]

DRIFT spectra of adsorbed pyridine were obtained for HPW on $Nb_2O_5$, $ZrO_2$, $TiO_2$, and $SiO_2$ catalysts. Catalyst samples were mixed with KBr powder 1:9 w/w. In order to remove physisorption water, samples were pretreated under vacuum at 150 °C/0.01 kPa for 1 h, followed by cooling at room temperature under $N_2$. After that, a small amount of pyridine (0.1 ml) was dropped onto samples and was left for 1 h. The samples with pyridine were then degassed under vacuum at 150 °C for 1 h with the purpose of removing the physisorbed pyridine and then analysed. The regions of 1540 $cm^{-1}$ and 1450 $cm^{-1}$ were reported for the Brønsted and Lewis acid sites, respectively.[37]

The measurements were performed using a Nicolet Nexus FTIR-Raman spectrometer at room temperature under $N_2$ atmosphere to prevent interference by the gaseous environment in the chamber. The spectra were taken in the region between 4000 and 400 $cm^{-1}$.

### 2.3.6 Powder X-ray diffraction (XRD)

X-rays were discovered in 1895, allowing scientists to investigate crystalline materials and to identify their structure, since each crystalline solid has its unique characteristics.[38] X-rays with a wavelength of the order of $10^{-10}$ m (1 Å) are required to probe atomic distances since their wavelength is comparable to the size of atoms.[39] The X-rays can pass through a sample and provide information on the structural arrangement.

When X-ray photons interact with electrons, some photons from the incident beam will be reflected with the angle of this reflected wave being equal to the angle of the incident wave. The directions in which X-rays are scattered depend on several factors, as expressed in Bragg's law (**equation 2.8**). The Bragg's law applies when constructive interference occurs from X-rays scattered by parallel planes of atoms which give diffraction peak.

$$n\lambda = 2d\sin\theta \qquad (\mathbf{2.8})$$

Here $\lambda$ is the incident X-ray wavelength, $n$ is an integer value (the order of the reflection), $d$ is the lattice spacing between layers of atoms, and $\theta$ is the angle between the incident rays and the surface of the crystal. Constructive interference occurs when the path length difference between incident and reflected beams of two rays is similar to the wavelength of one monochromatic beam which is created by X-ray source by bombarding a metal with high energy electrons and then collimating the beam into one wavelength as shown in **Figure 2.7**.

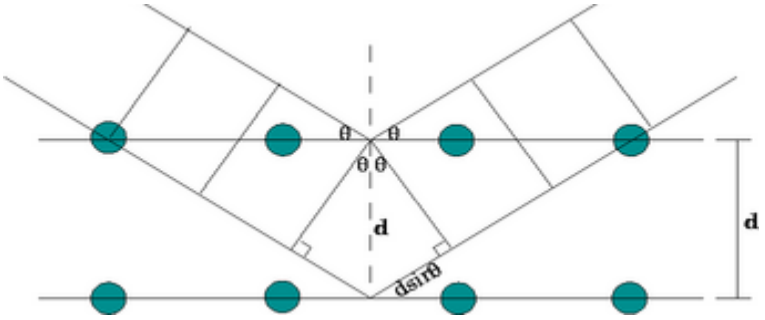


**Fig. 2.7**. Diagram of Bragg's Law reflection.[40]

Powder X-ray diffraction (XRD) spectra of catalysts were recorded on a PANalytical Xpert diffractometer which was equipped with a Ge monochromator giving monochromatic CuKα radiation ($\lambda$ = 1.542 Å). Typically, the powdered sample was placed on a sample holder and exposed to X-ray radiation at room temperature. The pattern was recorded in the range of $2\theta$ between $10^{o}$ and $70^{o}$ and attributed using the JCPDS database.

## 2.3.7 Microcalorimetry

Differential heats of ammonia adsorption on the catalysts were measured by a pulse method in a gas flow system at 150 $^{o}$C. Flow adsorption microcalorimetry involves the use of a carrier gas passing continuously through the adsorption cell. In order to determine the amounts of gas adsorbed, flow calorimetry must be used in combination with another technique such as TGA, MS, GC, etc.[41-42]

In our microcalorimetry set-up, a Setaram C80 Calvet calorimeter was fitted with a Metrohm DMS Titrino 716 titrator to determine the amount of unabsorbed ammonia (**Figure 2.8**).

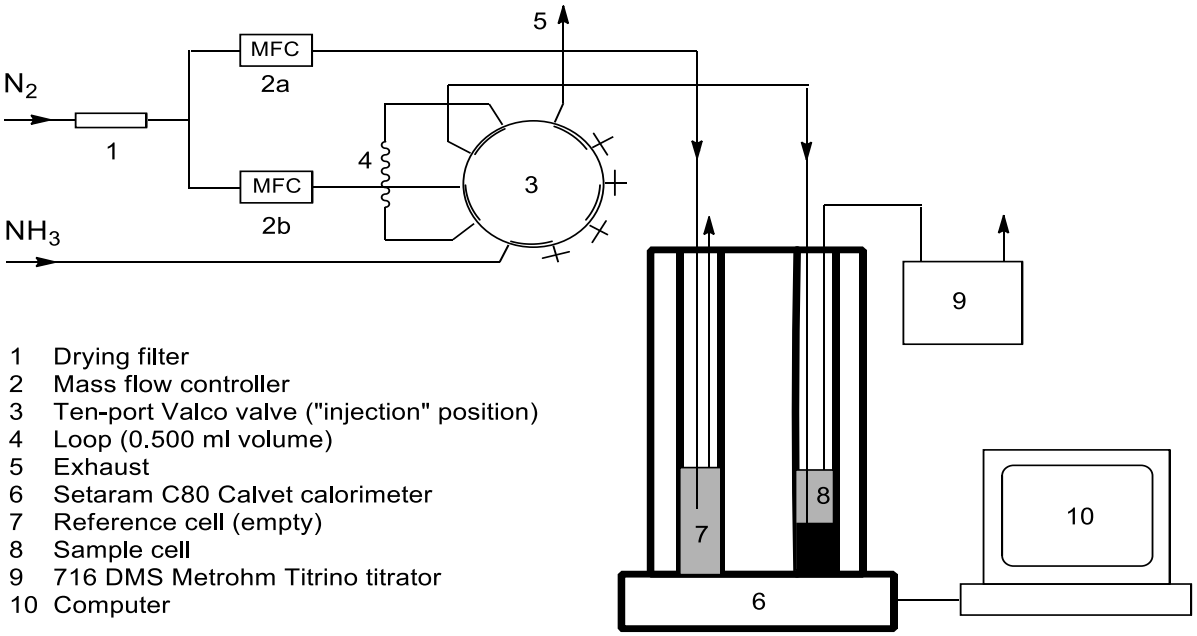


**Fig. 2.8.** Adsorption microcalorimetry set-up.

The catalyst sample (0.5-1 g) was placed in a stainless steel percolation cell of 2.8 $cm^3$ volume which was set in the sample compartment of the C80 calorimeter and pre-treated in situ at 150 $^oC$ in a dry nitrogen flow (20 mL $min^{-1}$) for 1.5 h. After temperature and heat flux stabilisation, the measurement of adsorption heat was performed by successive pulses of gaseous ammonia (0.5 mL, 0.02 mmol) into the $N_2$ flow using a stainless steel loop fitted in a 10 port Valco valve.

Sufficient time (~30 min) was allowed after each pulse for adsorption equilibrium to be established. The precise amount of ammonia in the pulse was determined by titration with sulfamic acid (see below) in a blank test. The downstream gas flow after the sample cell was passed through the titration vessel (50 mL) containing an aqueous buffer solution made of 1 M $NH_4Cl$ (15 mL) and saturated boric acid (1 mL) to absorb any ammonia broken through the catalyst sample. This ammonia was titrated with an aqueous solution of 0.01 M sulfamic acid using a Metrohm combined pH glass electrode with an end point

set at pH 5.0, as described elsewhere.[43] The amount of ammonia adsorbed was determined as the difference between the amount of ammonia supplied in the pulse and the amount of ammonia broken through the sample cell.

From these results, the differential enthalpies of ammonia adsorption per mole of ammonia adsorbed were obtained. Extrapolation of these values to zero ammonia uptake gave the initial enthalpy of ammonia adsorption, $\Delta H_{NH3}$. Typically, in the first 4-5 pulses, the entire ammonia supplied was adsorbed on the catalyst sample, without any ammonia breakthrough observed. This allowed accurate determination of the $\Delta H_{NH3}$ values without the need of ammonia titration. The mean absolute error in $\Delta H_{NH3}$ was found to be ±3 kJ $mol^{-1}$.

## 2.4 Catalyst testing

### 2.4.1 Product analysis

Gas chromatography was used for product separation and quantitative analysis of the gas-phase catalytic reactions.

#### 2.4.1.1 Gas chromatography (GC)

Gas chromatography (GC) is widely used in research and industry for product separation and the quantitative analysis of the gas-phase and liquid-phase catalytic reactions.[30]

In GC, the volatilized sample is injected into a heated injector port and transported by the mobile phase, which is usually an inert carrier gas that serves to introduce it into a heated column.

The column has a stationary phase which is a microscopic layer of liquid on an inert solid support, inside glass or metal tubing, called a column. The most common means by which samples are injected into the column is a split/splitless injector (**Figure 2.9**) since little loading of the injected sample is required.

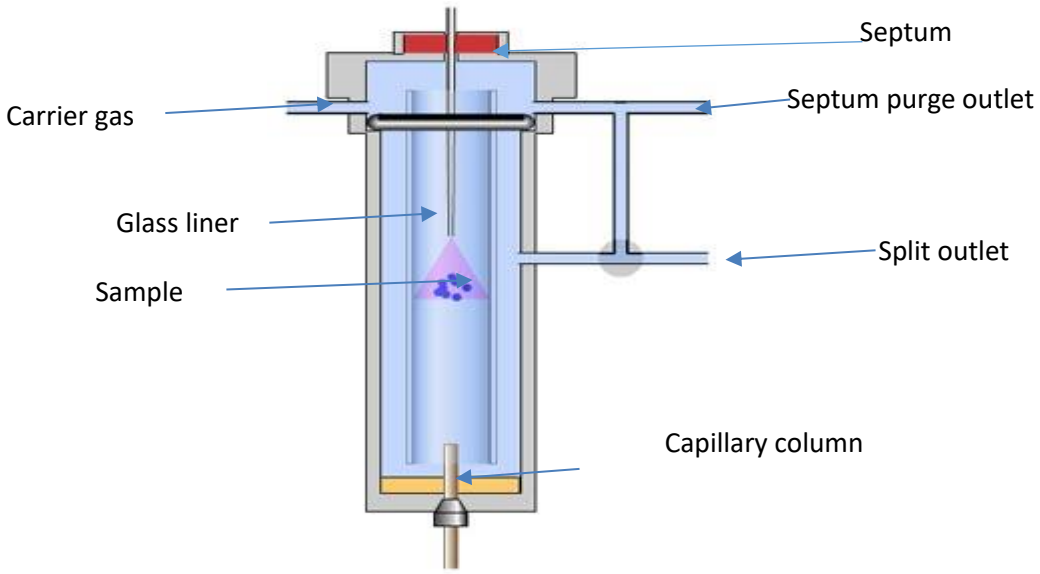


**Fig. 2.9.** Split-splitless vaporising injector.

The mixed gases of the sample are distributed between the carrier gas and the stationary phase of the column. The separated gases then elute from the GC column and interact with the detector. A flame ionisation detector (FID) is a commonly used detector that is sensitive to ionized molecules in a hydrogen-air flame, and that is particularly useful for analysing organic compounds.

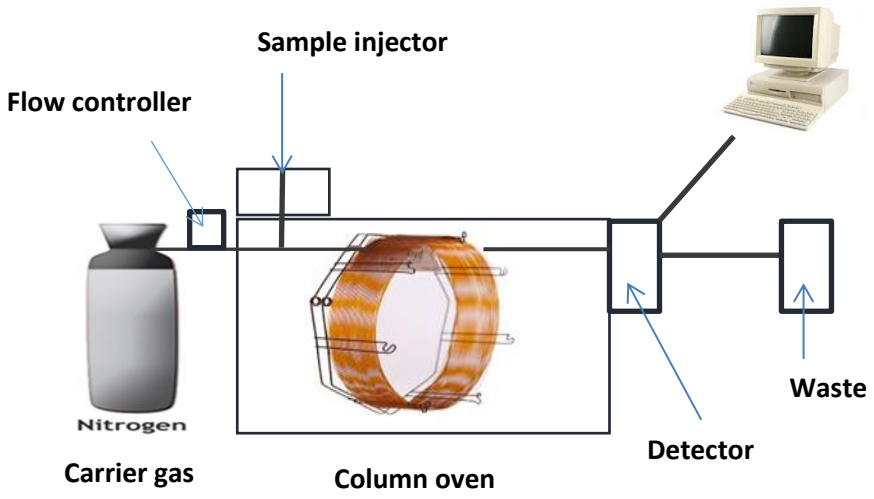


**Fig. 2.10.** Schematic representation of gas chromatograph.

### 2.4.1.2 Quantitative analysis of products

Analytical chemistry has a range of linear correlations and additivity schemes that have been proposed and used to interpret experimental data. For example, in gas chromatography (GC), the retention indices for a broad range of compounds can be estimated using an additivity scheme based on parameters such as the carbon number (CN) with functional group increments and column polarity. A method to predict gas chromatographic response factors for the trace-level analysis of volatile organic compounds based on the effective carbon number concept has been developed.[44-45]

In this work, the response of the commonly used set-up of GC with FID has been examined using the effective carbon number (ECN). The ECN for many compounds can be calculated from the heteroatoms and functional groups in the molecule and is used to obtain the relative molar response factor which can be calculated using equation (2.9) as proposed by Scanlon and Willis.[46]

$$F_{\text{molar}} = \frac{(\text{ECN of reference})}{(\text{ECN of compound})} \qquad (\mathbf{2.9})$$

The molecular weights, boiling points, retention times, effective carbon number (ECN), relative molar of response factor ($F_{\text{molar}}$) and response factor ($K$) for the compounds involved in the dehydration of methanol and ethanol are given in **Table 2.1**.

**Table 2.1**. *Molecular weights, boiling points, GC retention times and response factors for compounds involved in dehydration of methanol and ethanol.*

| **Compound** | **Molecular weight (g/mol)** | **Boiling point (°C)** | **Retention time (min)** | **Effective carbon number (ECN)** [47] | **Relative of molar response factor** | **Response factor (*K*)** |
|---|---|---|---|---|---|---|
| Methanol | 32 | 65 | 2.72 | 0.4 | 1.0 | 1.0 |
| Ethanol | 46 | 78 | 3.13 | 1.4 | 1.0 | 1.0 |
| Dimethyl ether | 46 | -24 | 1.17 | 1.0 | 2.5 | 0.4 |
| Diethyl ether | 74 | 35 | 1.30 | 3.0 | 2.1 | 0.4 |
| Ethylene | 28 | - 104 | 1.12 | 1.9 | 1.3 | 0.7 |
| Methane [a] | 16 | - 164 | 4.40 | 1.0 | 2.5 | 0.4 |
| Ethane [a] | 30 | - 89 | 4.70 | 2.0 | 5.0 | 0.2 |
| Propene [a] | 44 | -42 | 5.80 | 3.0 | 7.5 | 0.1 |

[a] Retention times using column B.

### 2.4.2 Fixed–bed reactor for catalyst testing

The dehydration of alcohols was carried out under atmospheric pressure in a Pyrex fixed-bed down flow reactor (9 mm internal diameter) fitted with on-line GC analysis (Varian Star 3400 CX instrument with a 30 m×0.32 mm×0.5 µm SUPELCOWAX 10 capillary column (column A) and a flame ionization detector) as shown in **Figure 2.11**. For a more accurate analysis of $C_1$-$C_3$ hydrocarbon products, a 60 m x 0.32 mm GSGasPro capillary column (column B) was used, which allowed for the full separation of these hydrocarbons. The temperature in the reactor was controlled by a Eurotherm controller using a thermocouple placed at the top of the catalyst bed.

The gas feed containing alcohol vapor in nitrogen was obtained by passing nitrogen flow controlled by a Brooks mass flow controller through a saturator, which held liquid alcohols at a controlled temperature (±1$^{o}$C) to maintain the chosen alcohols partial pressure (**Table 2.2**).

Before reaction, the catalysts were pretreated in situ at the reaction temperature for 1 h under $N_2$ flow. At regular time intervals, the downstream gas flow was analyzed by the on-line GC to obtain alcohol conversion and product selectivity. The selectivity was defined as the percentage of alcohol converted into a particular product taking into account reaction stoichiometry.

**Table 2.2.** *The vapour partial pressure of alcohols at saturation temperatures used in experiments (calculated from reference book [47]).*

| **Reactant** | **Temperature (°C)** | **Partial vapour pressure (kPa)** |
|---|---|---|
| Methanol | 0 | 3.83 |
| | 25 | 16.7 |
| Ethanol | 0 | 1.48 |
| | 25 | 7.66 |
| Isopropanol | 0 | 0.95 |

The product yields ($Y_P$), total conversion ($X$) and the selectivity of a particular product ($S$) were calculated using equations (2.10), (2.11) and (2.12), respectively.

$$Y_P = \frac{(S_P \times K_P \times A)}{S_r + (\sum S_P \times K_P \times A)} \times 100 \qquad (\mathbf{2.10})$$

$$X = \sum Y_P \qquad (\mathbf{2.11})$$

$$S = \frac{Y_P}{X} \times 100 \qquad (\mathbf{2.12})$$

In equation (2.10), $S_r$ is the peak area of the unreacted substrate; $S_p$ is the peak area of the product, $K_p$ is the response factor of the product relative to the substrate, $A$ is the stoichiometry factor of the product relative to the substrate. For example, for ethylene and ether product in dehydration of ethanol, stoichiometry factor $A$ = 1 and 2, respectively.

Carbon balance was estimated as the percentage of the reacted carbon atoms found in organic products. Typically, it was close to 100% within ±5% experimental error. Non-analysed gaseous by-products and coke deposited on the catalyst had little effect on the carbon balance and were neglected unless stated otherwise.

The activation energy ($E_a$) for methanol and ethanol dehydration was measured using 0.2 g catalyst samples under differential conditions (conversion less than 10%) where the reaction rate becomes approximately linearly proportional to the change in conversion. Therefore, the activation energy can be calculated directly from the incremental change in conversion. The activation energy was calculated using the Arrhenius equation (2.13).

$$K = Ae^{-\frac{E_a}{RT}} \qquad (\mathbf{2.13})$$

Here $K$ is the reaction rate constant, $A$ is the pre-exponential factor, $E_a$ is the activation energy, $R$ is the gas constant, and $T$ is the absolute temperature. *A* plot of ln $K$ against $1/T$ gives a straight line, from which the activation energy can be determined.[47, 49]

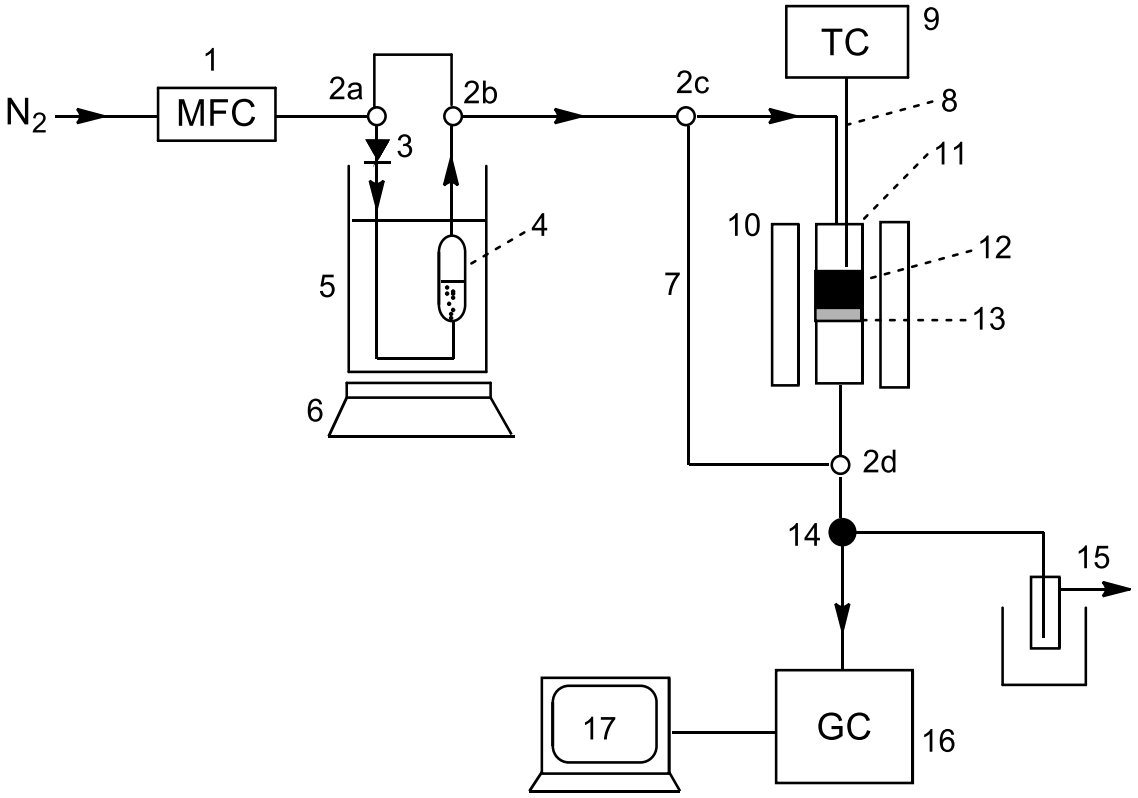


Key: (1) Brooks mass flow controller, (2) 3-way valve, (3) check valve (non-return), (4) saturator containing liquid substrate, (5) temperature controlled water bath, (6) stirring hotplate, (7) bypass, (8) thermocouple, (9) Eurotherm temperature controller, (10) furnace, (11) Pyrex tubular reactor, (12) catalyst bed, (13) glass wool support, (14) Valco multiposition sampling valve with air actuator, (15) product trap, (16) Varian gas chromatograph, (17) computer.

**Fig. 2.11.** Continuous flow fixed-bed reactor set-up for alcohol dehydration in the gas phase.

The conditions of the GC analysis are shown in **Figure 2.12-2.13**. Typical GC traces for the dehydration of methanol and ethanol are shown in **Figure 2.14-2.15**, respectively. GC chromatogram for light hydrocarbons from dehydration of methanol is shown in **Figure 2.16.**

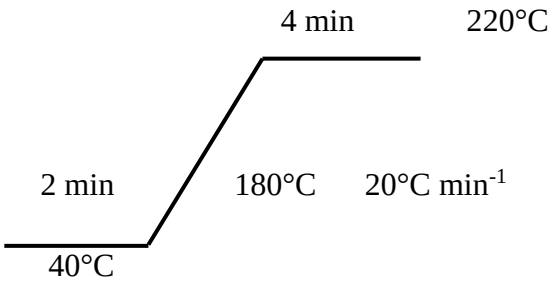


**Fig. 2.12.** Temperature programme (column A) used for methanol and ethanol dehydration in gas phase.

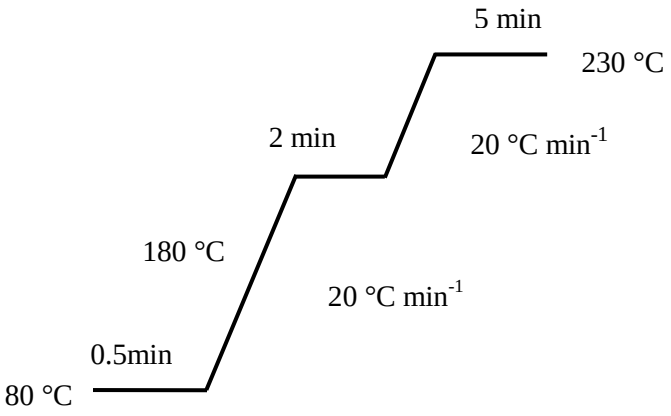


**Fig 2.13.** Temperature programme (column B) of GC analysis for all reactions tested.

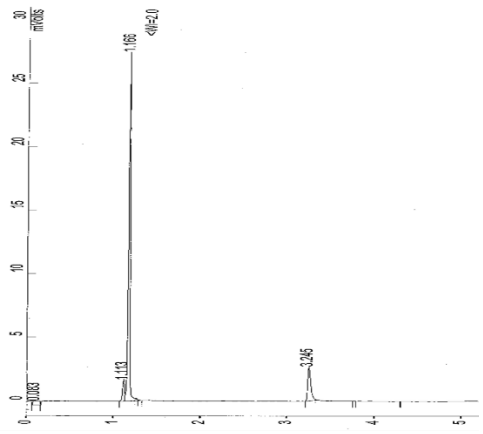


**Fig. 2.14.** GC trace using column A for the gas phase dehydration of methanol over 20%HSiW/$SiO_2$ at 250ºC showing two product peaks (1.11 and 1.16 min for light hydrocarbons and dimethyl ether, respectively) and the unreacted methanol peak (3.24 min).

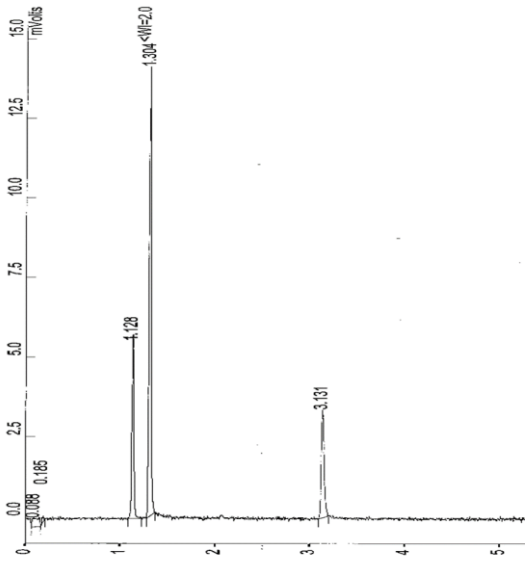


**Fig. 2.15.** GC trace using column A for the gas phase dehydration of ethanol over 20 % HSiW/$SiO_2$ at 120 ºC showing 2 product peaks (1.12 and 1.30 min for ethene and diethyl ether, respectively) and the unreacted substrate peak (3.13 min).

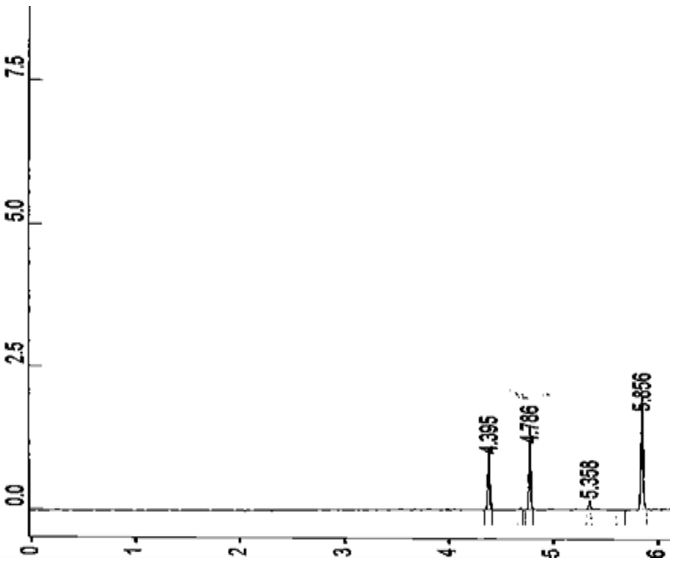


**Fig. 2.16.** GC trace using column B for the gas phase dehydration of methanol over 20%HSiW/$SiO_2$ at 250 $^oC$ showing light product peaks (4.39, 4.78 and 5.85 min for methane, ethane, and propane, respectively).

GC traces for the dehydration of isopropanol and 4-methyl-2-pentanol are given in **Figure 2.17-2.18**, respectively.

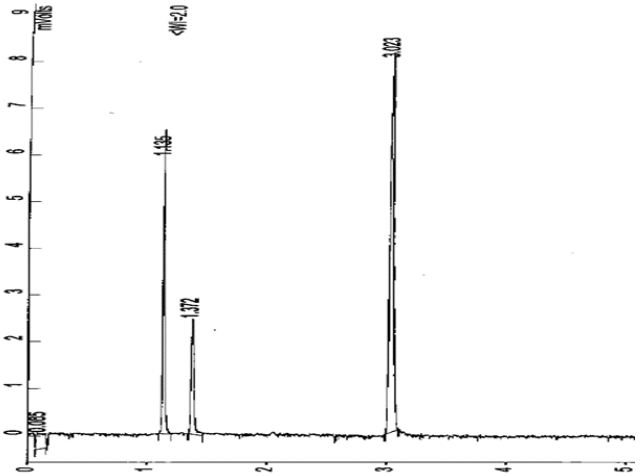


**Fig. 2.17.** GC trace using column A for the gas phase dehydration of isopropanol over $Cs_{2.25}H_{0.75}PW_{12}O_{40}$ showing the 2 product peaks (1.13 and 1.37 min for propene and di-isopropyl ether, respectively) and the unreacted isopropanol peak (3.02 min).

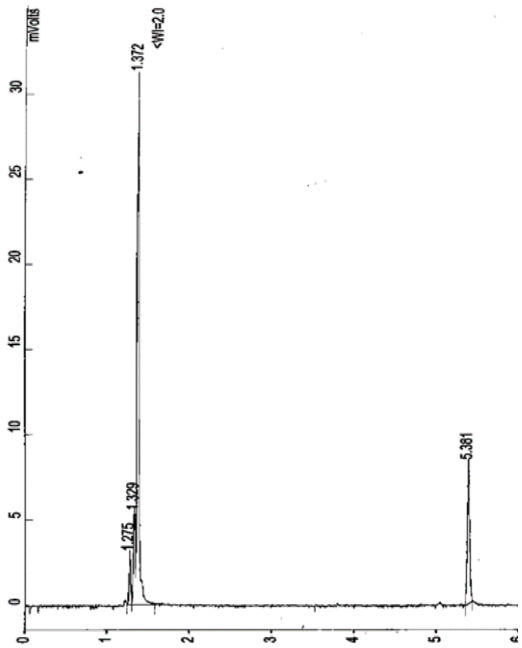


**Fig. 2.18.** GC trace using column A for the gas phase dehydration of 4-methyl-2-pentanol over $Cs_{2.5}H_{0.5}PW_{12}O_{40}$ showing minor and major product peaks (minor products at 1.27 and 1.32 min, major at 1.37 min for alkene isomers) and the unreacted 4-methyl-2-pentanol peak (5.38 min).

## 2.5 References


1. Y. Izumi, M. Ono, M. Kitagawa, M. Yoshida, K. Urabe, Micropor. Mater, 5 (1995) 255.
2. A. M. Alsalme, P. V. Wiper, Y. Z. Khimyak, E. F. Kozhevnikova, I. V. Kozhevnikov, J. Catal., 276 (2010) 181.
3. G. C. Bond, S. J. Frodsham, P. Jubb, E. F. Kozhevnikova, I. V. Kozhevnikov, J. Catal., 293 (2012) 158.
4. Y. Lim, R. S. Drago, M. W. Babich, N. Wong, P. E. Doan, J. Am. Chem. Soc., 109 (1987) 169.
5. N. Uekawa, T. Kudo, F. Mori, Y. J. Wu, K. Kakegawa, J. Colloid Interface Sci., 264 (2003) 378.
6. T. L. Stuchinskaya, M. Musawir, E. F. Kozhevnikova, I. V. Kozhevnikov, J. Catal., 231 (2005) 41.
7. L. Matachowski, A. Drelinkiewicz, D. Mucha, J. Krys´ciak-Czerwenka, R. Rachwalik, Appl. Catal., A 469 (2014) 239.
8. A. Zieba, L. Matachowski, E. Lalik, A. Drelinkiewicz, Catal. Lett., 127 (2009) 183.
9. L. Matachowski, A. Zieba, M. Zembala, A. Drelinkiewicz, Catal. Lett., 133 (2009) 49.
10. K. Kaneko, J. Membr. Sci., 96 (1994) 59.
11. K. W. Sing, F. Rodrguez-Reinoso et al. (Eds.), Characterization of Porous Solids II, Elsevier, Amsterdam, 1991.
12. K. K. Unger, J. Roquerol, K. S. W. Sing, H. Kral (Eds.), Characterization of Porous Solids, Elsevier, Amsterdam, 1988.

13. J. Roquerol, F. Rodriguez-Reinoso, K. S. W. Sing, K. K. Unger (Eds.), Characterization of Porous Solids III, Elsevier, Amsterdam, 1994.
14. J. T. Richardson, Principles of Catalyst Development, Plenum Press, New York, 1989.
15. G. Leofanti, M. Padovan, G. Tozzola, B. Venturelli, Catal. Today, 41 (1998) 207.
16. G. C. Bond, Heterogeneous Catalysis, 2nd ed., Oxford University Press, Oxford, 1987.
17. J. M. Thomas, W. J. Thomas, Principles and Practice of Heterogeneous Catalysis, VCH, Weinheim, 1997.
18. G. Attard, C. Barnes, Surfaces, Oxford University Press, Oxford, 1998.
19. M. Bowker, The Basis and Application of Heterogeneous Catalysis, Oxford University Press, Oxford, 1998.
20. S. Brunauer, P. H. Emmet, E. Teller, J. Am. Chem. Soc., 60 (1938) 309.
21. C. B. G. Attard, Surfaces, Oxford University Press, Oxford, 1998.
22. A. R. Katritzky, E. S. Ignatchenko, R. A. Barcock, V. S. Lobanov, M. Karelson, Anal. Chem., 66 (1994) 1799.
23. K. Kaneko, J. Membr. Sci., 96 (1994) 59.
24. S. J. Gregg, K. S. W. Sing, Adsorption, Surface Area and Porosity, Academic Press, London, 1982.
25. T. L. Hill, J. Chem. Phys., 14 (1946) 263.
26. D. M. Young, A. D. Crowell, Physical Adsorption of Gases, Butterworths, London, 1962.
27. R. Hetterley, PhD. Thesis, Department of Chemistry, University of Liverpool, UK, 2008.
28. P. Patnaik, Dean's Analytical Chemistry Handbook, 2nd ed., McGraw-Hill Education, New York, 2004.

29. https://www.perkinelmer.com.cn/Catalog/Family/ID/Standard%20Furnaces%20and%20Furnace%20Accessories%20for%20TGA%207 (accessed 10/08/2017).
30. J. Mendham, R. C. Denney, J. D. Barnes, M. J. K Thomas, Vogel's Textbook of Quantitative Chemical Analysis, Preston Education Ltd, United Kingdom, 2000.
31. E. Furimsky, Ind. Eng. Chem. Res. Ind. Eng. Chem. Prod. R.D., 18 (1979) 206.
32. M. Thompson, J. N. Walsh, Inductively Coupled Plasma Spectrometry, Blackie, Untied State of America, 1989.
33. L. M. Harwood, C. J. Moody, J. M. Percy, Experimental Organic Chemistry: Standard and Microscale, Blackwell Science, Oxford, 2001.
34. G. Schwedt, The Essential Guide to Analytical Chemistry, John Wiley & Sons, Chichester, England, 1997.
35. T. Pham, D. Shi, D. Resasco, Top. Catal., 57 (2014) 706.
36. E. Lichtfouse, J. Schwarzbauer, D. Robert, Environmental Chemistry Green Chemistry and Pollutants in Ecosystems, Springer, Berlin, 2005.
37. G. Seo, J. Lim, J. Kim, J. Catal., 114 (1988) 469.
38. P. W. Atkins, Physical Chemistry, Oxford University Press, Oxford, 1998.
39. P. Atkins, J. Paula, Atkins' Physical Chemistry, 7th ed., Oxford University Press, Oxford, 2002.
40. http://laser.physics.sunysb.edu/~czayas/report/index.html
41. A. Auroux, Catal. Today, 19 (2002) 205.
42. D. R. Brown, A. J. Groszek, Langmuir, 16 (2000) 4207.
43. G. T. Kerr, A. W. Chester, Thermochimica Acta, 3 (1971) 113.
44. J. E. Szulejko, Y. H. Kim, K. H. Kim, J. Sep. Sci., 36 (2013) 3356.
45. R. L. Grob, E. F. Barry, Modern Practice of Gas Chromatography, Wiley, Untied State of America, 2004.

46. C. Perego, S. Peratello, Catal. Today, 52 (1999) 133.

47. H. Purnama, T. Ressler, R.E. Jentoft, H. Soerijanto, R. Schlogl, R. Schomacker, Appl. Catal. A 259 (2004) 83.

48. D. R. Lide, Handbook of Chemistry and Physics, 84th ed., CRC Press, Boca Raton, 2003.

49. C. Perego, S. Peratello, Catal. Today, 52 (1999) 133.

# Chapter 3. Catalyst characterisation

This chapter concentrates mainly on the results of catalyst characterisation. This characterisation comprised the investigation of surface area and pore texture, elemental content, thermal stability, the state of heteropoly acids on the catalyst surface, crystallinity, and the nature and the strength of acid sites. To this end, various techniques were used, such as nitrogen adsorption, ICP-AES (inductively coupled plasma atomic emission spectroscopy), TGA (thermogravimetric analysis), XRD (X-ray diffraction), IR (infrared spectroscopy) and microcalorimetry.

## 3.1 Surface area and porosity

### 3.1.1 Introduction

The physical adsorption of nitrogen molecules at boiling temperature (77 K) was employed as a technique to determine the total surface area, pore volume and pore size distributions of the solid catalysts prepared in this study. A Micromeritics ASAP 2010 instrument was used to measure the surface area and to characterize the porous texture of the catalysts.

The first step in this method is to create the $N_2$ adsorption isotherm, which is found by plotting the amount of $N_2$ adsorbed against its relative pressure. The shape of the isotherm depends on the porous texture of individual solids. Solid materials can be classified into six isotherm types on the basis of their shapes according to the IUPAC classification.[1-2] **Figure 3.1** shows the four isotherm types commonly presented in catalyst characterisation. Types I, II, IV and VI isotherms correspond to microporous, macroporous, mesoporous and uniform ultramicroporous solids, respectively. Types I and IV isotherms are explained in more detail because of their relevance to the catalysts in this study.

The type IV isotherm occurs in mesoporous solids. At low relative pressures, an adsorption monolayer is formed, while at high relative pressures, a multilayer formation occurs until condensation takes place, giving a sharp increase in the observed volume of adsorbed gas.

With microporous solids (Type I), a strong interaction between the pore walls and adsorption gas takes place at very low relative pressures. A higher pressure is required to fill the pores completely. After the microporous have been filled, the adsorption continues on the external surface, as is the case with mesoporous. Zeolites are typical examples of microporous catalysts and are used for comparative purposes in this study.

When saturation of the adsorbate $N_2$ is reached, desorption is carried out in the opposite way to adsorption. With mesoporous solids, however, the desorption takes place at a pressure lower than that at which capillary condensation occurs, giving a hysteresis loop. **Figure 3.2** shows the four hysteresis shapes that have been classified by IUPAC.[3-5]

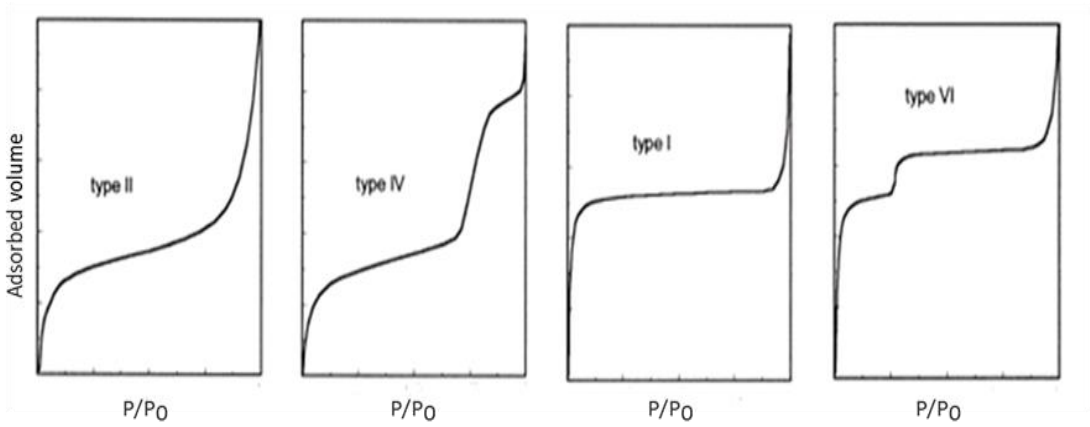


**Fig. 3.1.** The four types of adsorption isotherms found with $N_2$ adsorption.[4]

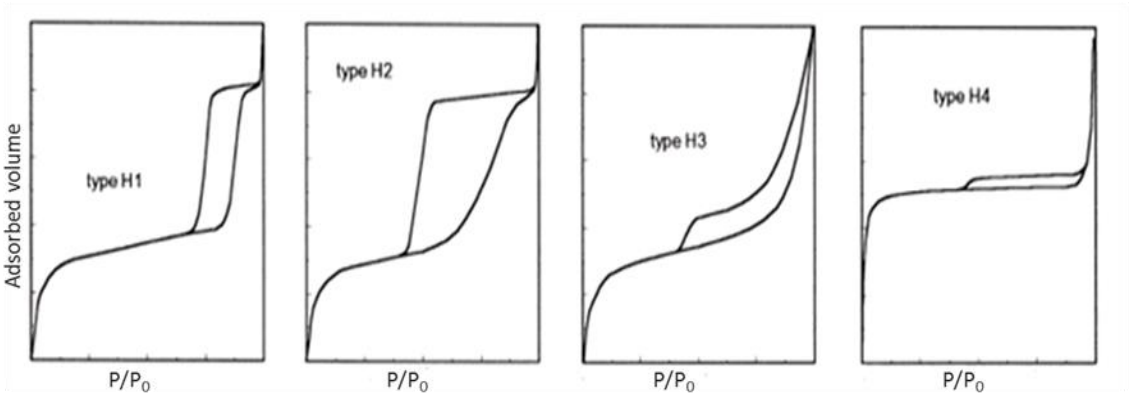


**Fig. 3.2.** The four hysteresis shapes usually observed with $N_2$ adsorption.[4]

Types H1 and H2 hysteresis are found when analysing solids consisting of particles crossed by channels close to cylindrical in shape, or made by aggregates or agglomerates that are spheroidal in shape. In more detail, H1 hysteresis is observed with solid samples that consist of pores with uniform size and shape, while H2 hysteresis is observed in samples that have pores of non-uniform size and shape. The causes of H1 and H2 hysteresis are a different size of the pore mouth and pore body (e.g. ink bottle-shaped pores) and/or a different behaviour in adsorption and desorption in near cylindrical pores. Most mesoporous catalysts display type H1 and H2 hysteresis adsorption isotherms.

Types H3 and H4 hysteresis isotherms are found in solid samples that consist of aggregates or agglomerates of particles forming slit-shaped pores (plates or edged particles similar to cubes), with non-uniform and uniform size and/or shape, respectively. The microporous materials such as zeolites and active carbon are good examples of these types of hysteresis isotherms. The absence of hysteresis indicates that the solids possess blind cylindrical, cone-shaped and/or wedge shaped pores. Since catalyst pores are usually irregular, however, only solids with a much reduced hysteresis loop will be observed.[4, 6]

The general procedure for the measurement of surface area and porosity was described in **Section 2.3.1.** The total surface area of the catalysts was calculated using the Brunauer-Emmett-Teller (BET) method. The pore size distribution and the total pore volumes were determined using the Barrett, Joyner, and Halenda (BJH) method.[7-8]

### 3.1.2 HPW-based catalysts

The texture (surface area, pore diameter, and pore volume) of bulk Keggin HPAs and supported HPW catalysts have been studied previously.[9-11]

The disadvantages of the lower surface area and the solubility of bulk Keggin HPAs in polar media can be avoided by placing HPAs on a support. The interaction between the protons of the HPA with hydroxyl groups on the surface of the support can occur by ligand exchange mechanisms or form surface complexes by coordination. **Figure 3.3** presents these two mechanisms.[12, 13]

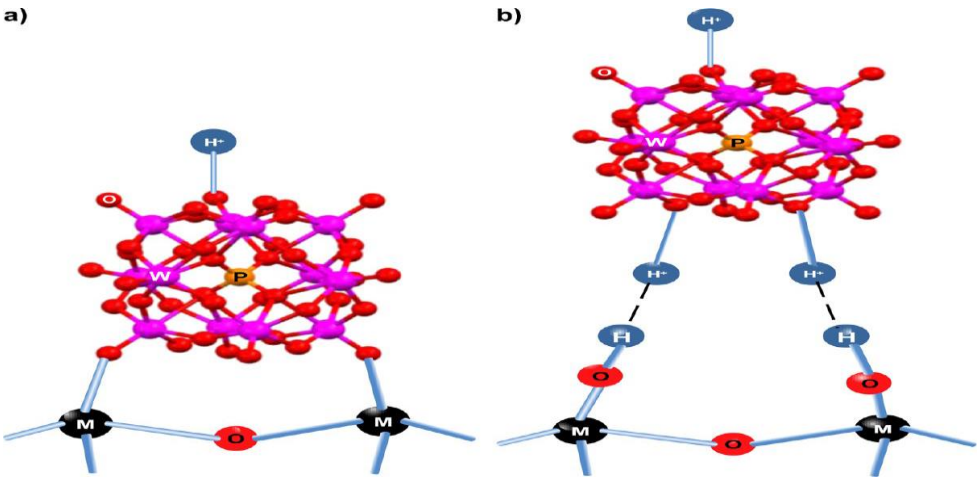


**Fig. 3.3.** Two types of interaction mechanism: (a) exchange mechanism, (b) coordination mechanism.[14]

The reaction between the surface hydroxyl groups (M−OH) and the HPA protons to produce water in the ligand exchange mechanism occurs as shown in equations 3.1 and equation 3.2.

$$M\text{-}OH_{(s)} + H^{+}{}_{(aq)} \rightarrow MOH_2{}^{+}{}_{(s)} \quad (3.1)$$

$$MOH_2{}^{+}{}_{(s)} + (HPA_n)^{-1}{}_{(aq)} \rightarrow M(HPA_n)_{(s)} + H_2O_{(l)} \quad (3.2)$$

Here, M and $MOH_{(s)}$ are a metal ion and surface hydroxyl, respectively, and $HPA_n$ is the heteropolyanion. A good example of this type of mechanism is when heteropoly anions interact with MgO. In this mechanism, however, heteropoly anions would be strongly adsorbed on the surface of the support, which could lead to a loss of HPA acidity and catalytic activity.[14-16]

Another mechanism involves coordination of protonated surface hydroxyl groups with the heteropolyanion to form a surface complex (equation 3.3); the acid strength of this complex depends on interaction of the bulk Keggin HPA with the support, as well as the cation present in the HPA.[14]

$$MOH_2{}^{+}{}_{(s)} + (HPA_n)^{-1}{}_{(aq)} \rightarrow MOH_2{}^{+}(HPA_n)^{-1}{}_{(s)} \quad (3.3)$$

The texture for HPW and HSiW catalysts as bulk, and supported on different oxide supports with sub-monolayer HPA loadings (5-20 wt%), is shown in **Table 3.1**. All the catalysts used here were mesoporous materials with average pore diameters of 22 – 230 Å. The texture of the bulk HPAs was in agreement with the literature.[17, 18]

**Table 3.1**. *Catalyst characterisation*

| **Catalysts** [a] | **$S_{BET}$**[b] **($m^2g^{-1}$)** | **Pore volume** [c] **($cm^3g^{-1}$)** | **Pore size** [d] **(Å)** |
|---|---|---|---|
| $Nb_2O_5$ | 183 | 0.15 | 33 |
| $ZrO_2$ | 145 | 0.10 | 26 |
| $TiO_2$ (P25 Degussa) | 44 | 0.10 | 90 |
| $SiO_2$ (Aerosil 300) | 300[e] | | |
| $H_3PW_{12}O_{40}$ | 2 | 0.04 | 81 |
| $H_4SiW_{12}O_{40}$ | 9 | 0.02 | 71 |
| $H_3PMo_{12}O_{40}$ | 12 | 0.02 | 32 |
| 15%HPW/$Nb_2O_5$ | 126 | 0.11 | 34 |
| 15%HPW/$ZrO_2$ | 120 | 0.07 | 24 |
| 15%HPW/$TiO_2$ | 45 | 0.20 | 174 |
| 5%HPW/$SiO_2$ | 235 | 0.86 | 146 |
| 10%HPW/$SiO_2$ | 237 | 1.02 | 173 |
| 15%HPW/$SiO_2$ | 202 | 1.00 | 169 |
| 20%HPW/$SiO_2$ | 213 | 0.81 | 152 |
| 5%HSiW/$SiO_2$ | 168 | 0.76 | 181 |
| 10%HSiW/$SiO_2$ | 244 | 1.16 | 191 |
| 15%HSiW/$SiO_2$ | 221 | 1.02 | 185 |
| 20%HSiW/$SiO_2$ | 200 | 0.90 | 180 |

[a] All HPA catalysts calcined at 150 °C under a vacuum for 1.5 h; in-house-made supports, $ZrO_2$ and $Nb_2O_5$, calcined at 400 °C in air for 5 h and $Cs_3PW_{12}O_{40}$ at 300 °C in air for 3 h. [b] BET surface area. [c] Single point total pore volume. [d] Average BET pore diameter. [e] Manufacturer's value

The pure oxides, $Nb_2O_5$ and $ZrO_2$, were prepared in order to obtain supported catalysts with a high surface area. Indeed, all HPA catalysts based on $Nb_2O_5$, $ZrO_2$, $TiO_2$ and $SiO_2$ possess relatively high surface areas.

For HPA catalysts supported on $Nb_2O_5$ and $ZrO_2$, the surface area was reduced. In contrast, the surface area of $TiO_2$ supported catalysts practically did not change. Regarding pore diameter, titania based catalysts possessed larger pores and zirconia based ones smaller pores, with niobia catalysts lying in between.

Supporting heteropoly acids on silica increases the total surface area of the catalyst up to 244 $m^2/g$ for 10% $HSiW/SiO_2$. As can be seen in **Table 3.1**, the total surface area per gram of the $HPW/SiO_2$ catalysts decreases with an increase of HPA loading (10-20 wt%), which is probably due to the decrease in the amount of silica.

The nitrogen adsorption-desorption isotherm for bulk HPAs is shown in **Figure 3.4**. The adsorption isotherms were a type II that is usually observed for nonporous materials.[3] This is in agreement with results reported by Misono *et al*.[19, 20]

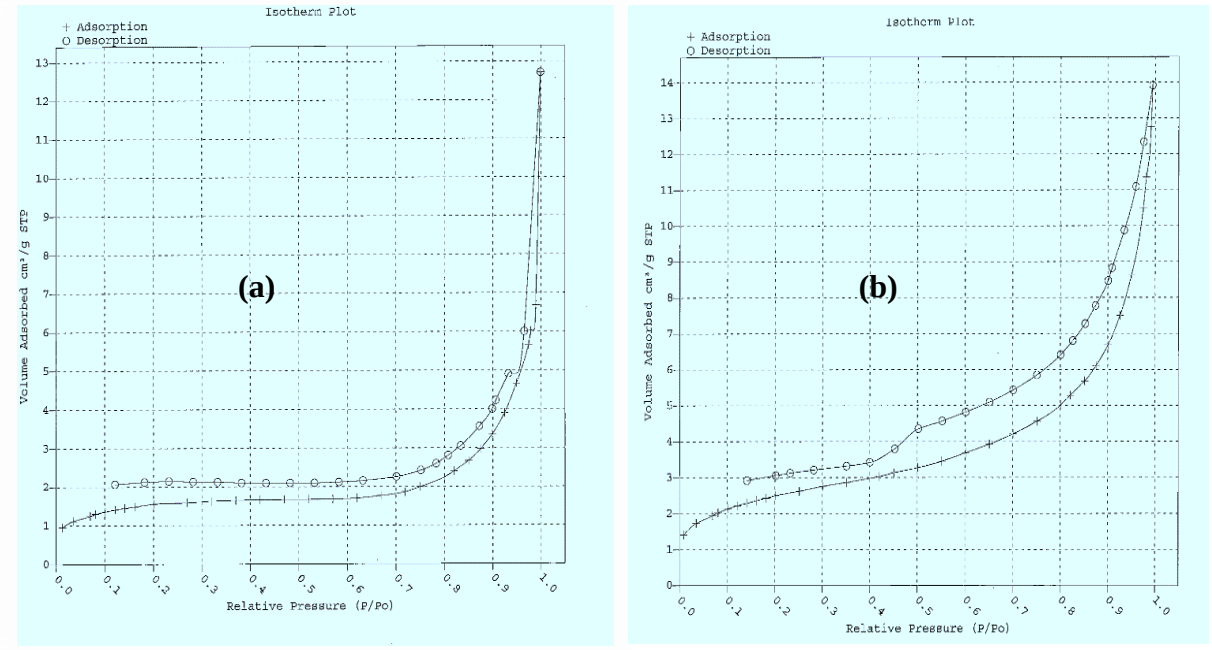


**Fig. 3.4.** $N_2$ adsorption-desorption on: (a) $H_3PW_{12}O_{40}$ and (b) $H_4SiW_{12}O_{40}$.

The adsorption-desorption isotherm for supported HPAs is shown in **Figure 3.5**. The adsorption isotherm of HPW supported on $Nb_2O_5$ shows a type IV characteristic of mesoporous materials, and this isotherm possesses a H2 type hysteresis loop: an indication of non-uniform sized and/or

shaped mesopores. The adsorption isotherm for 15%HPW/$ZrO_2$ possessing a large surface area presents as type I with an H3 hysteresis loop, indicating the presence of non-uniform micro/mesoporous structures.

**Figures 3.5 (c)** and **(d)** show the isotherm when HPW is supported on $TiO_2$ and $SiO_2$, respectively, showing type II isotherms in both cases with a hysteresis loop (type H3) indicating the presence of non-uniform size and/or shape mesopores. These results are in agreement with previous studies.[21-24]

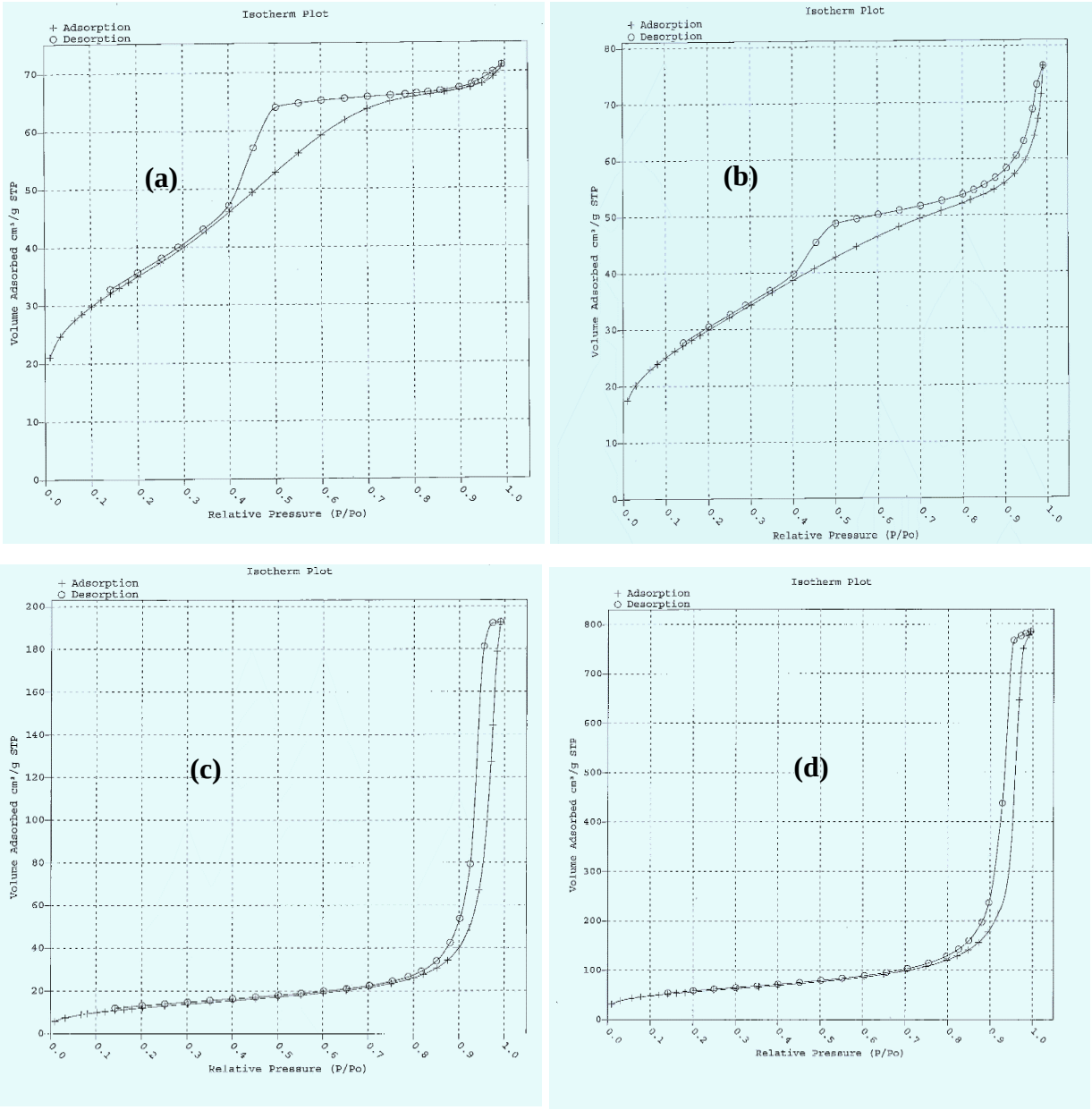


**Fig. 3.5.** $N_2$ adsorption isotherm for: (a)15%HPW/ $Nb_2O_5$, (b) 15%HPW/ $ZrO_2$, (c) 15%HPW/ $TiO_2$ and (d) 15%HPW/ $SiO_2$.

Another method of solving the problem of the lower surface area can be by exchanging the HPAs protons completely or partially with metal ions without affecting the primary structure (as described in **Section 1.3.3.3.1**). Salts of HPAs with large monovalent cations of $Cs^+$ have a rigid microporous/mesoporous structure and surface areas over 100 $m^2$ $g^{-1}$. These also possess high thermal stability and low solubility in polar solvents.[9, 25-27]

$Cs_xH_{3-x}PW_{12}O_{40}$ have been reported to have high surface areas, and these salts have been extensively studied using $^{31}P$ NMR, XRD, electron diffraction, atomic force microscopy (AFM) and scanning electron microscopy by Misono *et al*.[9]

CsPW possesses a bimodal distribution of pores with micropores ranging from 0.5-1 nm (peak at 0.65 nm and mostly > 0.75 nm), and mesopores (peak at 4-5 nm). It has been suggested that the micropores account for approximately 70% of the total surface area of CsPW and correspond to the spaces between the crystal planes.[9] The mesopores are formed from spaces between nanocrystallites (10-20 nm) and between aggregates in the region of 100-500 nm in size. **Figure 3.6** is a schematic representation of the bimodal pore size distribution in CsPW.

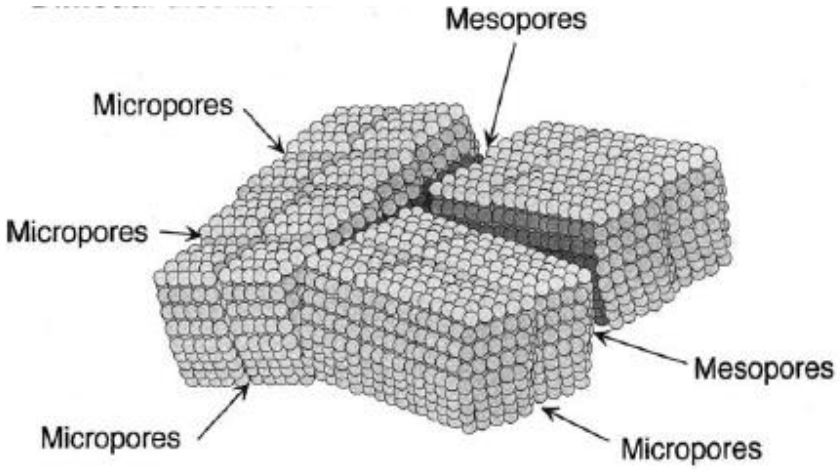


**Fig. 3.6** The bimodal pore size distribution in $Cs_{2.5}H_{0.5}PW_{12}O_{40}$.[28]

The BET isotherm and the pore size distribution for the CsPW used in our study is shown in **Figure 3.7**. A type IV $N_2$ adsorption isotherm is observed for CsPW, which is characteristic of mesoporous materials (2 nm < pore diameter < 50 nm). Also, a type H2 hysteresis loop is observed, indicating the presence of mesopores which are of non-uniform shape. In addition, the steep increase of the adsorption amount in the low pressure region observed for CsPW suggests the presence of micropores as well as mesopores. The pore size distribution of CsPW was derived from the desorption isotherm by the BJH (Barret-Joyner-Halenda) method. A sharp peak appeared at about 40 Å diameter. This result is in good agreement with other researchers.[19, 29]

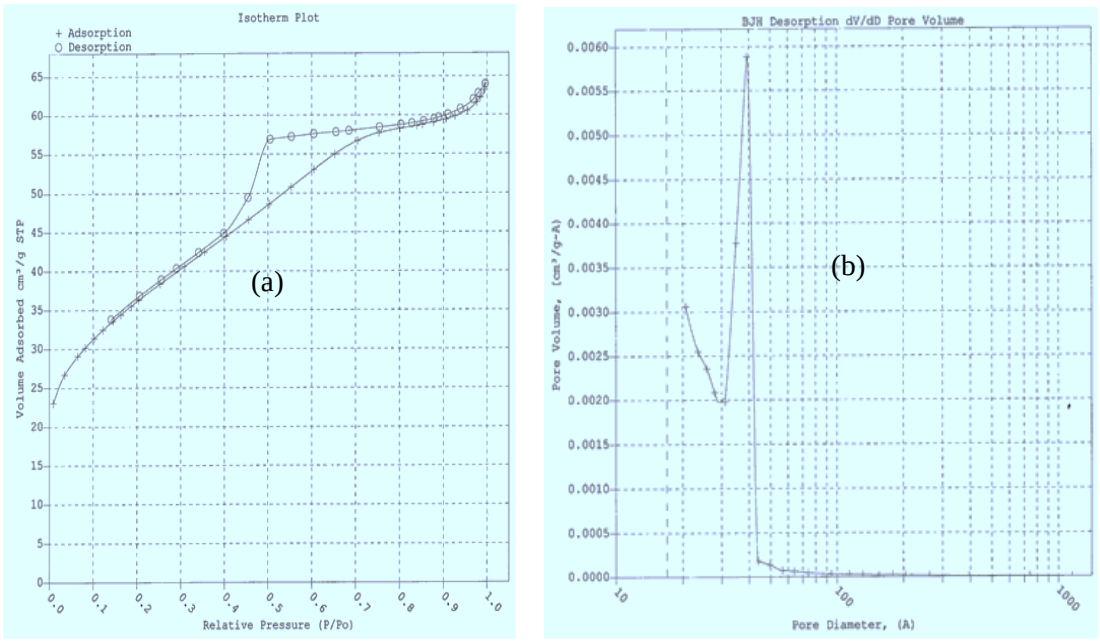


**Fig. 3.7.** $N_2$ adsorption-desorption on $Cs_{2.5}H_{0.5}PW_{12}O_{40}$ (a), and pore size distribution for $Cs_{2.5}H_{0.5}PW_{12}O_{40}$ by BJH method (b) (the catalyst was pre-treated at 250 °C in vacuum).

Core-shell catalysts comprising an HPA (shell) supported on its insoluble neutral salts (core), such as HPW/$Cs_3$PW and HPW/$K_3$PW, have attracted interest due to their possible advantages over the corresponding bulk acidic heteropoly salts such as $Cs_nH_{3-n}PW$ and $K_nH_{3-n}PW$.[30] It is claimed that the core-shell catalysts have a larger number of accessible surface acid sites than the corresponding bulk salts of the same total composition, and, further, that these acid sites are stronger than those in the bulk salts. As a result, the core-shell HPA catalysts could have higher catalytic activities than their bulk counterparts. Moreover, there is evidence that some bulk heteropoly salts, e.g. $Cs_2$HPW, are in fact core-shell materials.[30-31] The texture for the salts $Cs_nH_{3-n}PW$ and core-shell catalysts HPW/$Cs_3$PW used in this study is shown in **Table 3.2**, in relation to their preparation conditions, such as aging and calcination temperature.

**Table 3.2.** *Bulk salts $Cs_nH_{3-n}PW$ and core-shell catalysts HPW/$Cs_3$PW*

| **Catalyst** | **BET surface area[a]** $m^2g^{-1}$ | **Pore volume[b]** $cm^3g^{-1}$ | **Pore diameter[c]** Å |
|---|---|---|---|
| $Cs_3PW_{12}O_{40}$ ($Cs_3$PW) | 145 | 0.111 | 31 |
| $Cs_{2.5}H_{0.5}PW_{12}O_{40}$ | 117 | 0.073 | 25 |
| $Cs_{2.25}H_{0.75}PW_{12}O_{40}$ | 128 | 0.070 | 22 |
| 15% HPW/$Cs_3$PW ($H_2O$)[d] | 146 | 0.124 | 34 |
| 15% HPW/$Cs_3$PW (MeOH)[e] | 135 | 0.131 | 39 |
| 15% HPW/$Cs_3$PW (Washed)[f] | 133 | 0.111 | 34 |
| 25% HPW/$Cs_3$PW ($H_2O$)[d] | 116 | 0.070 | 24 |

[a] Obtained using the BET method. [b] Single point total pore volume of pores. [c] Average pore diameter. [d] Prepared in water. [e] Prepared in methanol. [f] $Cs_3$PW washed with water before wet impregnation of HPW.

It can be seen in **Tables 3.1-3.2** that $ZrO_2$ and $Cs_3PW$ both possess similar BET surface areas. This suggests that the dispersion of HPW on $Cs_3PW$ and $ZrO_2$ should be similar. On the other hand, the oxide support would interact strongly with the heteropoly acid, diminishing the strength of its acid sites and therefore reducing the catalytic activity of the heteropoly acid (acid site effects are described in **Section 3.6**). When the neutral heteropoly salt is used as the core for the core-shell particle formation, it is therefore anticipated that it would generate stronger proton sites than when applying for a more basic oxide support due to the weak interaction between the heteropoly acid and its neutral salt.[9]

The BET isotherm for 15% HPW/$Cs_3PW$ as core-shell materials behaves in line with the corresponding bulk acidic heteropoly salts ($Cs_nH_{3-n}PW$), as shown in **Figure 3.8**. This data is in agreement with previous studies.[9, 30-31]

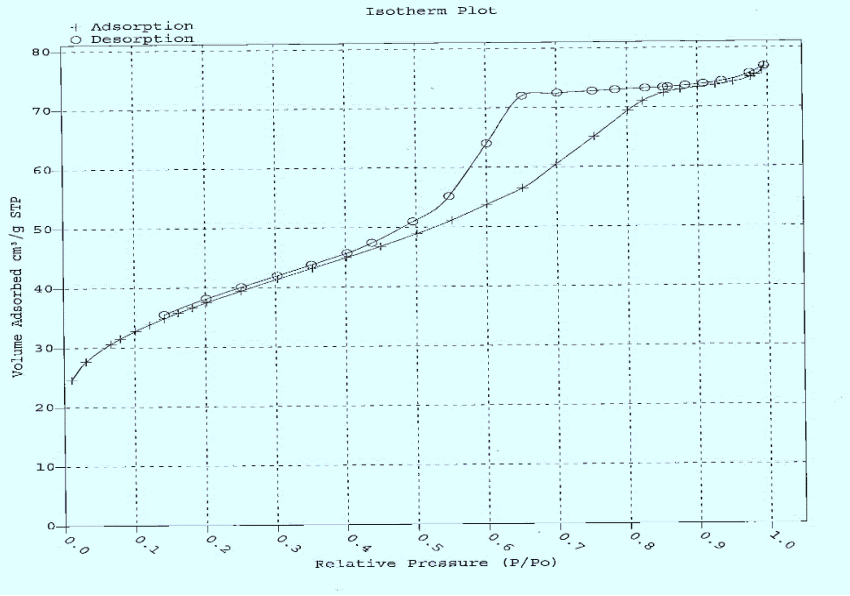


**Fig. 3.8.** The nitrogen adsorption-desorption isotherm of 15%HPW/$Cs_3PW$.

## 3.2 Thermogravimetric analysis (TGA)

In this study, a Perkin Elmer TGA 7 instrument was used to determine the water content in catalysts by heating catalyst samples from 25 to 700 °C under nitrogen flow with a heating rate of 20 °C per minute. This technique was also used to evaluate the thermal stability of the catalysts under study.

Solid heteropoly compounds (heteropoly acids and salts) accommodate a large amount of water of crystallisation (up to 30 molecules per Keggin unit). Depending on the amount of hydration water, and on the counter cation, several crystallographic arrangements exist (**Table 3.3**).

**Table 3.3.** *Crystal structures of 12-tungstophosphoric acid hydrates.*[9]

| **Hydrate** | **Crystal type** |
|---|---|
| $H_3PW_{12}O_{40}{\cdot}29\ H_2O$ | cubic |
| $H_3PW_{12}O_{40}{\cdot}21\ H_2O$ | orthorhombic |
| $H_3PW_{12}O_{40}{\cdot}14\ H_2O$ | triclinic |
| $H_3PW_{12}O_{40}{\cdot}6\ H_2O$ | cubic |

TGA analysis was conducted on bulk HPAs, supported HPW and $Cs_{2.5}PW$ to measure the amount of physisorbed water removed at temperatures up to 150 °C.

### 3.2.1 Bulk HPAs

The thermal behaviour of HPA catalysts has already been reported, with the results being in agreement with previous studies.[9, 27, 32-33]

**Figures 3.9-3.12** show the TGA analysis of $H_3PW_{12}O_{40}$, $H_4SiW_{12}O_{40}$, and $H_3PMo_{12}O_{40}$ hydrates. Three main peaks can be observed. The first peak, at a temperature below 100 °C corresponds to the loss of physisorbed and hydration waters in the sample. The second peak, in the temperature range of 100 – 280 °C, is accounted for by the loss of ca. six $H_2O$ molecules per Keggin unit, and the dehydration of a relatively stable hexahydrate $H_3PW_{12}O_{40}.6H_2O$ in which the waters are hydrogen-bonded to the acidic protons. These stronger bound waters are suggested to hydrate the three acidic protons in HPW, forming dioxonium ions $H_5O_2^+$.[9] The third peak, in the range of 300 – 600 ºC, is attributed to the loss of all acidic protons and the beginning of the decomposition of the Keggin structure to evolve 1.5 water molecules per Keggin unit. **Figure 3.13** shows a fragment of the crystal structure of the hexahydrate $H_3PW_{12}O_{40}\cdot 6\ H_2O$ determined by single-crystal X-ray analysis.[33]

It has been suggested that the water forms because of the extraction of oxygen from the anion by the protons, apparently without collapse of the Keggin structure of the anion but with some rearrangement of its secondary structure (equation 3.4).[9]

$$H_3PW_{12}O_{40} \rightarrow PW_{12}O_{38.5} + 1.5H_2O \qquad (3.4)$$

Decomposition of $H_3PW_{12}O_{40}$ to its constituent oxides $WO_3$ and $P_2O_5$ occurs above 550 °C (equation 3.5).[33]

$$H_3PW_{12}O_{40} \rightarrow 12WO_3 + 1/2P_2O_5 + 3/2H_2O \qquad (3.5)$$

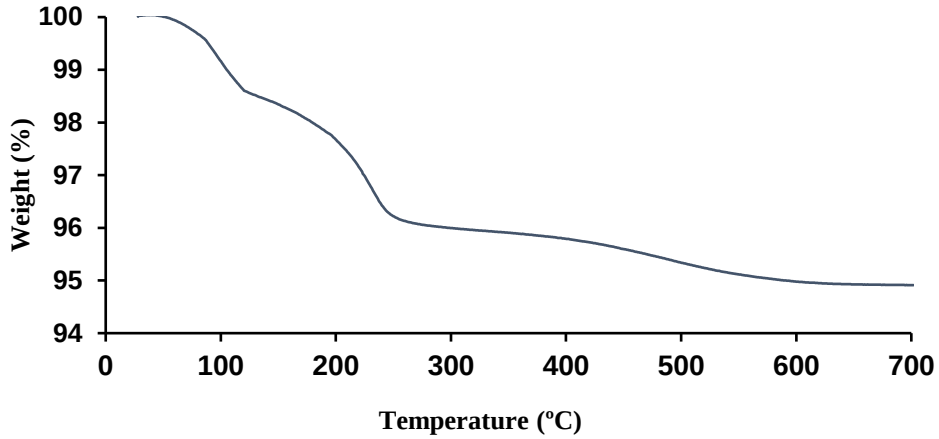


**Fig. 3.9.** TGA analysis of $H_3PW_{12}O_{40}$ hydrate.

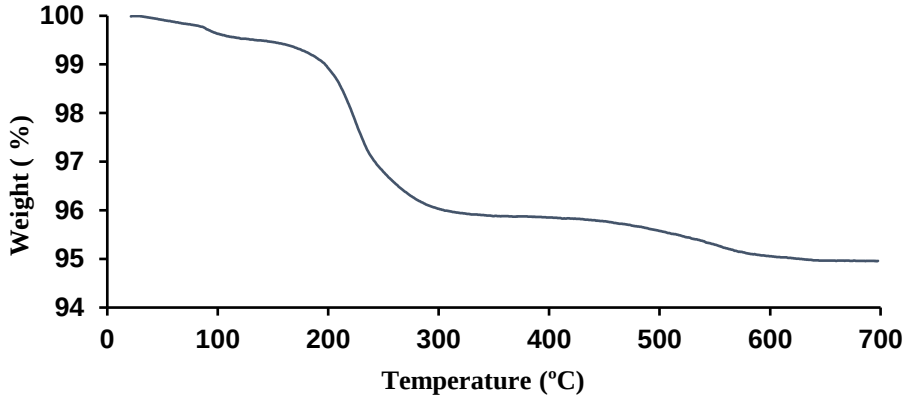


**Fig. 3.10.** TGA for HPW after pre-treatment at 150°C/0.5 Torr for 1.5 h.

It is known that $H_4SiW_{12}O_{40}$ and $H_3PMo_{12}O_{40}$ are less stable than $H_3PW_{12}O_{40}$.[9] The data presented in Figures 3.11 and 3.12 shows good agreement with that reported in the literature.[27]

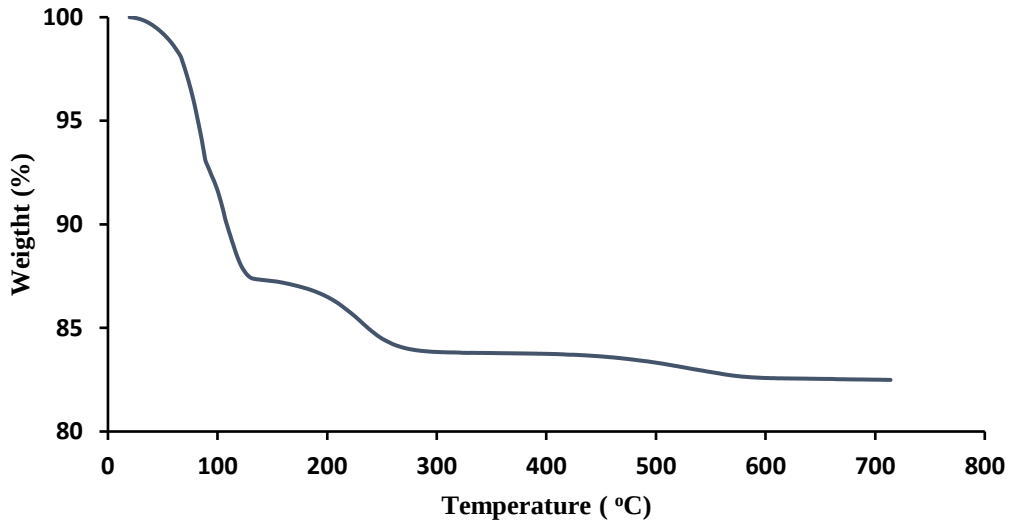


**Fig. 3.11.** TGA analysis of $H_4SiW_{12}O_{40}$.

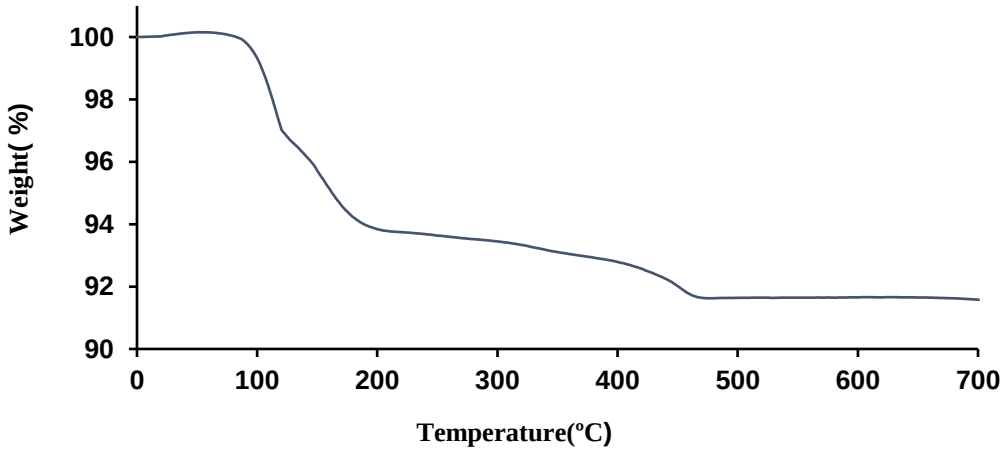


**Fig. 3.12.** TGA analysis of $H_3PMo_{12}O_{40}$.

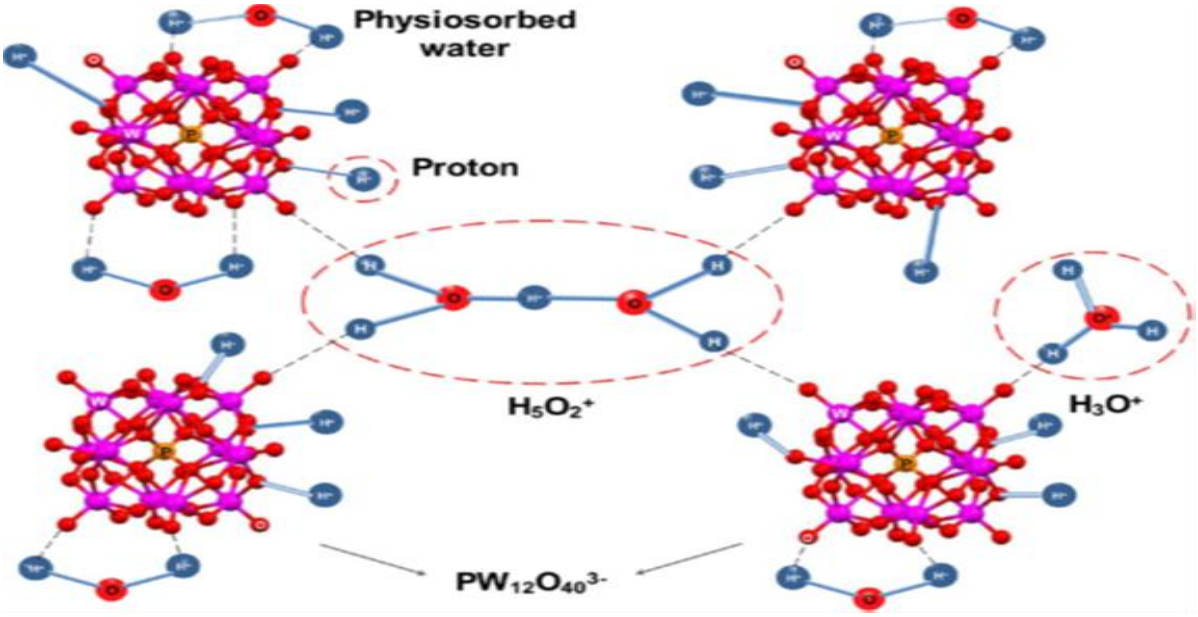


**Fig. 3.13.** Protonic species in $H_3PW_{12}O_{40}\cdot 6H_2O$.[14]

Differential thermal analysis (DTA) and differential scanning calorimetry (DSC) have also been used to estimate the thermal stability of heteropoly acids. Two general features have been shown: endotherms below 400 °C and exotherms above. The endotherms correspond to the loss of water of crystallisation and the exotherms to the decomposition to the constituent oxides.[33]

### 3.1.2 $Cs_nH_{3-n}PW$

The acidic $Cs^+$ salt $Cs_{2.5}H_{0.5}PW_{12}O_{40}$ has been found to be thermally stable up to 600 ºC and insoluble in polar solvents.[25] **Figure 3.14** shows the thermal analysis of $Cs_{2.5}H_{0.5}PW_{12}O_{40}$, and the loss in weight of 3% up to a temperature of 300 ºC, which corresponds to the removal of physisorbed water and / or crystallisation water, as reported by Essayem *et al*.[34] The TGA profile of a neutral Cs salt ($Cs_3PW_{12}O_{40}$) is presented in **Figure 3.15**.

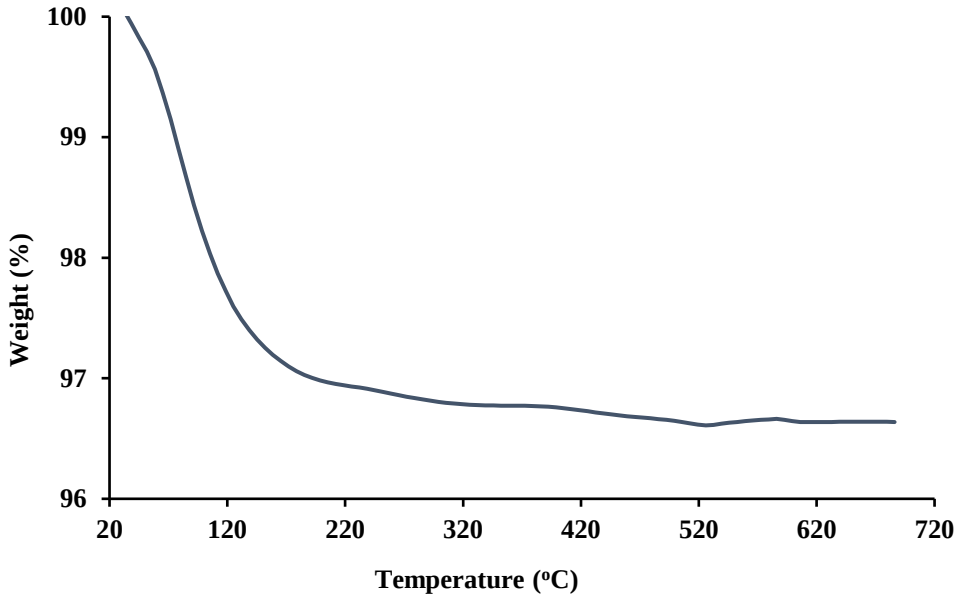


**Fig. 3.14.** TGA analysis of $Cs_{2.5}H_{0.5}PW_{12}O_{40.}$

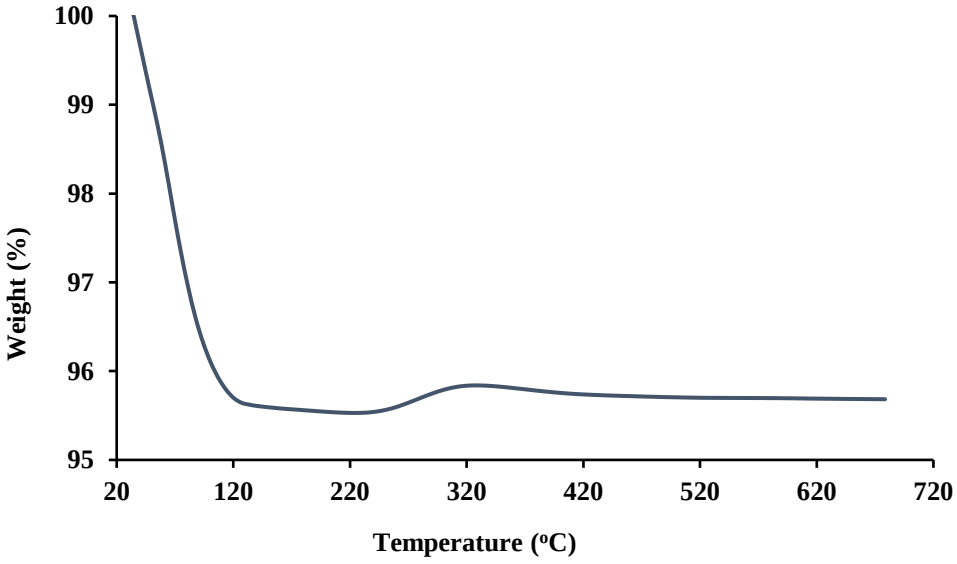


**Fig. 3.15.** TGA analysis of $Cs_3PW_{12}O_{40}$.

### 3.1.3 Supported HPAs

The TGA results for HPA supported catalysts, along with $Nb_2O_5$, $ZrO_2$, $SiO_2$, and $TiO_2$, supports are shown in **Figures 3.16–3.19**. The most significant weight loss in these catalysts was found at temperatures below 300 °C, which corresponds to the removal of adsorbed water and/or crystallisation water. These results are close to those reported in the literature.[23, 35]. It should be noted that $Nb_2O_5$ and $ZrO_2$ were prepared in the lab while $TiO_2$ was supplied by Aldrich. $Nb_2O_5$ and $ZrO_2$ accommodate a large amount of water during the preparation stage. Silica is well known to rehydrate upon treatment with water while titania is usually too inert to rehydrate in bulk, although it still could rehydrate to some extent at the surface.

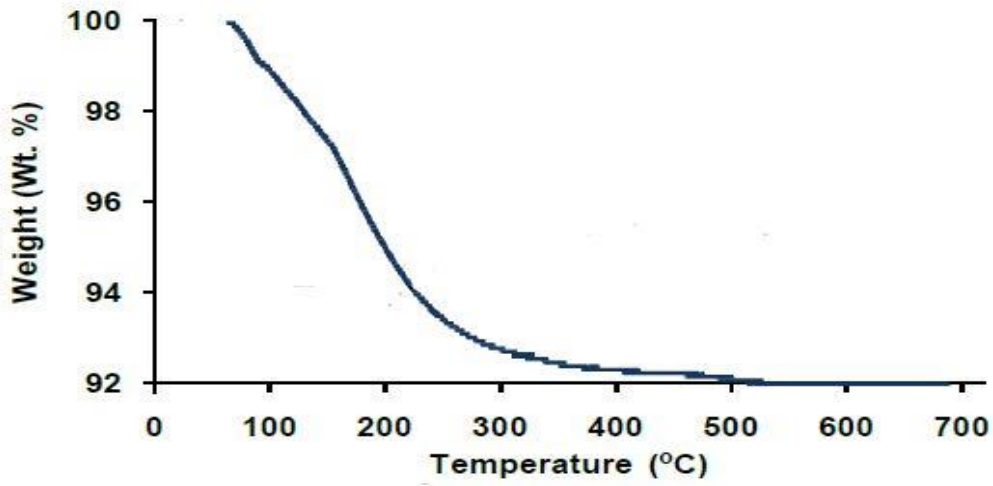


**Fig. 3.16.** TGA analysis of 15%HPW/$Nb_2O_5$.

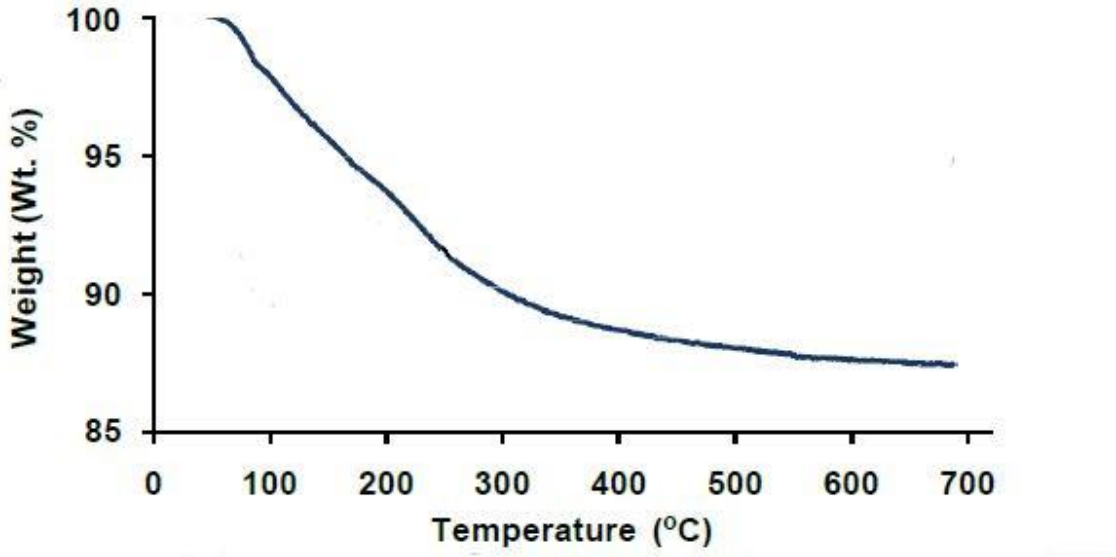


**Fig. 3.17.** TGA analysis of 15%HPW/$ZrO_2$.

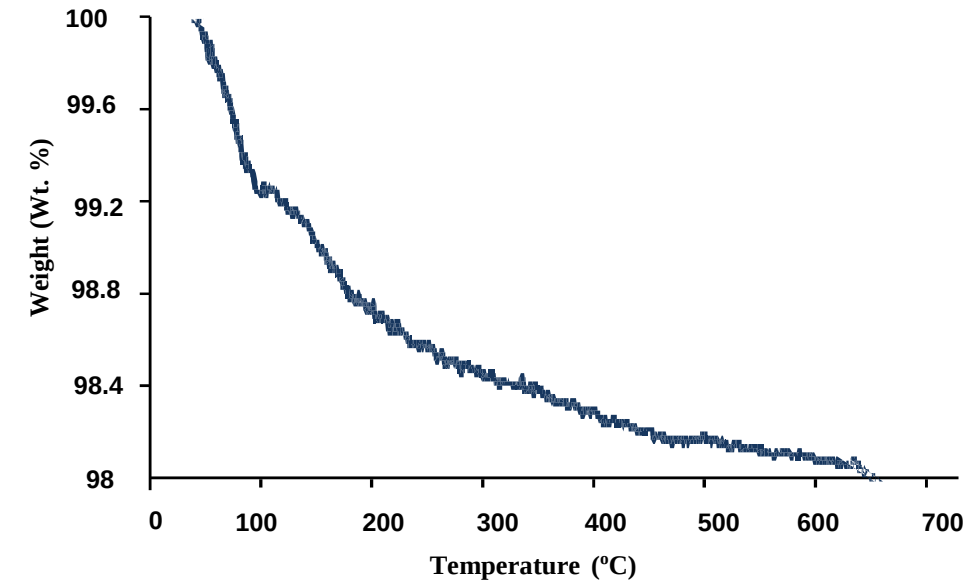


**Fig. 3.18.** TGA analysis of 15%HPW/$TiO_2$.

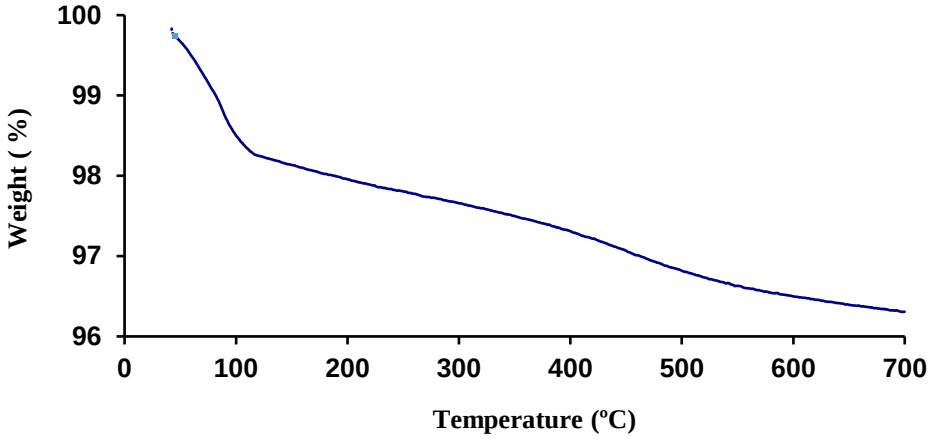


**Fig. 3.19.** TGA analysis of 15% HPW/$SiO_2$.

The temperature of water evolution from the pure silica support was about 30 degrees lower than from HPW catalysts (**Figure 3.19**). The weight loss above 250 °C can be attributed to the dehydroxylation of the silica support. Equation 3.6 represents the reversible dehydration/rehydration of silica below 400 °C (from IR data). A secondary structural effect at a temperature of about 400 °C may involve reactions of isolated SiOH groups.[36]

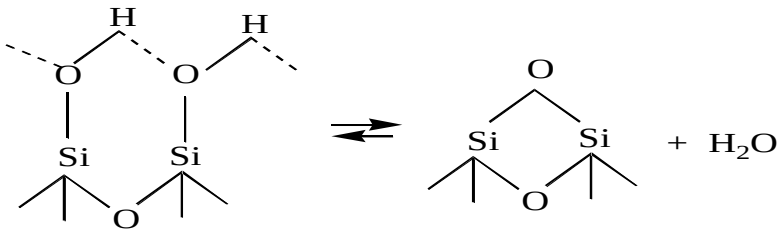


**(3.6)**

## 3.3 Fourier transform infrared spectroscopy (FTIR)

### 3.3.1 Introduction

The general experimental procedure for our FTIR measurement is described in Section 2.3.5. Infrared spectroscopy is one of the most frequently used techniques for the characterisation of heteropoly compounds. The majority of the characteristic infrared active bands of the Keggin anion are recorded in the fingerprint region between 1200 and 500 $cm^{-1}$.[10, 33] It has been reported by Choi *et al.* that the characteristic IR bands for bulk HPW calcined at 300 $^oC$ were at 1080 $cm^{-1}$ (P-$O_a$ in the central tetrahedron, as presented in **Section 1.3.2. Figure 1.7**), 984 $cm^{-1}$ (terminal W=$O_d$), 897 $cm^{-1}$ (W-$O_b$-W) and 812 $cm^{-1}$ (W-$O_c$-W), associated with the asymmetric vibrations in the Keggin polyanion.[37]

### 3.3.2 Supported HPAs

The state of $H_3PW_{12}O_{40}$ on the surface of $Nb_2O_5$, $ZrO_2$, $TiO_2$ and $SiO_2$ has been investigated by various techniques such as XRD, FTIR, $^{31}P$ MAS NMR and others.[23, 33, 38-44]

Okumura *et al*. reported that $H_3PW_{12}O_{40}$ forms in the $H_3PO_4 - WO_3 - Nb_2O_5$ system and partially decomposes upon calcination at 500 $^oC$.[38] Recently, Srilatha *et al.* found decomposition of HPA in a 25%HPW/$Nb_2O_5$ catalyst between 400 – 500 $^oC$, with profound loss of catalyst activity in the esterification of fatty acids.[42]

Kumbar *et al.*, meanwhile, found both fragmented and intact HPA in 20%HPW/$TiO_2$ calcined at 700 $^oC$.[41] In HPW/$ZrO_2$ calcined at 750 $^oC$, the HPA has been claimed to be stabilised by $ZrO_2$, if its loading does not exceed a monolayer (15 wt%).[39] In an earlier study, however, $H_3PW_{12}O_{40}$ on $ZrO_2$ had been found to decompose above 500 $^oC$.[43] Moreover, Sawant *et al.* found that $H_3PW_{12}O_{40}$ is present on the mixed support $ZrO_2$–MCM-41 even after calcination at 850 $^oC$.[40]

This result should be treated with caution, however, since these calcination temperatures are higher than the temperature of the decomposition of bulk $H_3PW_{12}O_{40}$.

In our experiment, we examined the state of HPA on $Nb_2O_5$, $ZrO_2$, $TiO_2$ and $SiO_2$ with sub-monolayer HPA coverage. The FTIR spectra were measured using 10% catalyst mixtures with KBr.

The results obtained for the catalysts under study are shown in **Figures 3.20-3.21.**

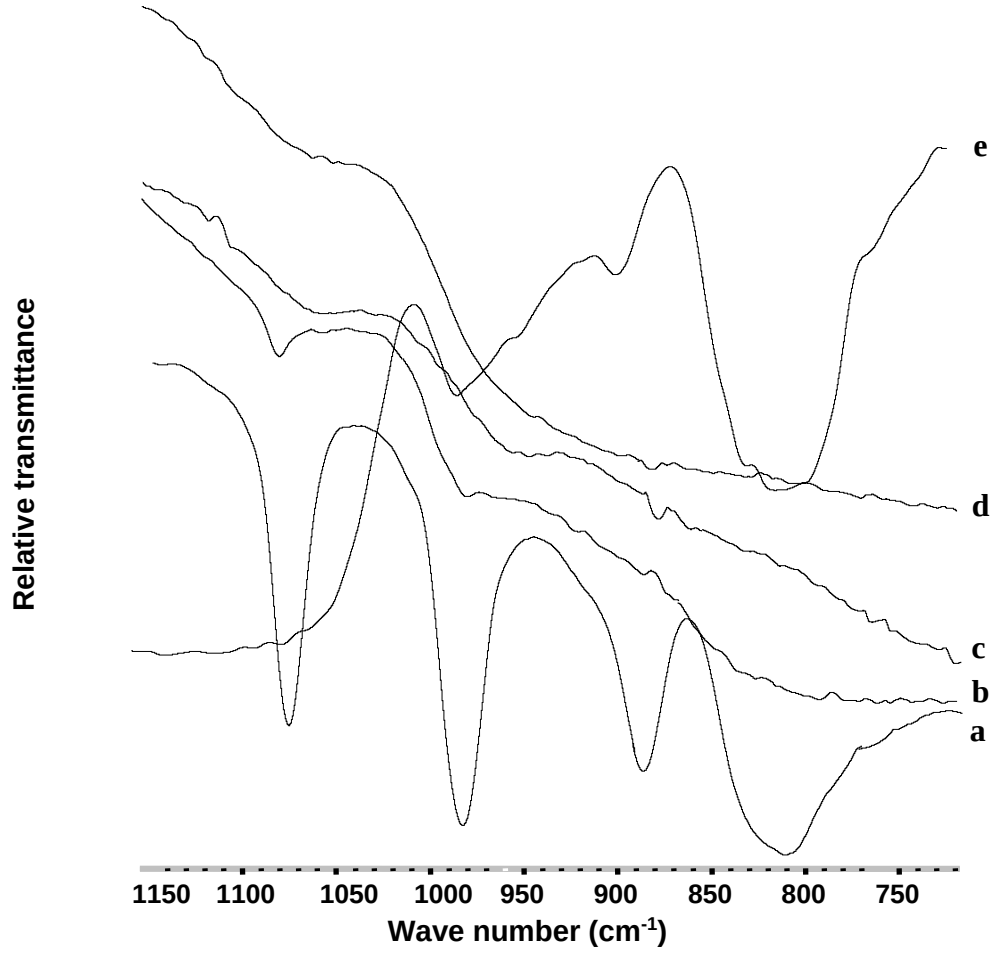


**Fig. 3.20.** FTIR spectra of (a) bulk $H_3PW_{12}O_{40}$ (b) 15%$H_3PW_{12}O_{40}/TiO_2$, (c) 15%$H_3PW_{12}O_{40}/ZrO_2$, (d) 15%$H_3PW_{12}O_{40}/Nb_2O_5$, and (e) 15%$H_3PW_{12}O_{40}/SiO_2$.

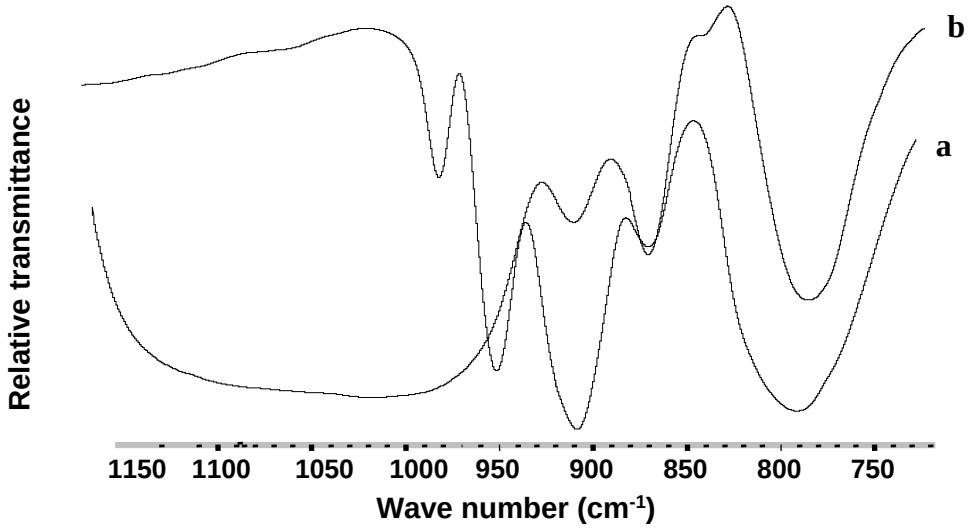


**Fig. 3.21.** FTIR spectra of (a) $H_4SiW_{12}O_{40}$ and (b) 20 %$H_4SiW_{12}O_{40}/SiO_2$.

**Figure 3.20** shows the IR spectra of the catalysts in the range between 750 and 1150 $cm^{-1}$. Bulk HPA (spectrum (a)) exhibits four infrared bands characteristic of the Keggin structure: 1080, 983, 890 and 812 $cm^{-1}$, which is in agreement with previous studies.[9] The spectra (b), (c) and (d) represent supported HPA catalysts calcined at 300 $^oC$ and at this temperature, HPA should remain intact.[9]

In fact, the 15%HPA/$TiO_2$ catalyst (spectrum (b)) clearly exhibited the Keggin unit vibrations at 1080 (P-O) and 983 $cm^{-1}$ (W=O), however, their intensity was much weaker compared to those in the spectrum (a). Also, no vibrations of the bridging W-O-W groups appeared in this spectrum. This is probably due to the bridging O atoms in HPA having a higher negative charge than the terminal ones, in particular, when the HPA interacts more strongly with its support, causing restriction of W-O-W vibrations.

On the contrary, HPW/$ZrO_2$ and HPW/$Nb_2O_5$ did not show any Keggin unit bands (spectra (c) and (d)). This may be explained by a strong interaction between the HPA and its support. Spectrum (e) for 15%HPW/$SiO_2$ exhibits strong infrared bands at 1100 and 806 $cm^{-1}$ and a weak shoulder band at 984 $cm^{-1}$. The strong bands from silica masked the HPA vibrations at 1080 and 812 $cm^{-1}$, but the vibrations at 983 $cm^{-1}$ (W=O) and 890 $cm^{-1}$ (W-O-W) appeared at their normal positions, indicating the presence of an intact Keggin structure. Significantly, it is clear from spectrum (e) that the Keggin structure of HPW is quite stable and remains intact after supporting HPW on silica.[9]

Further evidence of the stability of HPA/$SiO_2$ is represented in **Figure 3.21**. The FT-IR spectrum of bulk HSiW shows four characteristic peaks at 980, 950, 930 and 780 $cm^{-1}$. These four peaks are just shifted a little in the case of HSiW/$SiO_2$. These shifts correspond to interactions between the $OH^-$ group on the surface of the $SiO_2$ support and the oxygen atoms of the HSiW. This result is in agreement with other reports.[45, 46] From these results, it can be inferred that the HPA/support interaction increases in the series: $SiO_2$ < $TiO_2$ < $Nb_2O_5$, $ZrO_2$.

### 3.3.3 $Cs_nH_{3-n}PW$ and core–shell HPA catalysts

The protons in Keggin HPAs can be readily exchanged, totally or partially, by different cations without affecting the primary Keggin structure of the heteropoly anion. The FTIR spectrum for $Cs_{2.5}H_{0.5}PW_{12}O_{40}$ was investigated by Choi *et al*. and it was found that bulk tungstophosphoric acid and its $Cs^+$ salt showed the characteristic IR bands at ca. 1080 $cm^{-1}$ (P-O in the central tetrahedron), 984 $cm^{-1}$ (terminal W=O), 897 and 812 $cm^{-1}$ (W-O-W) associated with asymmetric vibrations in the Keggin polyanion.[37]

CsPW is distinctively characterised by a split in the W=O band at 984 $cm^{-1}$ due to a direct interaction between the polyanion and $Cs^{+}$. The spectra of $Cs_3PW_{12}O_{40}$ also exhibited absorption bands due to $PW_{12}O_{40}^{3-}$ ions.[37, 47]

**Figure 3.22** exhibits absorption bands characteristic of the Keggin structure, with the band at 985 $cm^{-1}$ being split into two peaks and the band at 806 $cm^{-1}$ having a shoulder. The splitting and shoulder appeared to intensify for the water treated samples. This is suggested to be the result of changes in the hydration state rather than because of an alteration of the Keggin structure.[47]

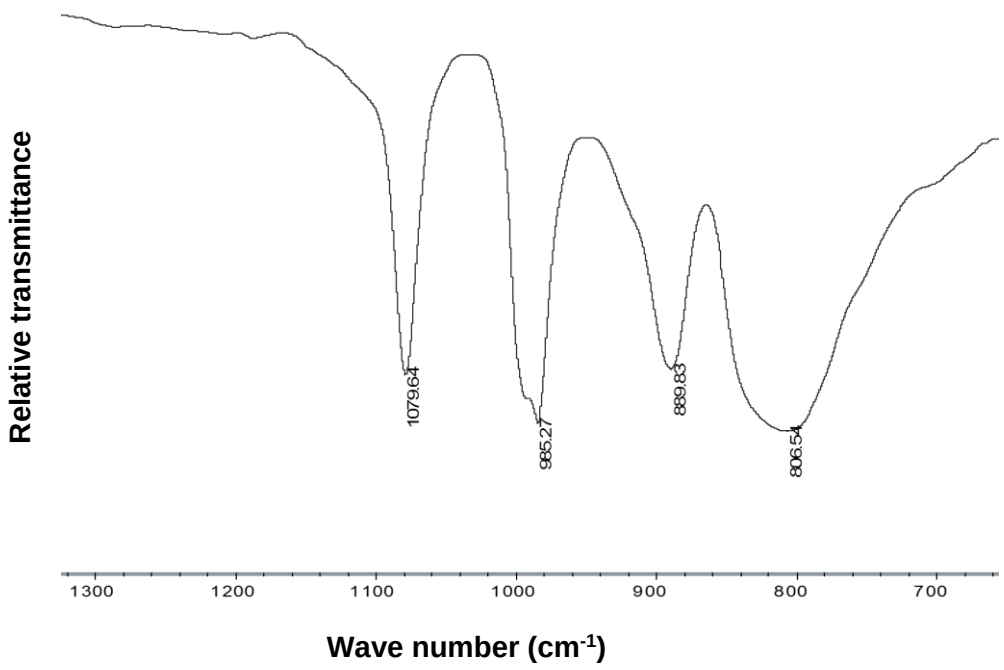


**Fig. 3.22.** FTIR spectrum of $Cs_{2.5}PW$.

The core, consisting of the neutral heteropoly salt, and the shell comprising the heteropoly acid itself was also characterised by FTIR to study the state of the Keggin structure. **Figure 3.23** shows absorption bands characteristic of the Keggin structure for 15%HPW/$Cs_3$PW and 25%HPW/$Cs_3$PW.

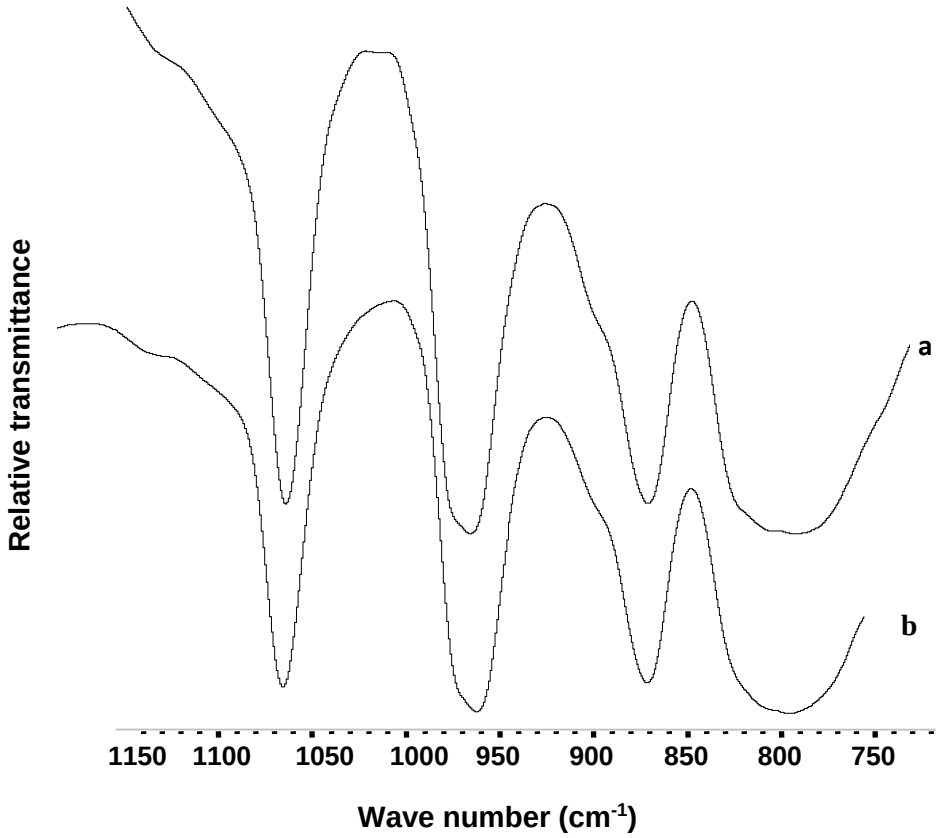


**Fig. 3.23.** FTIR spectra of (a) 15% HPW/$Cs_3$PW and (b) 25%HPW/$Cs_3$PW.

To sum up, both $Cs_nH_{3-n}$PW and core–shell HPA catalysts maintain the structure and symmetry given by heteropoly acid Keggin units.

## 3.4 Powder X-ray diffraction

### 3.4.1 HPW-based catalysts

The XRD diffraction patterns are obtained using the experimental procedure described in **Section 2.3.6.** The supported HPA catalysts on $Nb_2O_5$, $ZrO_2$, $TiO_2$ and $SiO_2$ were studied as part of this research, and no crystalline phase of $H_3PW_{12}O_{40}$ was found in these catalysts calcined at 300 $^oC$, which indicates a high dispersion of HPA on the catalyst surface.[22] The XRD results obtained are close to those reported by other researchers.[39, 49, 48-49]

The XRD data for $H_3PW_{12}0_{40}$, $Cs_nH_{3-n}PW$ and the core–shell HPA catalysts under investigation are shown in **Figure 3.24**. It can be seen that all the catalysts under investigation have a similar structure. These results are also in agreement with other reports.[30-31, 50] In the cited references, the HPW diffraction pattern is present at 10.3, 25.4, 34.6, 37.7 and 53.2$^o$ of 2θ. The cesium salts exhibit XRD diffraction peaks that are slightly shifted to higher values from that of the parent $H_3PW_{12}O_{40}.6H_2O$, however.[50] This can be explained by the larger lattice constant of $Cs_3PW$ (a = 12.14 Å) in comparison with $H_3PW_{12}0_{40}.6H_20$ (a = 11.86 Å).

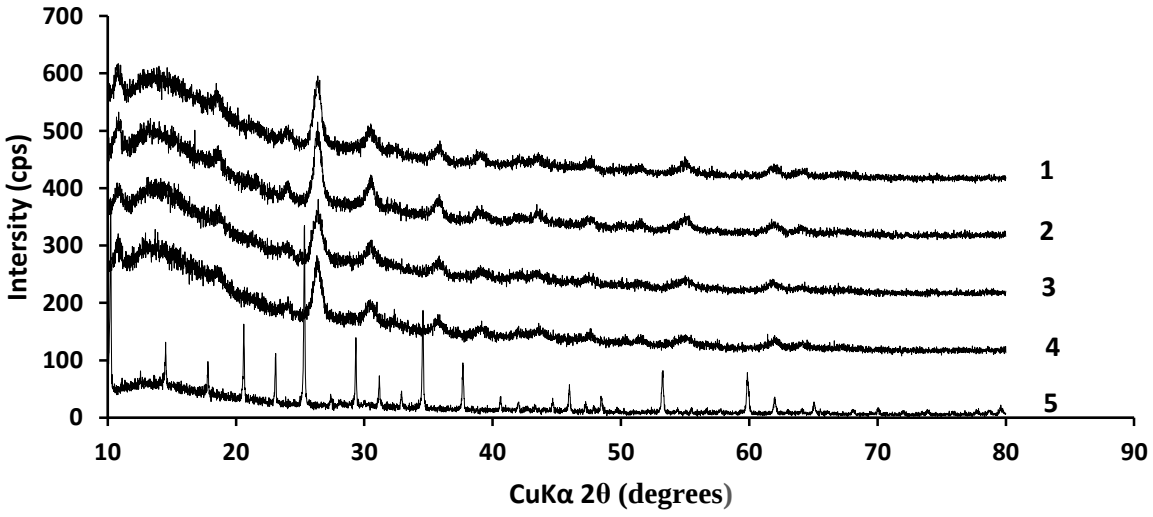


**Fig. 3.24.** XRD patterns for (1) 15% HPW/$Cs_3PW$, (2) 25% HPW/$Cs_3PW$, (3) $Cs_{2.25}PW$, (4) $Cs_{2.5}PW$, and (5) HPW.

### 3.4.2 HZSM-5 zeolites

The XRD patterns for HZSM-5 zeolites with Si/Al atomic ratios of 10, 17, 30, 43, and 120 are represented in **Figure 3.25** and show their MFI structure and high crystallinity.

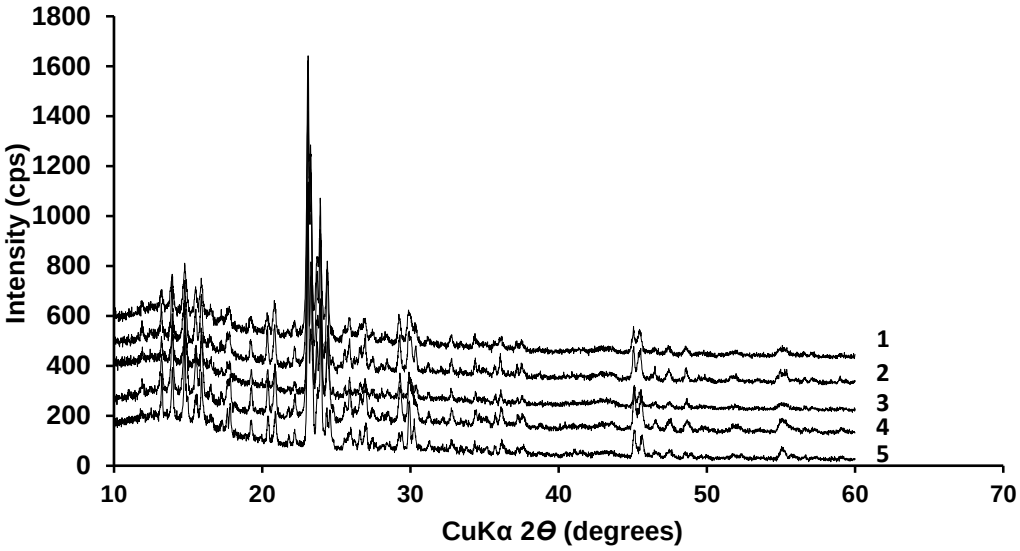


**Fig. 3.25.** XRD pattern for HZSM-5: (1) Si/Al = 10, (2) Si/Al = 17, (3) Si/Al = 30, (4) Si/Al = 43 and (5) Si/Al = 120.

## 3.5 Measurement of acidity

This section aims to characterise the acidity of the investigated catalysts using techniques such as microcalorimetry of ammonia adsorption in a gas-solid system to determine the strength of acid sites, and Fourier transforms infrared spectroscopy (FTIR) to determine the nature of acid sites (Brønsted and Lewis) by adsorption of pyridine. The experimental procedures for these measurements are described in more detail in chapter two.

## 3.5.1 Microcalorimetry of ammonia adsorption

### *3.5.1.1 HPW-based catalysts*

Differential heats of ammonia adsorption on the catalysts were measured by a pulse method in a gas flow system at 150 $^{o}$C. Flow adsorption microcalorimetry involves the use of a carrier gas passing continuously through the adsorption cell. To determine the amounts of gas adsorbed, flow calorimetry must be used in combination with another technique such as TGA, MS, GC, etc.[51, 52] In our microcalorimetry set-up, a Setaram C80 Calvet calorimeter was fitted with a Metrohm DMS Titrino 716 titrator to determine the amount of unadsorbed ammonia. The amount of ammonia adsorbed was determined as the difference between the amount of ammonia supplied in the pulse and the amount of ammonia broken through the sample cell. From these results, the differential enthalpies of ammonia adsorption per mole of ammonia adsorbed were obtained. Extrapolation of these values to zero ammonia uptake gave the initial enthalpy of ammonia adsorption, $\Delta H_{NH3}$.

Typically, the entire ammonia supplied was adsorbed on the catalyst sample in the first four or five pulses, without any ammonia breakthrough being observed. This allowed accurate determination of the $\Delta H_{NH3}$ values without the need for ammonia titration. The mean absolute error in $\Delta H_{NH3}$ was found to be ±3 kJ mol$^{-1}$. The measurement procedure is illustrated in **Figures 3.26-3.28.**

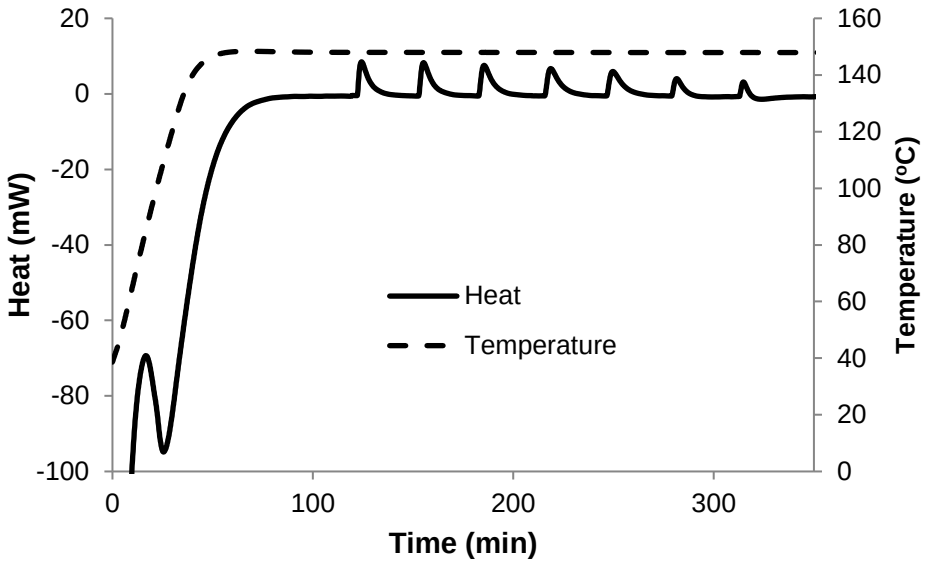


**Fig. 3.26.** Microcalorimetry of ammonia adsorption for $Cs_{2.5}H_{0.5}PW_{12}O_{40}$ at 150 °C.

**Table 3.3** displays the initial enthalpies of ammonia adsorption, $\Delta H_{NH3}$, for the catalysts studied measured at the gas-solid interface under flow conditions at 150 °C. Some of these were determined previously by TG-DSC,[22] others were measured in this work by ammonia adsorption microcalorimetry. The acid strength of the catalysts decreases in the order: HPW > $Cs_{2.5}H_{0.5}PW$ ≈ $Cs_{2.25}H_{0.75}PW$ > $HPW/SiO_2$ ≈ $HSiW/SiO_2$ > $HPW/TiO_2$ > $HPW/Nb_2O_5$ > $HPW/ZrO_2$. It also decreases in the order of oxide supports: $SiO_2$ > $TiO_2$ > $Nb_2O_5$ > $ZrO_2$, which indicates increasing interaction between the HPA and support in that order, as discussed previously.[22]

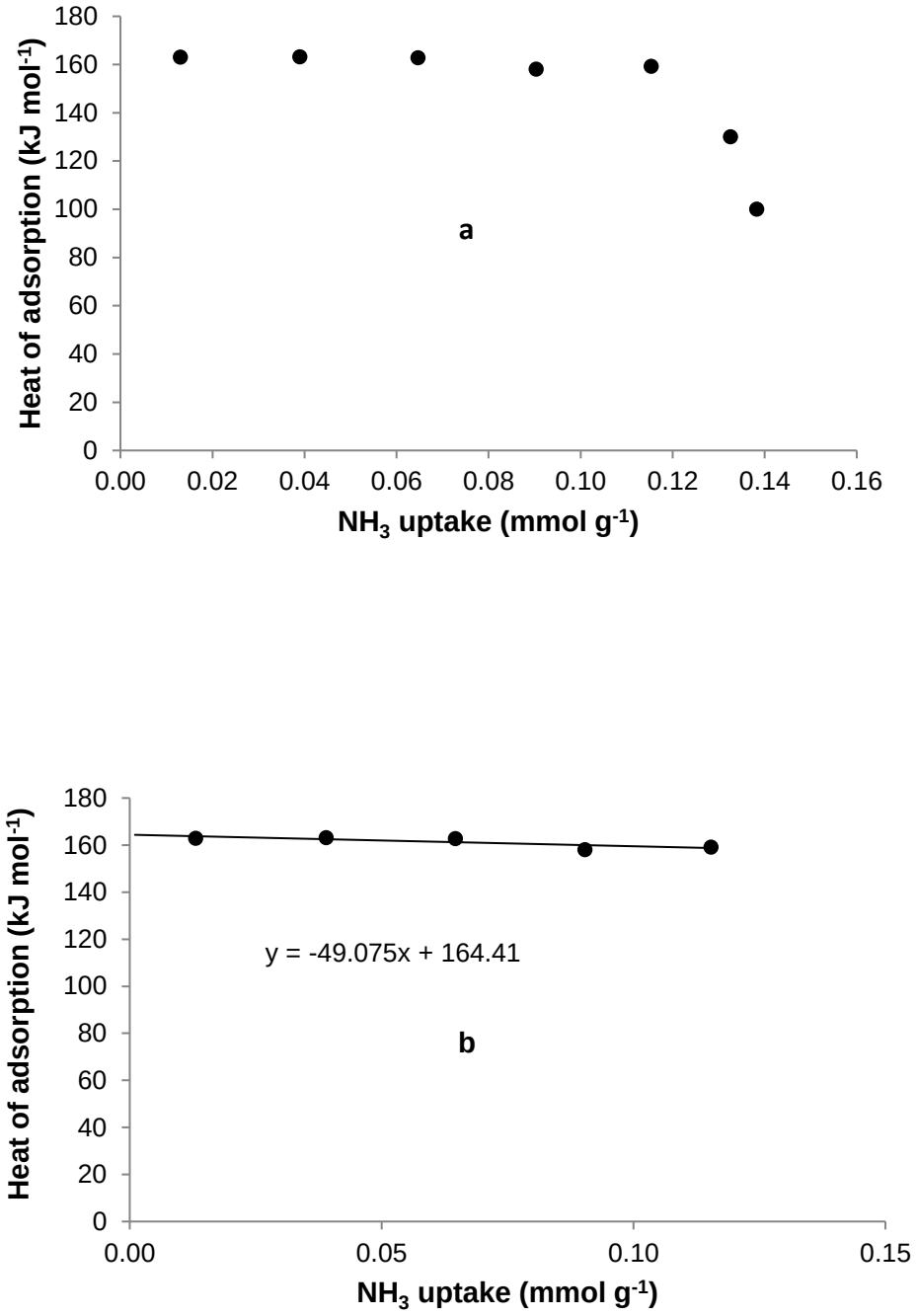


**Fig. 3.27**. Differential heat of ammonia adsorption as a function of ammonia uptake for $Cs_{2.5}H_{0.5}PW_{12}O_{40}$ at 150 ºC (a) and extrapolation to zero uptake (b) ($\Delta H_{NH3}$ = -164.4 kJ mol$^{-1}$).

**Table 3.3** *Initial enthalpy of $NH_3$ adsorption at 150 $^oC$ (±3 kJ $mol^{-1}$).*

| Catalyst | Calcination temperature ($^o$C) | $\Delta H$ (kJ/mol) |
|---|---|---|
| $H_3PW_{12}O_{40}$ | 150 | -197 |
| $H_4SiW_{12}O_{40}$ | 150 | -171 |
| $Cs_{2.5}H_{0.5}PW_{12}O_{40}$ | 150 | -164 |
| $Cs_{2.25}H0_{.75}PW_{12}O_{40}$ | 150 | -162 |
| 15%HPW/$Cs_3$PW | 150 | -151 |
| 25%HPW/$Cs_3$PW | 150 | -165 |
| 15% $H_3PW_{12}O_{40}/Nb_2O_5$ | 150 | -132 |
| 15% $H_3PW_{12}O_{40}/ZrO_2$ | 150 | -121 |
| 15% $H_3PW_{12}O_{40}/SiO_2$ | 150 | -154 |
| 15% $H_4SiW_{12}O_{40}/SiO_2$ | 150 | -154 |
| 15% $H_3PW_{12}O_{40}/TiO_2$ | 150 | -143 |

Also, it can be seen that 25%HPW/$Cs_3$PW and $Cs_{2.25}H_{0.75}$PW have practically the same acid strength within experimental error: -165 and -162 kJ $mol^{-1}$, respectively. Unexpectedly, the acid strength of the 15%HPW/$Cs_3$PW core-shell material (-151 kJ $mol^{-1}$) was found to be significantly lower than that of the bulk salt, $Cs_{2.5}H_{0.5}$PW (-164 kJ $mol^{-1}$). These results contradict the report by Matachowski *et al.* from which the acidity of the core-shell catalysts HPW/$Cs_3$PW could be anticipated to be stronger than that of the corresponding bulk salts, $Cs_nH_{3-n}PW$.[30]

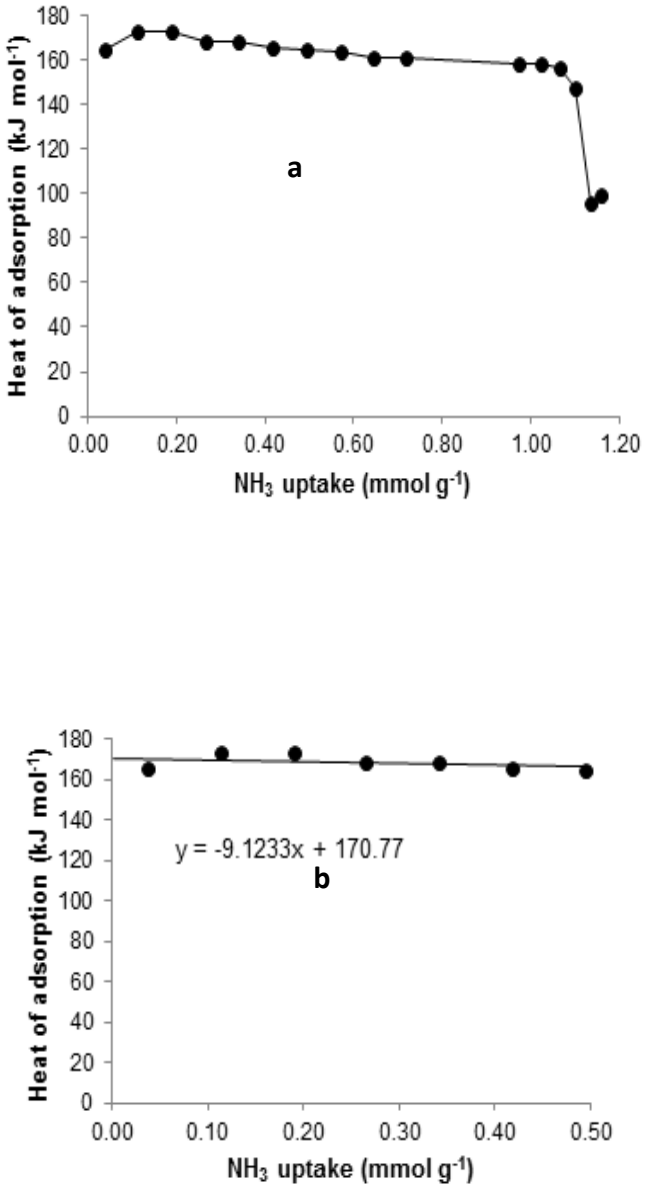


**Fig. 3.28.** Differential heat of ammonia adsorption on bulk HSiW as a function of ammonia uptake at 150 $^{o}$C (a), and extrapolation to zero $NH_3$ uptake (b) (pre-treatment at 150 $^{o}$C/2 h in $N_2$ flow; 0.2756 g sample weight, 0.0210 mmol $NH_3$ pulse; $\Delta H_{NH3}$ = -171±3 kJ mol$^{-1}$).

### *3.5.1.2 HZSM-5 zeolites*

The differential heat of ammonia adsorption on HZSM-5 zeolites (Si/Al = 10, 30 and 120) was measured at ambient pressure after pre-treatment at 150 °C in dry $N_2$ flow by a pulse method in a gas flow system using a Setaram C80 Calvet calorimeter.

The results for HZSM-5 are shown in **Figure 2.29**. The values of $\Delta H_{NH3}$ for HZSM-5 zeolites are somewhat lower that those reported in the literature ($\Delta H_{NH3}$=131-150 kJ mol$^{-1}$, Si/Al=20-70).[53,54] This can be explained by the lower pre-treatment temperature in our work (150 °C) to match the conditions of catalyst testing in MeOH dehydration. In calorimetric studies, zeolites are usually pre-treated at 400 – 500 °C in vacuum, which results in higher $\Delta H_{NH3}$ values.[54]

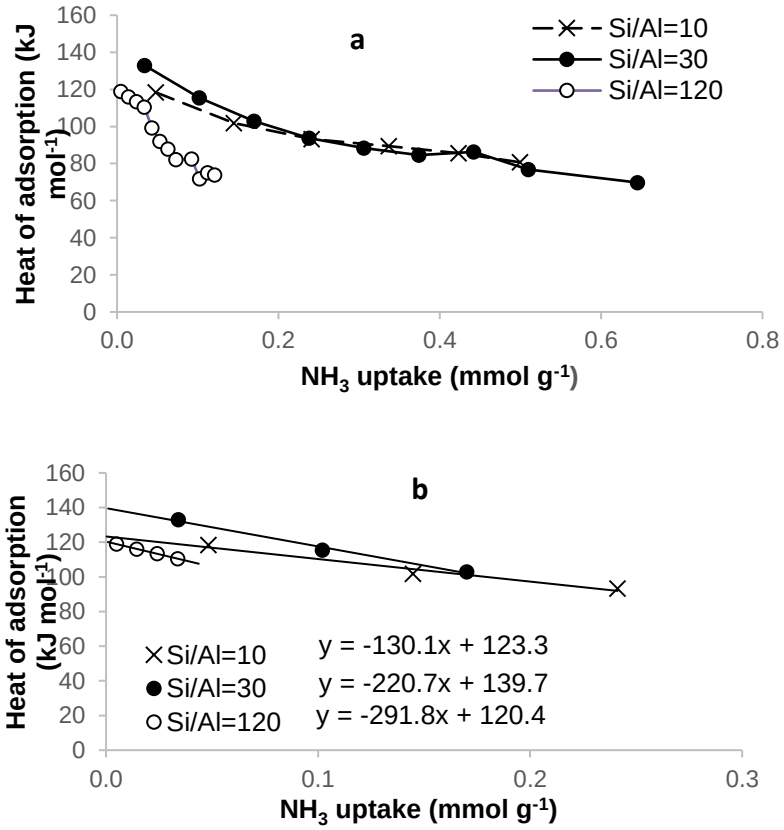


**Fig. 3.29.** Differential heat of ammonia adsorption on HZSM-5 as a function of ammonia uptake at 150 °C (a) and extrapolation to zero $NH_3$ uptake (b) (pre-treatment at 150 °C/2 h in $N_2$ flow): HZSM-5(10), 0.2130 g sample weight, 0.0206 mmol $NH_3$ pulse, $\Delta H_{NH3}$ = -123±5 kJ mol$^{-1}$; HZSM-5(30), 0.3029 g sample weight, 0.0206 mmol $NH_3$ pulse, $\Delta H_{NH3}$ = -140±3 kJ mol$^{-1}$; HZSM-5(120), 0.4086 g sample weight, 0.00412 mmol $NH_3$ pulse, $\Delta H_{NH3}$ = -120±3 kJ mol$^{-1}$.

### 3.5.2 FTIR study of pyridine adsorption

Adsorption of pyridine as a base on the surface of solid acids is one of the most common applications for the characterisation of surface acidity as the fundamental step to understanding the reaction mechanisms in heterogeneous catalysis.[39, 55] The use of IR spectroscopy to detect adsorbed pyridine allows the two different acid sites to be identified. The pyridinium ion displays a vibration at 1540 $cm^{-1}$, which is attributed to the C-C stretching vibration of the ion, indicating the presence of Brønsted acid sites. On the other hand, the band at ~1450 $cm^{-1}$ shows a pyridine complex on Lewis acid sites.

Bulk $H_3PW_{12}O_{40}$ and $Cs_{2.5}H_{0.5}PW_{12}O_{40}$ pre-treated at temperatures below 300 $^oC$ are known to possess strong Brønsted acid sites.[9] It has been reported, however, that CsPW-based catalysts and H-ZSM-5 have both Brønsted and Lewis acid sites.[9, 56]

Alsalme *et al.* reported that Lewis acid sites in HPA/$Nb_2O_5$, HPA/$ZrO_2$, and HPA/$TiO_2$ catalysts were mainly originated from the oxide support since these have been reported to exhibit Lewis acid sites. Brønsted acid sites were provided by the HPA as well as oxide supports in the case of $Nb_2O_5$ and $ZrO_2$.[22] It is notable that HPW supported on $SiO_2$ contains only a very small amount of Lewis acid sites compared to other carries, since $SiO_2$ is relatively inert towards HPAs.[22, 38] **Figure 3.30** shows DRIFT spectra of adsorbed pyridine on 15%HPW/$SiO_2$ as well as 15%HSiW/$SiO_2$. These catalysts possessed both Brønsted and Lewis acid sites, as confirmed by strong IR bands. Our results are in agreement with previous studies.[22, 39, 41, 57-58]

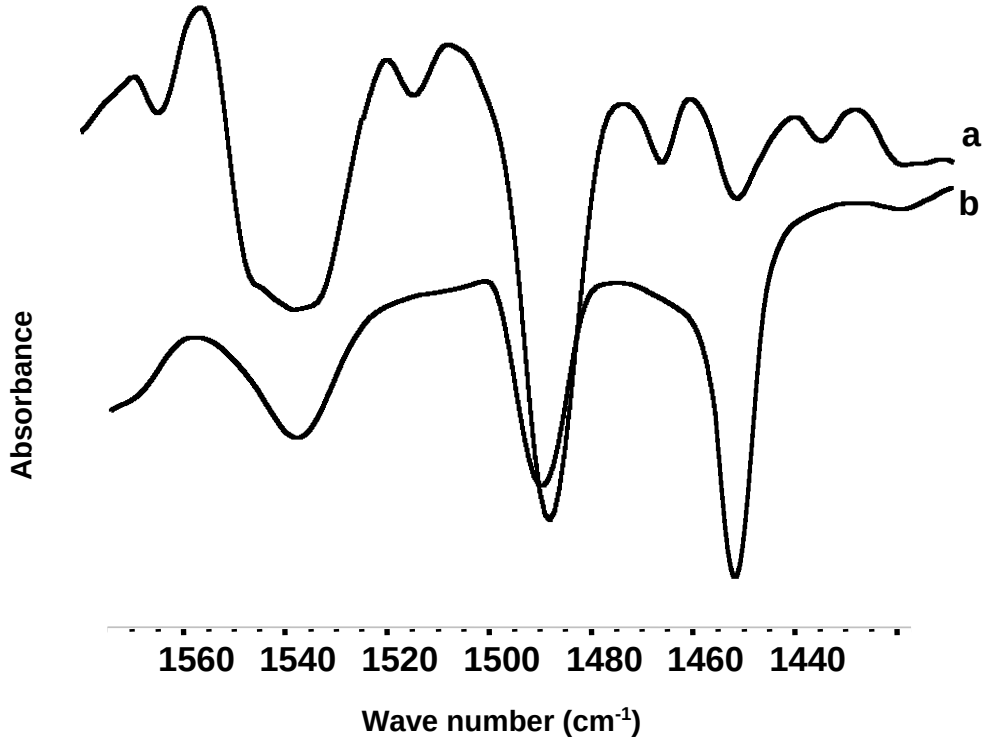


**Fig. 3.30.** DRIFT spectra of pyridine adsorbed on (a) 15%$H_3PW_{12}O_{40}/SiO_2$ and (b) 15%$H_4SiW_{12}O_{40}/SiO_2$.

## 3.6 Conclusion

The texture of catalysts was characterised by $N_2$ physisorption. All the HPA catalysts under study were mesoporous materials with average pore diameters of 22 – 230 Å. Our supported HPA catalysts had surface areas above 100 $m^2\ g^{-1}$ up to 244 $m^2\ g^{-1}$, except for 15%HPW/$TiO_2$, which had a surface area of 45 $m^2\ g^{-1}$. Assuming a cross section of 144 $Å^2$ for HPW and HSiW molecules [17–20] the 15% HPA loading will correspond to monolayer HPA coverage of 45 $m^2\ g^{-1}$. Therefore, all supported HPA catalysts could be viewed as having submonolayer HPA coverage. Fine HPA dispersion on the catalyst surface has been confirmed by XRD analysis.

The initial enthalpies of ammonia adsorption ($\Delta H_{NH3}$) for HPA catalysts have been measured by ammonia adsorption calorimetry. The acid strength of HPA catalysts decreases in the order: HPW > HSiW > $Cs_{2.5}H_{0.5}PW$ ≈ $Cs_{2.25}H_{0.75}PW$ > HPW/$SiO_2$ ≈ HSiW/$SiO_2$ > HPW/$TiO_2$ > HPW/$Nb_2O_5$ > HPW/$ZrO_2$. The acid strength notably decreases in the order of supports: $SiO_2$ > $TiO_2$ > $Nb_2O_5$ > $ZrO_2$, which indicates increasing interaction between the HPA and support in that order.

## 3.7 References


1. K. K. Unger, J. Roquerol, K. S. W. Sing, H. Kral (Eds.), Characterisation of Porous Solids I, Elsevier, Amsterdam, 1988.
2. J. Roquerol, F. Rodriguez-Reinoso, K. S. W. Sing, K. K. Unger, Characterisation of Porous Solids III, Elsevier, Amsterdam, 1994.
3. S. J. Gregg, K. S. W. Sing, Adsorption, Surface Area and Porosity, Academic Press, London, 1982.
4. G. Leofanti, M. Padovan, G. Tozzola, B. Venturelli, Catal. Today, 41 (1998) 207.
5. K. Kaneko, J. Membr. Sci., 96 (1994) 59.
6. K. W. Sing, F. Rodrguez-Reinoso *et al*. (Eds.), Characterization of Porous Solids II, Elsevier, Amsterdam, 1991.
7. G. C. Bond, Heterogeneous Catalysis, 2nd ed., Oxford University Press, Oxford, 1987.
8. C. B. G. Attard, Surfaces, Oxford University Press, Oxford, 1998.
9. I. V. Kozhevnikov, Catalysts for Fine Chemicals.Vol. 2. Catalysis by Polyoxometalates, Wiley, Chichester, 2002.
10. T. Okuhara, N. Mizuno, M. Misono, Adv. Catal., 41 (1996) 113.
11. T. Okuhara, Chem. Rev., 102 (2002) 3641.
12. G. D. Yadav, Catal. Surv. Asia, 9 (2005) 117.
13. Y. Wu, X. Ye, X. Yang; X. Wang, W. Chu, Hu. Yucai, Ind. Eng. Chem. Res., 35 (1996) 2546.
14. C. Baroi, A. K. Dalai, Ind. Eng. Chem. Res., 53 (2014) 18611.
15. J. E. Herrera, J. H. Kwak, J. Z. Hu, Y. Wang, C. H. F. Peden, Top. Catal., 49 (2008) 259.
16. A. E. R. Khder, Appl. Catal., 343 (2008) 109.
17. G. T. Kerr, A. W. Chester, Thermochim. Acta, 3 (1971) 124.

18. F. Kapteijn, J.A. Moulijn, G. Ertl, H. Knözinger, F. Schüth, J. Weitkamp (Eds.), Handbook of Heterogeneous Catalysis, vol. 4, Wiley-VCH, Germany, 2008.
19. T. Okuhara, H. Watanabe, T. Nishimura, K. Inumaru, M. Misono, Chem. Mater., 12 (2000) 2230.
20. N. Mizuno, M. Misono, Chem. Rev., 98 (1998) 199.
21. E. López-Salinas, J.G. Hernández-Córtez, M. Cortéz, J. Navarrete, M. Yanos, A. Vázquez, H. Armendaris, T. López, Appl. Catal., 175 (1998) 43.
22. A. M. Alsalme, P. V. Wiper, Y. Z. Khimyak, E. F. Kozhevnikova, I. V. Kozhevnikov, J. Catal., 276 (2010) 181.
23. E. López-Salinas, J. G. Hernández-Cortéz a, I. Schifter a, E. Torres-Garc, J. Navarrete, A. Gutiérrez-Carrillo, T. López, P. P. Lottici, D. Bersani, Appl. Catal. A: Gen., 193 (2000) 215.
24. K. Okumura, K. Yamashita, K. Yamada, M. Niwa, J. Catal., 245 (2007) 75.
25. E. F. Kozhevnikova, E. Rafiee, I. V. Kozhevnikov, Appl. Catal. A, 260 (2004) 25.
26. I. V. Kozhevnikov, S. Holmes, M. R. H. Siddiqui, Appl. Catal. A, 214 (2001) 47.
27. M. Misono, Chem. Commun., (2001) 1141.
28. T. Okuhara, Catal. Today, 73 (2002) 167.
29. T. Yamada, Y. Yoshinaga, T. Okuhara, Bull. Chem. Soc. Jpn., 71 (1998) 2727.
30. L. Matachowski, A. Drelinkiewicz, D. Mucha, J. Krys´ciak-Czerwenka, R. Rachwalik, Appl. Catal. A, 469 (2014) 239.
31. L. Matachowski, A. Drelinkiewicz, E. Lalik, M. Ruggiero-Mikołajczyk, D. Mucha, J. Krys´ciak-Czerwenka, Appl. Catal. A, 469 (2014) 290.
32. P. A. Jalil, M. Faiz, N. Tabet, N. M. Hamdan, Z. Hussain, J. Catal., 217 (2003) 292.
33. J. B. Moffat, Metal-Oxygen Clusters, The Surface and Catalytic Properties of Heteropoly Oxometalates, Kluwer, New York, 2001.

34. N. Essayem, G. Coudurier, M. Fournier, J. C. Vedrine, Catal. Lett., 34 (1995) 223.

35. N. A. Comelli, L. M. Grzona, O. Masini, E. N. Ponzi, M. I. Ponzi, J. Chil. Chem. Soc., 49 (2004) 245.

36. B. A. Morrow, I. A. Cody, L. S. M. Lee, J. Phys. Chem., 80 (1976) 2761.

37. S. M. Choi, Y. Wang, Z. M. Nie, J. Liu, C. H. F. Peden, Catal. Today, 55 (2000) 117.

38. K. Okumura, K. Yamashita, M. Hirano, M. Niwa, J. Catal., 234 (2005) 300.

39. B. M. Devassy, F. Lefebvre, S. B. Halligudi, J. Catal., 231 (2005) 1.

40. D. P. Sawant, A. Vinu, F. Lefebvre, S. B. Halligudi, J. Mol. Catal. A, 262 (2007) 98.

41. S. M. Kumbar, G. V. Shanbhag, F. Lefebvre, S. B. Halligudi, J. Mol. Catal. A, 256 (2006) 324.

42. K. Srilatha, N. Lingaiah, B. L. A. P. Devi, R. B. N. Prasad, S. Venkateswar, P. S. S. Prasad, Appl. Catal. A, 365 (2009) 28.

43. E. Lopez-Salinas, J. G. Hernandez-Cortez, I. Schifter, E. Torres-Garcia, J. Navarrete, A. Gutierrez-Carrillo, T. Lopez, P. P. Lottici, D. Bersani, Appl. Catal. A, 193 (2000) 215.

44. G. Bond, S. Frodsham, P. Jubb, E. Kozhevnikova, I. Kozhevnikov, J. Catal., 293 (2012) 158.

45. C. R. Deltcheff, M. Fournier, R. Franck, R. Thouvenot, Inorg. Chem., 22 (1983) 207.

46. S. Zhao, Y. Jia, Y-F. Song, Catal. Sci. Technol., 4 (2014) 2618.

47. T. Nakato, M. Kimura, S. Nakata, T. Okuhara, Langmuir, 14 (1998) 319.

48. M. G. Kulkarni, R. Gopinath, L. C. Meher, A. K. Dalai, Green Chem., 8 (2006) 1056.

49. D. E. Lopez, K. Suwannakarn, D. A. Bruce, J. G. Goodwin, J. Catal., 247 (2007) 43.

50. L. Matachowski, A. Zie, M. Zembala, A. Drelinkiewicz, Catal. Lett., 133 (2009) 49.

51. A. Auroux, Catal. Today, 19 (2002) 205.

52. D. R. Brown, A. J. Groszek, Langmuir, 16 (2000) 4207.

53. M. Brandle, J. Sauer, J. J. Am. Chem. Soc., 120(1998) 1556.

54. A. Auroux, Top. Catal., 4 (1997) 71.

55. B. H. Davis, R. A. Keogh, S. Alerasool, D. J. Zalewski, D. E. Day, P. K. Doolin, J. Catal., 183 (1999) 45.

56. H. Benaissa, P. N. Davey, Y. Z. Khimyak, I. V. Kozhevnikov, J. Catal., 253 (2008) 244.

57. D. Andrew, D. Newman, R. Brown, P. Siril, A. F. Lee, K. Wilson, Phys. Chem. Chem. Phys., 8 (2006) 2893.

58. J. Zhang, M. Kanno, Y. Wang, H. Nishii, Y. Miura, Y. Kamiya, J. Phys. Chem., 115 (2011) 14762.

# Chapter 4. Dehydration of methanol to dimethyl ether over heteropoly acids catalysts

## 4.1 Introduction

Dimethyl ether (DME) is a multi-market product used as environment-friendly aerosol propellant, refrigerant and intermediate in the synthesis of chemicals such as olefins (ethylene and propylene), dimethyl sulfate, etc.[1] In recent years, DME has attracted much interest as a new clean fuel to supplement liquefied petroleum gas (LPG) and as a non-polluting diesel substitute due to its high cetane number, near-zero soot combustion and low $NO_x$ emission.[1, 2] DME is produced by equilibrium controlled dehydration of methanol (equation 4.1) in the gas-phase at 250-360 $^oC$ over solid-acid catalysts, typically γ-alumina.[1, 2] It can also be produced directly from the synthesis gas over multifunctional catalysts through methanol formation followed by dehydration to DME.[1] Over the years, much research has appeared on methanol dehydration focusing on the methanol-to-gasoline (MTG) and methanol-to-olefin (MTO) conversion and DME synthesis. The formation of DME is favorable at relatively low temperatures; whereas the MTG and MTO occur at higher temperatures. In addition to γ-alumina, acidic zeolites, especially MFI (HZSM-5), and heteropoly acids (HPAs) are among the most studied catalysts in methanol dehydration[3-16] (and references therein). These show significantly higher catalytic activities but as yet are less resistant to deactivation than γ-alumina.

$$2\ CH_3OH \rightarrow CH_3OCH_3 + H_2O \qquad (4.1)$$

Keggin-type HPAs comprising heteropoly anions of the formula $[XW_{12}O_{40}]^{n-}$, where X is the heteroatom ($P^V$, $Si^{IV}$, etc.), possess very strong Brønsted acidity.

In the last three decades, catalysis by HPAs has attracted much interest because of its potential to generate economic and environmental benefits;[17-20] several large-scale chemical processes

based on HPA catalysis have been commercialized.[20] In methanol-to-DME dehydration, Keggin HPAs have been found to exhibit higher catalytic activities than oxide and zeolite catalysts.[12, 15-16]

The aim of this work is to investigate a wide range of HPA catalysts in methanol-to-DME dehydration at a gas-solid interface in comparison with HZSM-5 zeolites (MFI structure, Si/Al = 10-120). Our primary goal is to examine the effect of catalyst acid strength on the reaction turnover rate in order to gain further evidence regarding the reaction mechanism for these two types of catalysts. Here we use experimental enthalpies of ammonia adsorption ($\Delta H_{NH3}$) as the catalyst acid strength parameters, which were measured microcalorimetrically under conditions close to those of the methanol-to-DME reaction. Among the HPA catalysts studied are $H_3PW_{12}O_{40}$ (HPW) and $H_4SiW_{12}O_{40}$ (HSiW) heteropoly acids as bulk and supported on $SiO_2$, $TiO_2$, $Nb_2O_5$ and $ZrO_2$ catalysts with sub-monolayer HPA coverage. Also studied are bulk acidic Cs salts of HPW, $Cs_{2.5}H_{0.5}PW_{12}O_{40}$ and $Cs_{2.25}H_{0.75}PW_{12}O_{40}$, there after abbreviated as $Cs_nH_{3-n}PW$. A good correlation between the turnover rates and catalyst acid strengths, represented by the initial enthalpies of ammonia adsorption, was established. This correlation holds for the HPA and HZSM-5 catalysts studied.

## 4.2 Mechanism of methanol-to-DME

Mechanism of methanol-to-DME dehydration is still debated. Formation of DME from methanol may be represented by two different pathways termed the associative pathway and the dissociative pathway (**Scheme 4.1**)[12, 14] (and references therein).

Both pathways are thought to take place at Brønsted acid sites. The associative (concerted) pathway, involves adsorption of two methanol molecules, which react and form the DME directly.

The dissociative (stepwise) pathway involves initial methanol adsorption, followed by water elimination, leading to adsorbed methyl group and water. The methyl group reacts with a second methanol molecule to form DME. Rate equations have been derived for the two pathways;[12, 14] however kinetics does not allow to discriminate these mechanisms.[12]

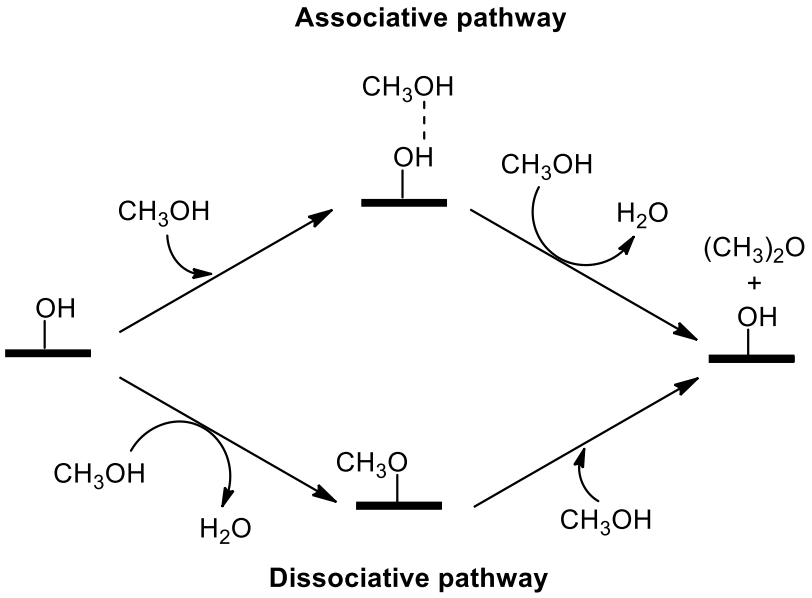


**Scheme 4.1.** Associative and dissociative pathways for methanol-to-DME dehydration.

Density functional theory (DFT) has been used to gain mechanistic insights into DME synthesis[12, 14, 16, 21-22] (and references therein). Earlier DFT calculations based on the cluster model[21, 22] point to the associative pathway dominating in the DME synthesis over acidic zeolites. More recent DFT study by Moses and Nørskov[14] based on the periodic model indicates that methanol-to-DME dehydration over HZSM-22 zeolite (1D channel system with 10 ring pores) occurs predominantly via the dissociative pathway. A linear correlation between the activation energy and catalyst acid strength has been found, which, however, cannot discriminate the mechanism as it will apply to both associative and dissociative mechanism.[14]

Iglesia *et al*. have studied the mechanism of methanol-to-DME dehydration over silica-supported Keggin tungsten HPA clusters $H_{8-n}X^{n+}W_{12}O_{40}$ (X = $P^{5+}$, $Si^{4+}$, $Al^{3+}$ and $Co^{2+}$).[12] Based on kinetic studies and DFT calculations, they proposed the associative mechanism for the reaction with HPA[12] as well as for the reaction over acidic Al-, Ga-, Fe- and B-MFI zeolites.[16] Linear correlations have been established between the logarithm of reaction turnover rate and deprotonation energy (DPE) of the HPA clusters and MFI zeolites derived from DFT calculations (different correlations for HPA and MFI zeolites).[12,16] Extrapolation of the rate/acid strength correlation for HPA catalysts to the DPE values characteristic of MFI zeolites (zeolites had greater DPE values than HPAs as derived from DFT calculations[12,16]) has indicated that the MFI zeolites can exhibit enhanced activity in methanol dehydration due to confinement effects within their microporous environment in comparison with the mesoporous HPA/$SiO_2$ catalysts.[16] This, however, needs to be further scrutinized because the DPE values for $SiO_2$-supported HPA clusters derived from DFT may be underestimated (i.e., catalyst acid strength overestimated) due to the DFT neglecting the effect of support on the acid strength of HPA.[23]

## 4.3 Thermodynamics of metanol-to-DME dehydration

It has been reported that the methanol-to-DME dehydration is an equilibrium controlled reaction.[1-2] Its thermodynamics has been reported for the industrially relevant temperature range of 250-360 $^{o}$C [27] (and references therein).

We calculated the equilibrium constant $K_p$ and equilibrium methanol conversion at lower temperatures relevant to this study using data[28] (as explain below). Since the reaction is volume neutral, its equilibrium is practically unaffected by the pressure and dilution.

The thermodynamic analysis includes calculation of the Gibbs free energy and equilibrium conversion for methanol-to-DME dehydration in the ideal gas system at 1 bar pressure. Initial thermodynamic data on the formation functions $\Delta_f G^o$ and $\Delta_f H^o$ together with $S^o$ and $C_p$ at standard conditions (298.15 K and 1 bar) are presented in **Table 4.1**.

**Table 4.1.** *Initial thermodynamic data (298.15 K, 1 bar).*[28]

| **Compound** | $\Delta_f H^o$ **kJ/mol** | $\Delta_f G^o$ **kJ/mol** | $S^o$ **J/mol K** | $C_p$ **J/mol K** |
|---|---|---|---|---|
| MeOH | -201.0 | -162.3 | 239.9 | 44.1 |
| DME | -184.1 | -112.6 | 266.4 | 64.4 |
| $H_2O$ | -241.8 | -228.6 | 188.8 | 33.6 |

Equations 4.2−4.6 are used for the calculations, where $K_p$ is the equilibrium constant and $X$ is the equilibrium conversion of methanol. These are practically independent of the pressure and dilution as the total number of moles of reactant and products does not change in the reaction ("volume neutral" reaction). $\Delta C_p$ was assumed to be independent of temperature, i.e., $\Delta C_p = \Delta C_p{}^o$. The results at selected temperatures are presented in **Table 4.2**.

$$\Delta H = \Delta H^o + \Delta C_p^o (T - 298.15) \quad (4.2)$$

$$\Delta S = \Delta S^o + \Delta C_p^o \ln(T/298.15) \quad (4.3)$$

$$\Delta G = \Delta H - T\Delta S \quad (4.4)$$

$$K_p = \frac{X^2}{4(1-X)^2} \quad (4.5)$$

$$X = \frac{2\sqrt{K_p}}{1+2\sqrt{K_p}} \quad (4.6)$$

**Table 4.2.** *Thermodynamics of methanol-to DME dehydrogenation.*[a]

| ***T*** **(°C)** | ***T*** **(K)** | ***ΔH*** **(kJ/mol)** | ***ΔG*** **(J/mol K)** | ***ΔS*** **(kJ/mol)** | $K_p$ | $lnK_p$ | ***x*** |
|---|---|---|---|---|---|---|---|
| 25 | 298.15 | -23.9 | -16.6 | -24.6 | 810 | 6.70 | 0.98 |
| 100 | 373.15 | -23.2 | -14.8 | -22.4 | 118 | 4.77 | 0.96 |
| 120 | 393.15 | -23.0 | -14.4 | -21.9 | 81.9 | 4.41 | 0.95 |
| 150 | 423.15 | -22.7 | -13.7 | -21.2 | 49.1 | 3.90 | 0.93 |
| 200 | 473.15 | -22.2 | -12.7 | -20.1 | 25.2 | 3.23 | 0.91 |
| 300 | 573.15 | -21.2 | -10.8 | -18.2 | 9.6 | 2.26 | 0.86 |

[a]At 1 bar, $\Delta C_p^o$ = 9.8 J/mol K.

The results are presented in **Figure 4.1**. As seen, equilibrium conversion in the temperature range of 25-300 $^{o}$C gradually decreases from 98 to 86%. This makes the low-temperature methanol-to-DME dehydration using more active catalysts (e.g., zeolites, HPA, etc.) economically desirable.

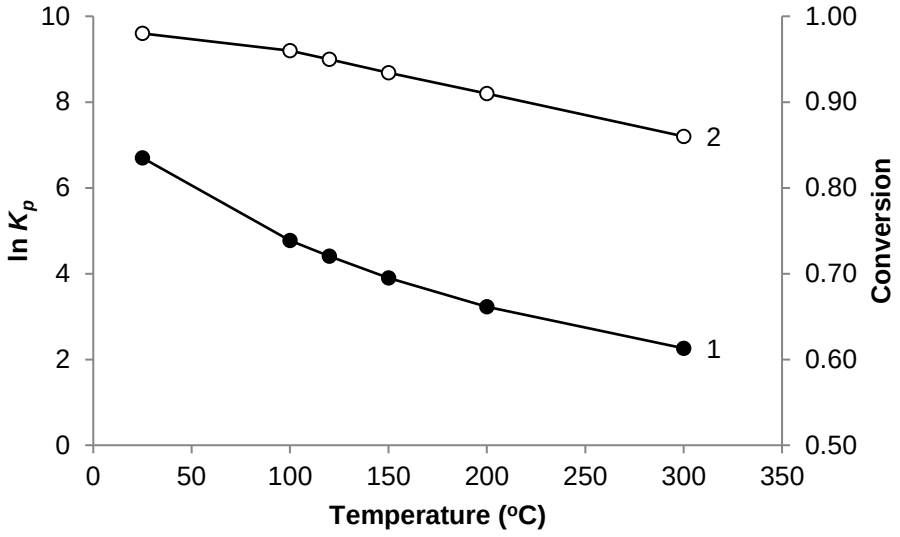


**Fig. 4.1.** Equilibrium constant $K_p$ (1) and methanol conversion (2) for methanol-to-DME dehydration as a function of temperature.

## 4.4 Methanol-to-DME dehydration over HPA catalysts

### 4.4.1 Measuring the rate of reaction

The experimental procedure was explained in detail in Chapter 2, but is briefly summarised here for clarity. The dehydration of methanol was carried out under atmospheric pressure in a Pyrex fixed-bed downflow reactor (9 mm internal diameter) fitted with on-line GC analysis (Varian Star 3400 CX instrument with a 30 m×0.32 mm×0.5 µm SUPELCOWAX 10 capillary column and a flame ionization detector) as described previously.[23-25]

The temperature in the reactor was controlled by a Eurotherm controller using a thermocouple placed at the top of the catalyst bed. The gas feed containing methanol vapor in nitrogen was obtained by passing nitrogen flow controlled by a Brooks mass flow controller through a saturator, which held liquid methanol at a controlled temperature (±1 $^{o}$C) to maintain the chosen methanol partial pressure.

Before reaction, the catalysts were pretreated in situ at the reaction temperature for 1 h in $N_2$ flow. At regular time intervals, the downstream gas flow was analyzed by the on-line GC to obtain methanol conversion and product selectivity. The selectivity was defined as the percentage of methanol converted into a particular product taking into account reaction stoichiometry; thus 100% DME selectivity would mean 1 mole of methanol converted to form 0.5 mole of DME. Typical reaction conditions, unless stated otherwise, were as follows: 0.20 g catalyst amount (45-180 μm particle size), 3.83 kPa MeOH partial pressure, 120 $^{o}$C (±0.5 $^{o}$C) temperature, 20 mL $min^{-1}$ gas flow rate ($N_2$ as a carrier gas), space time $W/F$ = 104 g h $mol^{-1}$, where $F$ is the molar flow rate of methanol (mol $h^{-1}$) and $W$ is the catalyst weight (g). The configuration of catalyst bed was appropriate to allow adequate plug-flow performance. It should be noted that methanol dehydration under the chosen conditions was a zero-order reaction hence not affected by axial dispersion in a plug-flow reactor.[26] Usually, reactions were carried out for 4 h, during which no catalyst deactivation was observed. In extended stability tests, the reaction length was up to 20 h. Reaction rates (in mol $h^{-1}g_{cat}^{-1}$) were calculated using the equation $r = XF/W$, where $X$ is the methanol conversion (typically under differential conditions at $X \leq 0.1$). The mean absolute percentage error in methanol conversion was ≤ 5%. Turnover frequencies (TOF) were calculated per surface Brønsted site as explained in the text.

## 4.4.2 The effect of temperature

The effect of temperature on methanol conversion and product selectivity for methanol dehydration over HPW, HSiW and $Cs_{2.5}H_{0.5}PW$ bulk catalysts and 20%HSiW/$SiO_2$ supported catalyst is shown in **Figure 4.2.** With the most active 20%HSiW/$SiO_2$ catalyst, methanol conversion reached an almost equilibrium value of 89% (93% at equilibrium, Table 4.2) with 100% DME selectivity at 150 $^oC$. At this temperature, the 20%HSiW/$SiO_2$ catalyst showed stable performance without deactivation for at least 4 h on stream (**Figure 4.3**); it also ran steadily for 20 h at 130 $^oC$ with 40% conversion and 100% DME selectivity (**Figure 4.4**).

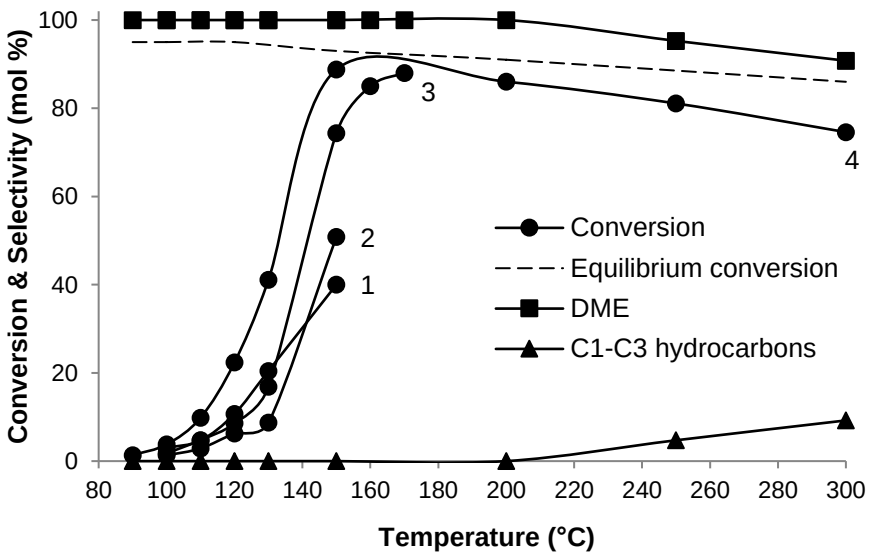


**Fig. 4.2.** Effect of temperature on methanol dehydration over HPW (1), HSiW (2) and $Cs_{2.5}H_{0.5}PW$ (3) bulk catalysts and 20%HSiW/$SiO_2$ supported catalyst (4) (0.20 g catalyst amount, 3.83 kPa methanol partial pressure, $N_2$ carrier gas, 20 mL $min^{-1}$ flow rate, space time $W/F$ = 104 g h $mol^{-1}$).

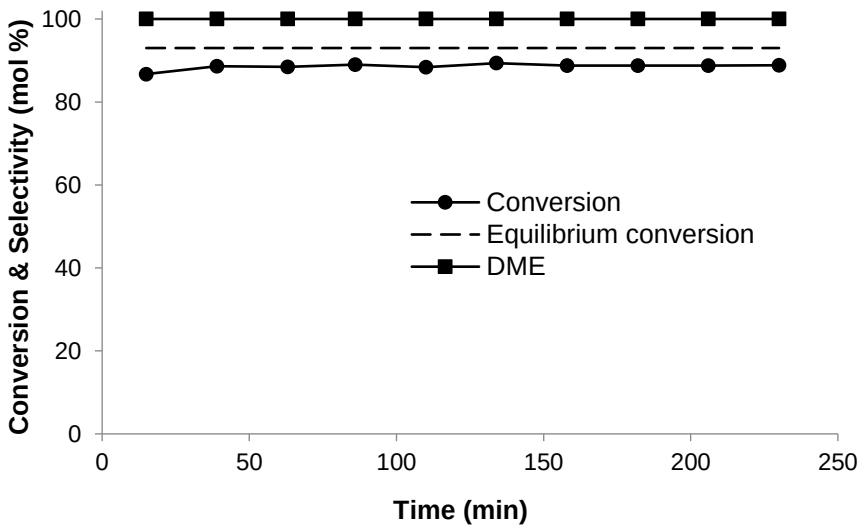


**Fig. 4.3.** Time course for methanol dehydration over 20%HSiW/$SiO_2$ (0.20 g) at 150 $^oC$ (3.83 kPa methanol partial pressure, 20 mL $min^{-1}$ flow rate, catalyst pretreatment at 150 $^oC$/1 h in $N_2$).

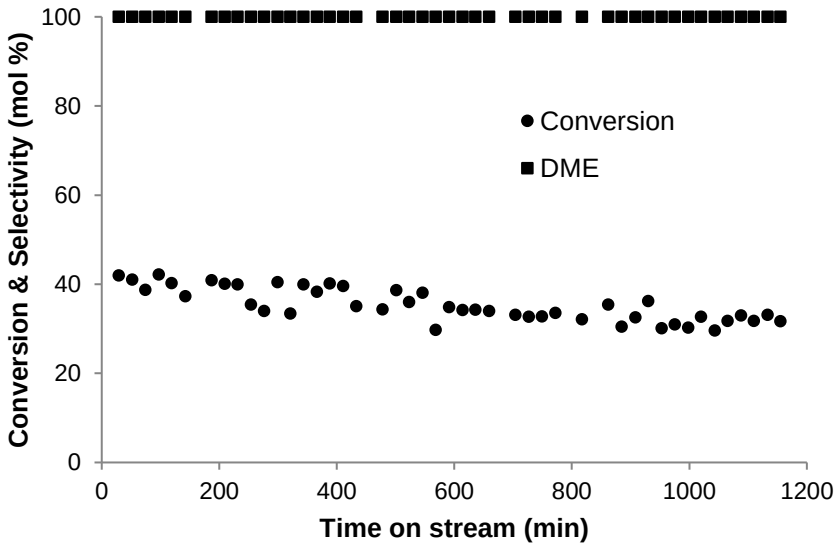


**Fig. 4.4.** Time course for dehydration of methanol over 20%HSiW/$SiO_2$ (0.20 g catalyst amount, 130 $^oC$, 3.83 kPa MeOH partial pressure, 20 mL $min^{-1}$ flow rate, catalyst pretreatment at 130 $^oC$/1 h in $N_2$).

At temperatures above 200 ºC, hydrocarbons (C1-C3 alkanes and alkenes) were also formed, decreasing DME selectivity (**Figure 4.2**). This was accompanied by catalyst deactivation probably due to coke formation as illustrated by the C H analysis of spent catalysts (**Table 4.3**). Blank tests showed no carbon present in fresh catalysts. These results are in agreement with previous reports on the methanol-to-hydrocarbon conversion over HPA catalysts. [3-4] Bulk $Cs_{2.5}H_{0.5}PW$ was less active than 20%$HSiW/SiO_2$ giving 88% conversion at 170 ºC with 100% DME selectivity. Bulk HPW and HSiW were even less active probably due to their low surface area (see **Chapter 3**, **Table 3.1**). At 150 ºC, the catalyst activity (methanol conversion, %) per unit catalyst weight decreased in the order: 20%$HSiW/SiO_2$ (89) > $Cs_{2.5}H_{0.5}PW$ (74) > HSiW (51) > HPW (40). This order is in line with the proton site densities of these catalysts, which are 0.28, 0.076, 0.042 and 0.019 mmol $g^{-1}$, respectively (see below).

**Table 4.3.** *Carbon deposits in spent catalysts.*

| **Catalyst** | **Temperature (°C)** | **C (%) (%)** | **H (%) (%)** |
|---|---|---|---|
| 20% $HSiW/SiO_2$ | 250 | 1.42 | 0.49 |
| 15% $HPW/TiO_2$ | 150 | 0.85 | 0.31 |
| HSiW | 150 | 1.34 | 0.66 |
| HPMo | 120 | 0.85 | 0.47 |
| HPW | 150 | 1.27 | 0.59 |
| $Cs_{2.5}H_{0.5}PW_{12}O_{40}$ | 150 | 0.84 | 0.27 |
| H-ZSM-5 (Si/Al=17) | 120 | 2.27 | 0.84 |

### 4.4.3 Kinetic studies

Kinetic studies under differential conditions, i.e., at methanol conversion ≤10%, showed that methanol-to-DME dehydration was zero order in methanol at methanol partial pressures 3-17 kPa and 120 $^{o}$C as illustrated in **Figure 4.5** for the reaction with 15%HSiW/$SiO_2$. The same results were obtained for 20%HSiW/$SiO_2$ and bulk HPW, HSiW and $Cs_{2.5}H_{0.5}PW$ catalysts. This is in agreement with the results reported by Iglesia *et al.*,[12] who have found a Langmuir-type rate equation for methanol dehydration over 5%HPA/$SiO_2$ catalysts, levelling off above 1 kPa methanol partial pressure at 160 $^{o}$C. Previously, zero order in alcohol has also been found in our group for ethanol and isopropanol dehydration over HPA catalysts in the same pressure range.[23-25]

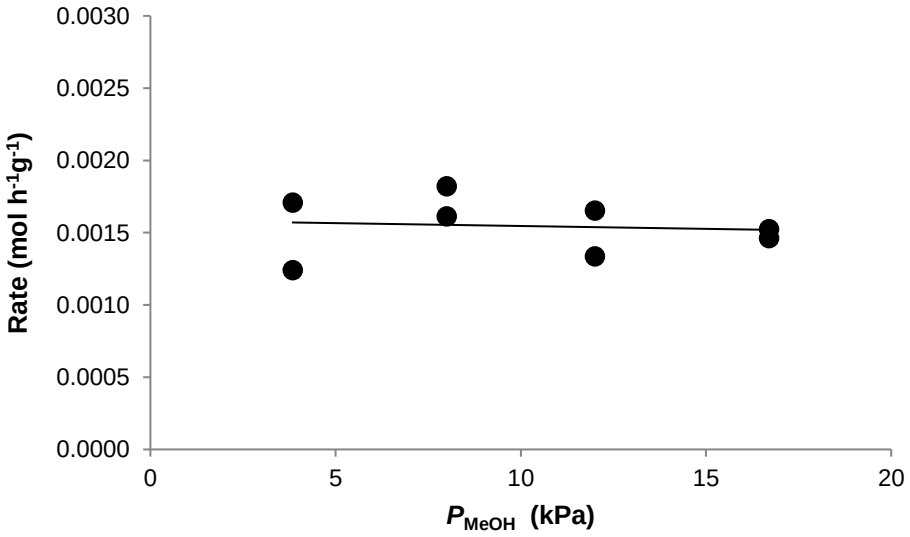


**Fig. 4.5.** Effect of methanol partial pressure on the rate of methanol dehydration over 15%HSiW/$SiO_2$ (0.20 g) at 120 $^{o}$C, 20 mL $min^{-1}$ flow rate, catalyst pretreatment at 120 $^{o}$C/1 h in $N_2$.

Methanol dehydration over 20%HSiW/$SiO_2$ obeyed the Arrhenius equation with an activation energy $E_a$ = 106 kJ $mol^{-1}$ in the temperature range of 90-130 $^oC$ (**Figure 4.6**). The same $E_a$ value was obtained when the temperature was raised and lowered. For the reaction over bulk HPW and HSiW, the activation energy was 82 and 85 kJ $mol^{-1}$, respectively (**Figure 4.7** and **Figure 4.8**). These high $E_a$ values indicate that methanol dehydration was not limited by mass transport, as it is generally suggested that the activation energy greater than 25 kJ $mol^{-1}$ indicates no diffusion limitation.[29] The absence of pore diffusion limitations was also backed up by the Weisz-Prater analysis [30] of the reaction system (Weisz-Prater criterion $C_{WP} = (1.2 – 3.7)\ 10^{-2} < 1$ indicating no internal diffusion limitations).[31]

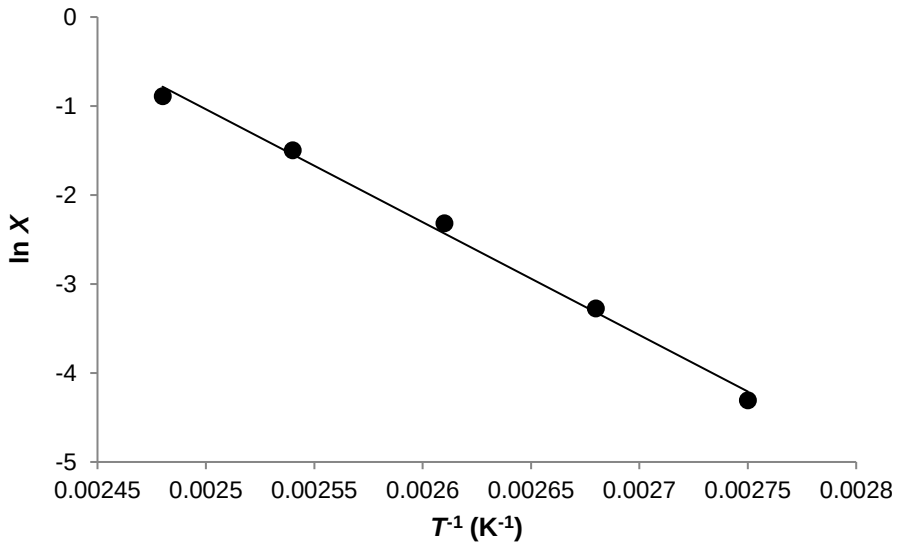


**Fig. 4.6.** Arrhenius plot for methanol dehydration over 20%HPW/$SiO_2$ where $X$ is the conversion of methanol (0.20 g catalyst amount, 3.83 kPa methanol partial pressure, $N_2$ carrier gas, 20 mL $min^{-1}$ flow rate, 90-130 $^oC$ temperature range; $E_a$ = 106 kJ $mol^{-1}$).

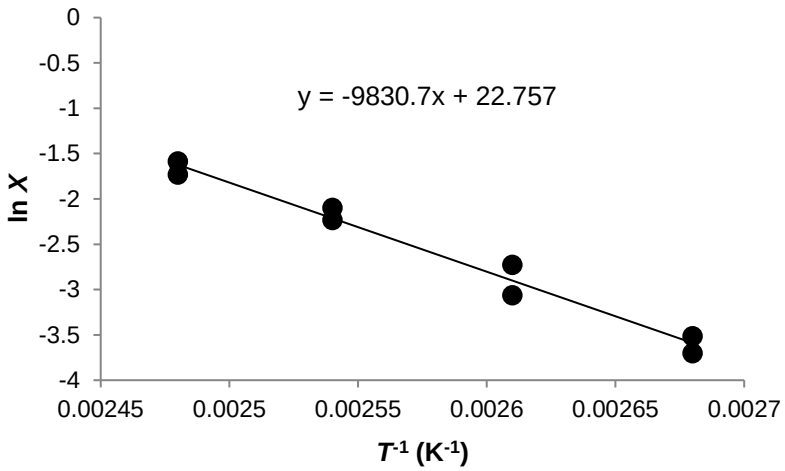


**Fig. 4.7.** Arrhenius plot for methanol dehydration over bulk HPW (0.20 g catalyst amount, 3.83 kPa MeOH partial pressure, $N_2$ carrier gas, 20 mL $min^{-1}$ flow rate, 100-130°C temperature range; $E_a$ = 81.7 kJ $mol^{-1}$).

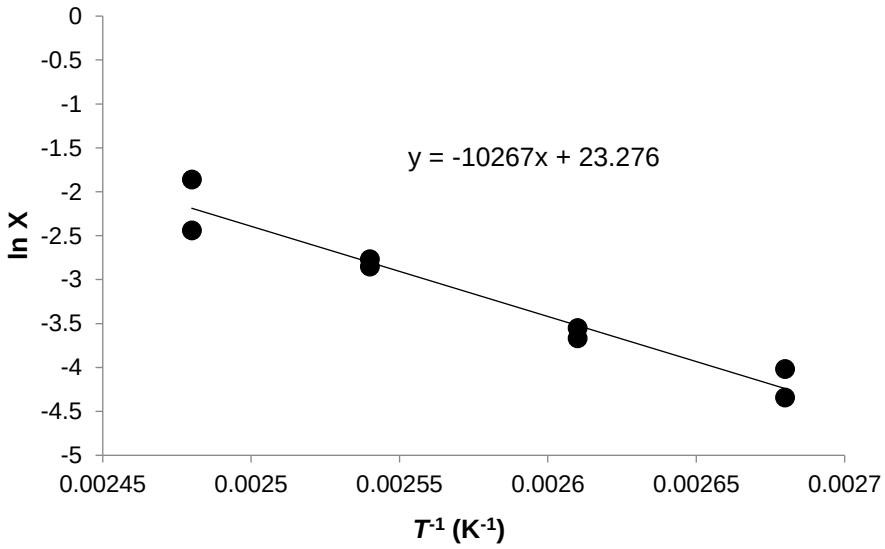


**Fig. 4.8.** Arrhenius plot for methanol dehydration over bulk HSiW (0.20 g catalyst amount, 3.83 kPa MeOH partial pressure, $N_2$ carrier gas, 20 mL $min^{-1}$ flow rate, 100-130°C temperature range; $E_a$ = 85.4 kJ $mol^{-1}$).

### 4.4.4 Turnover frequency (TOF)

Turnover frequency (TOF) is a more accurate measure of catalyst activity, which is directly related to the strength of acid sites. **Table 4.4** shows methanol conversion and turnover frequency (TOF) for the dehydration of methanol for all HPA catalysts studied at 120 $^{o}$C. At this temperature, the DME selectivity was 100%, without any byproducts observed. The results for silica-supported HPW at different HPA loadings 5-20 wt% indicate approximately first reaction order in HPA. The TOF values ($h^{-1}$) were calculated per surface proton site from the values of methanol conversion, which, given zero reaction order in methanol, are equivalent to the rate constants. The required densities of accessible proton sites were estimated as described elsewhere.[23-25] For supported HPA catalysts, which contained HPW or HSiW at sub-monolayer coverage, all HPA protons were assumed to be equally available for reaction (e.g., 0.16 and 0.21 mmol $g^{-1}$ proton density for supported 15% HPW and HSiW catalysts, respectively). This has been proved correct for silica-supported HPW by titration with $NH_3$[32] and pyridine.[33] For bulk HPW, HSiW and Cs salts of HPW, which have been suggested to catalyze alcohol dehydration through the surface type mechanism,[23-25] the number of surface protons was calculated using a Keggin unit cross section of 144 Å[17-20] and the catalyst surface areas (from Table 3.1 in chapter three): HPW (5.6 $m^2g^{-1}$, 0.019 mmol($H^+$) $g^{-1}$), HSiW (9.0 $m^2g^{-1}$. 0.042 mmol($H^+$) $g^{-1}$), $Cs_{2.5}H_{0.5}PW$ (132 $m^2g^{-1}$, 0.076 mmol($H^+$) $g^{-1}$) and $Cs_{2.25}H_{0.75}PW$ (128 $m^2g^{-1}$, 0.11 mmol($H^+$) $g^{-1}$). The TOF values thus obtained range from 0.8 $h^{-1}$ for 15%HPW/$Nb_2O_5$ to 53 $h^{-1}$ for bulk HPW indicating a strong effect of catalyst acid strength on the turnover reaction rate. This is further discussed in **Section 4.6**.

**Table 4.4.** *Dehydration of methanol over HPA catalysts*. [a]

| Catalyst | Conversion (%) | TOF [b] ($h^{-1}$) | DME selectivity (mol%) |
|---|---|---|---|
| 15%HSiW/$SiO_2$ | 13 | 6.0 | 100 |
| 15%HPW/$SiO_2$ | 16 | 9.9 | 100 |
| 15%HPW/$TiO_2$ | 8.7 | 5.4 | 100 |
| 15%HPW/$Nb_2O_5$ | 1.3 | 0.8 | 100 |
| 15%HPW/$ZrO_2$ | 1.7 | 1.0 | 100 |
| 5%HPW/$SiO_2$ | 7.1 | 13 | 100 |
| 10%HPW/$SiO_2$ | 14 | 13 | 100 |
| 20%HPW/$SiO_2$ | 24 | 11 | 100 |
| $Cs_{2.5}$PW | 8.6 | 11 | 100 |
| $Cs_{2.25}$PW | 13 | 12 | 100 |
| HPW | 11 | 53 | 100 |
| HSiW | 6.3 | 15 | 100 |

[a] 120°C, 0.20 g catalyst amount, 3.83 kPa MeOH partial pressure, $N_2$ carrier gas, 20 mL $min^{-1}$, 4 h time on stream. [b] Turnover frequency calculated as reaction rate per surface proton site.

## 4.5 Methanol-to-DME dehydration over HZSM-5 zeolites

Zeolites have been investigated extensively as the catalysts for methanol dehydration, especially HZSM-5 (MFI structure) [5, 7, 14, 16] (and references therein). Therefore, it was interesting to compare the turnover rates for HPA and HZSM-5 catalysts in the methanol-to-DME dehydration. For accurate comparison, it was essential that both catalysts were tested under the same conditions. Here we looked at commercial HZSM-5 zeolites with Si/Al atomic ratios of 10, 17, 30, 43 and 120, further denoted HZSM-5 (Si/Al).

### 4.5.1 The effect of temperature

The effect of temperature on methanol dehydration over HZSM-5(10) represents in **Figure 4.9**. Maximum methanol conversion 87% with 100% DME selectivity was achieved at 200°C (cf. 91% equilibrium conversion), with $C_2$-$C_5$ hydrocarbons appearing at 250 °C in agreement with previous report.[5] Therefore, the HZSM-5 catalyst is significantly less active than 20%HSiW/$SiO_2$ and $Cs_{2.5}H_{0.5}PW$ per unit catalyst weight.

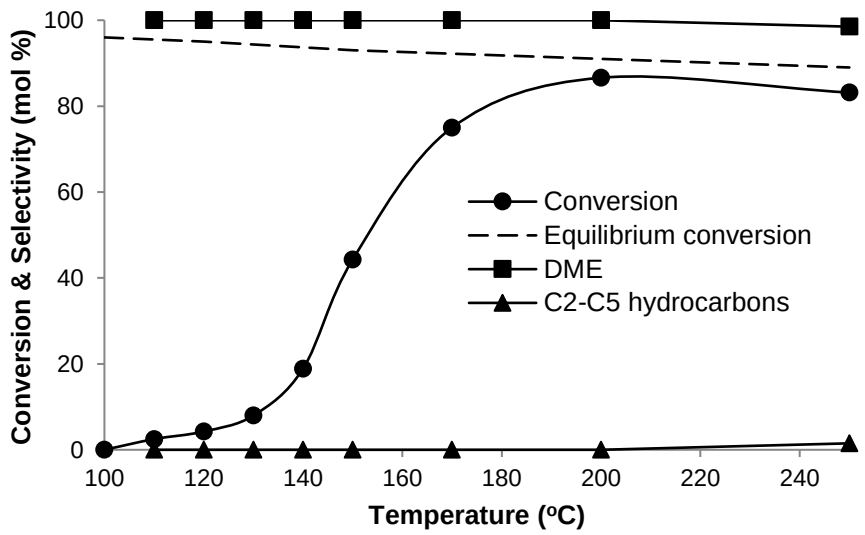


**Fig. 4.9.** Effect of temperature on methanol dehydration over HZSM-5 (Si/Al = 10) (0.20 g catalyst amount, 3.83 kPa methanol partial pressure, $N_2$ carrier gas, 20 mL $min^{-1}$ flow rate, space time *W/F* = 104 g h $mol^{-1}$).

Long-term testing demonstrated stable performance of HZSM-5(17) at 120 $^{o}$C and 200 $^{o}$C for 20 h on stream without catalyst deactivation (**Figure 4.10-4.11**).

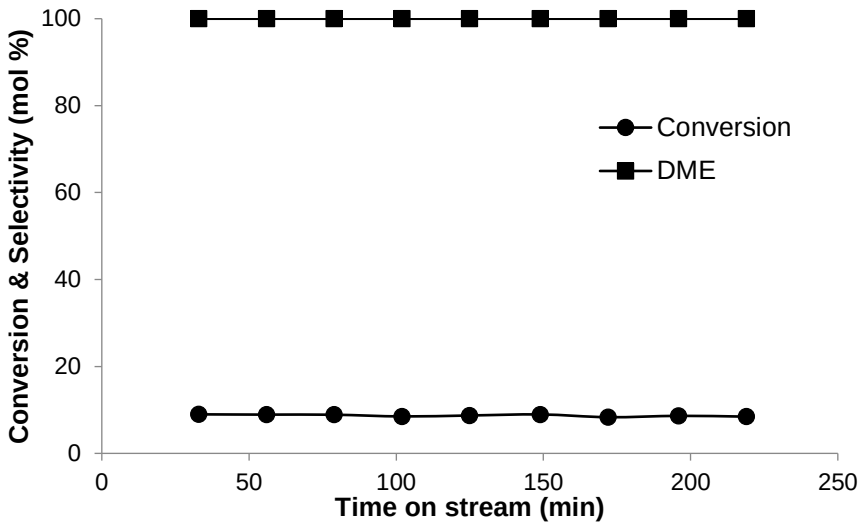


**Fig. 4.10.** Time course for dehydration of methanol over HZSM-5(17) (0.20 g catalyst amount, 120 $^{o}$C, 3.83 kPa methanol partial pressure, 20 mL min$^{-1}$ flow rate, catalyst pretreatment at 120 $^{o}$C/1 h in $N_2$).

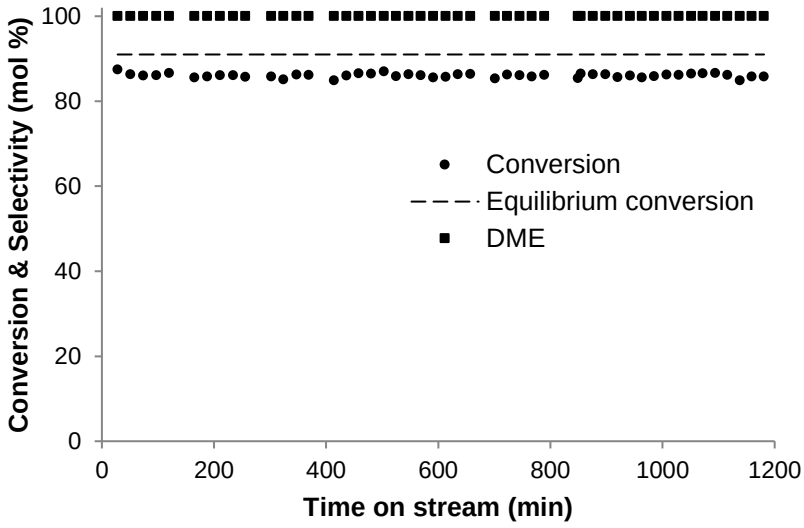


**Fig. 4.11.** Time course for methanol dehydration over HZSM-5(17) (200 $^{o}$C, 0.20 g catalyst amount, 3.83 kPa methanol partial pressure, $N_2$ carrier gas, 20 mL min$^{-1}$ flow rate, catalyst pretreatment at 200$^{o}$C/1 h in $N_2$).

## 4.5.2 Kinetic studies

Similar to HPA catalysts, the reaction with HZSM-5 had low order in methanol and high activation energy, e.g., for HZSM-5(10) the order in methanol was 0.23 at 3-17 kPa methanol partial pressure (**Figure 4.12**) and the activation energy $E_a$ = 95 kJ mol$^{-1}$ (**Figure 4.13**). This is in agreement with previous studies.[16]

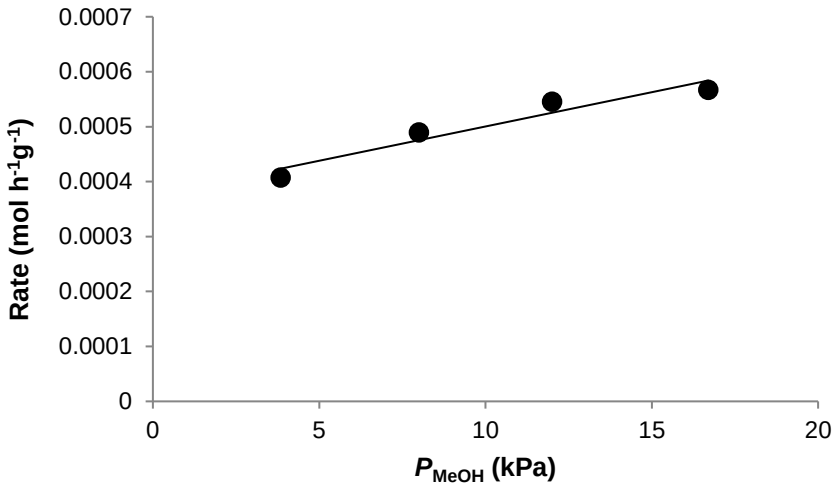


**Fig. 4.12.** Effect of methanol partial pressure on the rate of methanol dehydration over HZSM-5(10) (0.20 g) at 120°C, 20 mL min$^{-1}$ flow rate, catalyst pretreatment at 120°C/1 h in $N_2$; reaction order in methanol, 0.23.

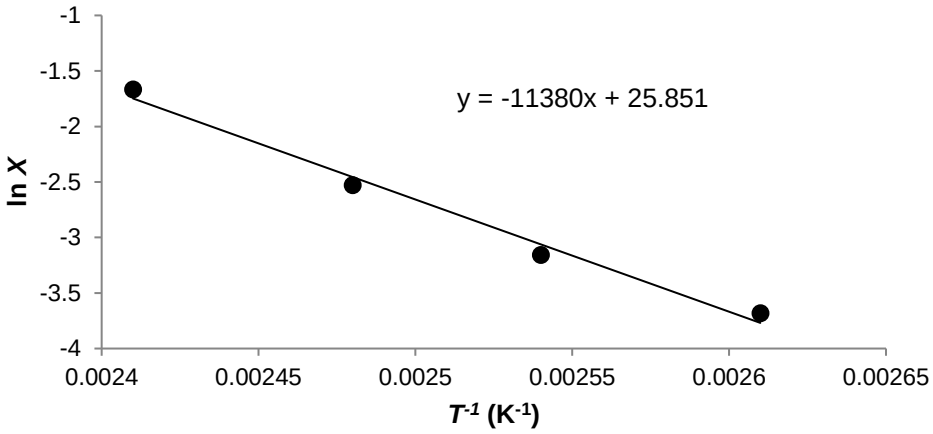


**Fig. 4.13.** Arrhenius plot for methanol dehydration over HZSM-5(10) (0.20 g catalyst amount, 3.83 kPa methanol partial pressure, $N_2$ carrier gas, 20 mL $min^{-1}$ flow rate, 110-140°C temperature range; $E_a$ = 95 kJ $mol^{-1}$).

## 4.5.3 Turnover frequency (TOF)

The values of TOF for HZSM-5 zeolites were determined at 120°C at differential conditions (methanol conversion <10%) (**Table 4.5**). The TOF values ($h^{-1}$) were calculated as the rate per zeolite proton site . The proton site densities were assumed to be equal to the Al content in zeolites and calculated from the Si/Al ratios . For highly crystalline HZSM-5 zeolites, this gives accurate enough acidities, which agree with experimental values.[16] The TOF values for the HZSM-5 zeolites studied range between 0.14 – 1.03 $h^{-1}$ and are much lower than those for HPA catalysts.

**Table 4.5** also shows the values of initial enthalpy of ammonia adsorption ($\Delta H_{NH3}$) for three selected HZSM-5 zeolites with Si/Al ratios of 10, 30 and 120. These were measured at 150 °C under flow conditions ($N_2$ carrier gas) after pretreament at 150 °C, i.e., under conditions close to those for methanol dehydration reaction. The $\Delta H_{NH3}$ values obtained range from -120 to -140 kJ $mol^{-1}$ and display the order of zeolite acid strength as follows: HZSM-5(10) < HZSM-5(30) > HZSM-5(120), i.e., the acid strength peaks for HZSM-5(30).

This order of zeolite acid strength is in agreement with the literature and has been discussed in detail elsewhere.[34] Therefore, the HZSM-5 zeolites have weaker acid sites than the most of HPA catalysts studied (see chater 3 Table 3.3), which agrees with the TOF values obtained for these catalysts. It should be noted that our $\Delta H_{NH3}$ values for HZSM-5 zeolites are predictably lower than those usually quoted in the literature, -130 to -150 kJ mol$^{-1}$ (Si/Al = 20-70).[34-35] The reason for this is that the latter values have been measured after pretreatment at 400-500 $^{o}$C, which generated stronger acid sites in zeolites.[34]

**Table 4. 5.** *Methanol dehydration over HZSM-5 zeolite catalysts* [a]

| **Si/Al**[b] | **Proton site density** [c] **mmol g$^{-1}$** | **Conversion %** | **DME selectivity mol%** | **Rate ×10$^{4}$ mol h$^{-1}$g$^{-1}$** | **TOF** [d] **h$^{-1}$** | **$\Delta H_{NH3}$**[e] **kJ mol$^{-1}$** |
|---|---|---|---|---|---|---|
| 10 | 1.52 | 4.4 | 100 | 4.2 | 0.28 | -123 |
| 17 | 0.93 | 8.7 | 100 | 8.4 | 0.91 | |
| 30 | 0.54 | 5.8 | 100 | 5.6 | 1.03 | -140 |
| 43 | 0.38 | 3.9 | 100 | 3.7 | 0.99 | |
| 120 | 0.14 | 1.1 | 100 | 1.1 | 0.77 | -120 |

[a] 0.20 g catalyst amount, 120$^{o}$C, 3.83 kPa methanol partial pressure, $N_2$ carrier gas, 20 mL min$^{-1}$, 4 h time on stream, catalyst pretreatment at 120$^{o}$C/1 h in $N_2$. [b] Si/Al atomic ratio from ICP analysis. [c] Calculated from Si/Al ratio. [d] TOF calculated as the rate per zeolite proton site. [e] Initial enthalpy of $NH_3$ adsorption at 150$^{o}$C.

**Figure 4.15** shows the plot of methanol conversion and TOF for methanol-to-DME dehydration over HZSM-5 zeolite catalysts versus Si/Al atomic ratio. Both dependencies peak at intermediate values of the Si/Al ratio (conversion at Si/Al = 17 and TOF at 30) and therefore both follow the trend in the acid strength of HZSM-5 zeolites (**Table 4.4**). Similar dependencies have been reported previously for other reactions; for a review see.[34]

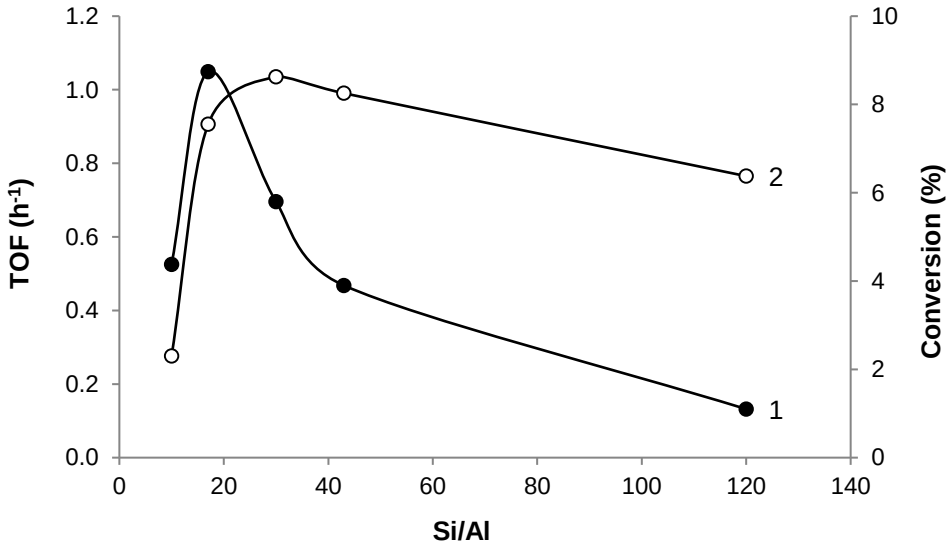


**Fig. 4.15.** Plot of methanol conversion (trace 1) and TOF (trace 2) for methanol-to-DME dehydration over HZSM-5 zeolite catalysts versus Si/Al atomic ratio (120 $^{o}$C, 0.20 g catalyst amount, 3.83 kPa methanol partial pressure, $N_2$ carrier gas, 20 mL $min^{-1}$ flow rate, catalyst pretreatment at 120$^{o}$C/1 h in $N_2$).

## 4.6 The relation between turnover rate and catalyst acid strength

The relationship between the rate of acid catalyzed reaction and the catalyst acid strength is well documented both in homogeneous and heterogeneous acid catalysis.[36-37] Usually, it is applied in the form of linear free energy relationship for a reaction with a series of acid catalysts of different acid strength. The first example of such relationship is the well-known Brønsted equation, which represents the relationship between the rate constant of acid- or base-catalyzed reaction and the ionization constant of the catalyst.[35] It is widely accepted that a reaction system (i.e., the series of reactants and/or catalysts involved) obeys a Brønsted-type relationship if reaction mechanism does not change within the series.[36] Therefore, the rate/acid strength relationship is an important mechanistic tool in acid catalysis.

**Figure 4.16** shows a fairly good linear relationship between the activity of HPA catalysts in methanol-to-DME dehydration, ln (TOF), and their initial enthalpy of ammonia adsorption ($\Delta H_{NH_3}$). Note that, for better compatibility, the two sets of parameters were determined experimentally under rather similar conditions: the TOF values are referred to the reaction at 120 °C in continuous flow reactor (**Table 4.3**) and the $\Delta H_{NH_3}$ values were measured at 150 °C under flow conditions after pretreatment at 150 °C. This relationship implies that Brønsted acid sites play an important role in methanol-to-DME dehydration over HPA catalysts, as represented in **Scheme 4.1**. As seen, both supported HPA catalysts, bulk Cs salts, and bulk HPA obey this plot. This indicates that all these HPA catalysts operate through the same mechanism of surface catalysis,[17–20] including the bulk HPAs, for which another mechanism, namely, a bulk catalysis mechanism, has hitherto been suggested[17] (for more discussion, see refs [23–25]). This relationship may be used to predict the activity of other Brønsted acid catalysts in methanol-to DME dehydration from their $\Delta H_{NH_3}$ values and vice versa.

The important result is that HZSM-5 zeolites also obey this relationship (**Figure 4.16**). This indicates that both HPA and HZSM-5 operate in the methanol-to-DME reaction through the same (or similar) mechanism, either associative or dissociative (**Scheme 4.1**). This also implies that confinement in HZSM-5 micropores hardly provides any enhancement of catalytic activity, compared to mesoporous HPA catalysts. The turnover rate of methanol dehydration for both catalysts is primarily determined by the strength of catalyst acid sites, regardless of the catalyst pore geometry. Evidence to the contrary[16] has come from the rate/acid strength correlation, where the acid strength of silica-supported HPA catalysts was represented by deprotonation energies derived from DFT calculations. The latter probably did not take into account the effect of support on the HPA acid strength, which is evident from the experimental $\Delta H_{NH_3}$ values. Therefore, the present study could serve as the basis for further investigations into the mechanism of methanol-to-DME dehydration.

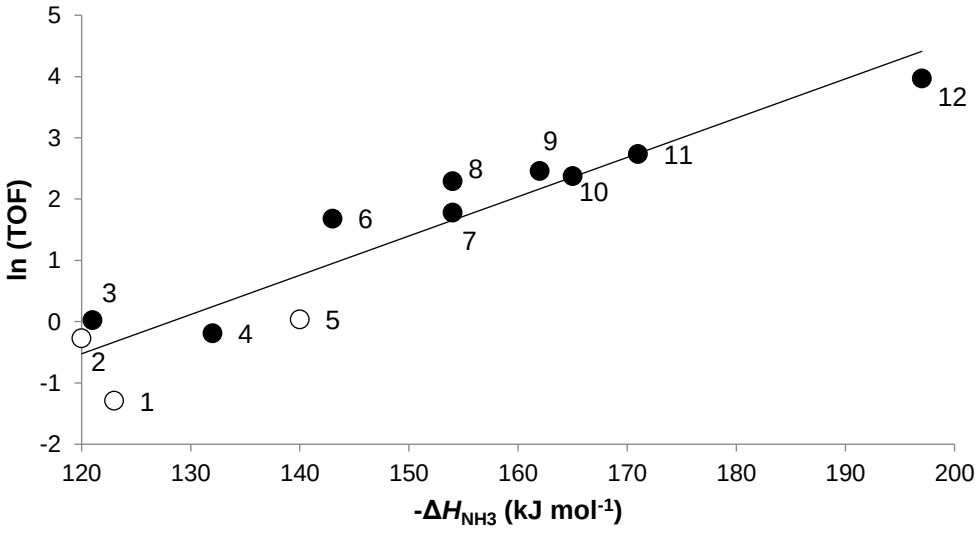


**Fig. 4.16.** Plot of ln (TOF) for methanol dehydration (TOF in $h^{-1}$) over tungsten HPA catalysts (closed circles) and HZSM-5 (open circles) versus initial heat of $NH_3$ adsorption (120 °C, 0.20 g catalyst amount, 3.83 kPa methanol partial pressure, $N_2$ carrier gas, 20 mL $min^{-1}$ flow rate; (1) HZSM-5(10), (2) HZSM-5(120), (3) 15%HPW/$ZrO_2$, (4) 15%HPW/$Nb_2O_5$, (5) HZSM-5(30), (6) 15%HPW/$TiO_2$, (7) 15%HPW/$SiO_2$, (8) 15%HSiW/$SiO_2$, (9) $Cs_{2.25}H_{0.75}PW$, (10) $Cs_{2.5}H_{0.5}$ PW, (11) bulk HSiW, (12) bulk HPW.

## 4.7 Conclusion

The methanol-to-DME dehydration has been studied at a gas-solid interface over a wide range of bulk and supported Brønsted acid catalysts based on tungsten Keggin heteropoly acids (HPA) and compared with the reaction over HZSM-5 zeolites (Si/Al = 10−120). Turnover rates for all these catalysts have been measured under zero-order reaction conditions. The HPA catalysts have been demonstrated to have much higher catalytic activities than the HZSM-5 zeolites. A good correlation between the turnover rates and catalyst acid strengths represented by the initial enthalpies of ammonia adsorption has been established. This correlation holds for all the HPA and HZSM-5 catalysts studied, which indicates that the methanol-to-DME dehydration with both HPA and HZSM- 5 catalysts occurs via the same (or similar) mechanism, either associative or dissociative. The turnover rate of methanol dehydration for both catalysts is primarily determined by the strength of catalyst acid sites, regardless of the catalyst pore geometry.

## 4.8 Reference


1. T. H. Fleisch, A. Basu, R. A Sills, J. Nat. Gas Sci. Eng., 8 (2012) 94.
2. F. Pontzen, W. Liebner, V. Gronemann, M. Rothaemel, B. Ahlers, Catal. Today, 171 (2011) 242.
3. T. Hibi, K. Takahashi, T. Okuhara, M. Misono, Y. Yoneda, Appl. Catal., 24 (1986) 69.
4. J. C. Highfield, J. B. Moffat, J. Catal., 98 (1986) 245.
5. S. Jiang, J. S. Hwang, T. Jin, T. Cai, W. Cho, Y. S. Baek, S. E. Park, Bull. Korean Chem. Soc., 25 (2004) 185.
6. V. Vishwanathan, Catal. Lett., 96 (2004) 23.
7. Y. Fu, T. Hong, J. Chen, A. Auroux, J. Shen, Thermochim. Acta., 434 (2005) 22.
8. D. Varisli, C. K. Tokay, A. Ciftci, T. Dogu, G. Dogu, Turk. J. Chem., 33 (2009) 355.
9. C. W. Seo, K. D. Jung, K. Y. Lee, K. S. Yoo, J. Ind. Eng. Chem., 15 (2009) 649.
10. M. Mollavali, F. Yaripour, S. Mohammadi-Jam, H. Atashi, Fuel Process. Technol., 90 (2009) 1093.
11. K. Lertjiamratn, P. Praserthdam, M. Arai, J. Panpranot, Appl. Catal. A., 378 (2010) 119.
12. R. T. Carr, M. Neurock, E. Iglesia, J. Catal., 278 (2011) 78.
13. A. Ciftci, D. Varisli, C. K. Tokay, N. A. Sezgi, T. Dogu, Chem. Eng. J., 207 (2012) 85.
14. P. G. Moses, J. K. Nørskov, ACS Catal., 3 (2013) 735.
15. R. M. Ladera, J. L. G. Fierro, M. Ojeda, S. Rojas, J. Catal., 312 (2014) 195.
16. A. L Jones, R. T. Carr, S. I. Zones, E. Iglesia, J. Catal., 312 (2014) 58.
17. T. Okuhara, N. Mizuno, M. Misono, Adv. Catal., 41 (1996) 113.
18. I. V. Kozhevnikov, Chem. Rev., 89 (1998) 171.
19. N. Mizuno, M. Misono, Chem. Rev., 98 (1998) 199.
20. I. V. Kozhevnikov, Catalysis by Polyoxometalates; Wiley & Sons: Chichester, England, 2002.

21. S. R. Blaszkowski, R. A. Van Santen, J. Phys. Chem., 101 (1997) 2292.

22. D. Lesthaeghe, V. Van Speybroeck, G. B Marin, M. Waroquier, Angew. Chem. Int. Ed., 45 (2006) 1714.

23. A. M.Alsalme, P. V. Wiper, Y. Z. Khimyak, E. F. Kozhevnikova, I. V. Kozhevnikov, J. Catal., 276 (2010) 181.

24. G. C. Bond, S. J. Frodsham, P. Jubb, E. F. Kozhevnikova, I. V. Kozhevnikov, J. Catal., 293 (2012) 158.

25. W. Alharbi, E. Brown, E. F. Kozhevnikova, I. V. Kozhevnikov, J. Catal., 319 (2014) 174.

26. F. Kapteijn, J. A. Moulijn, in Handbook of Heterogeneous Catalysis, G. Ertl, H. Knözinger, F. Schüth, J. Weitkamp, (Eds). Vol. 4, Wiley-VCH, Weinheim, 2008.

27. B. T. Diep, M. S Wainwright, J. Chem. Eng. Data, 32 (1987) 330.

28. W. M Haynes, CRC Handbook of Chemistry and Physics, (Eds.); CRC Press, 2012.

29. R. Klaewkla, M. Arend and W. F. Hoelderich, Mass Transfer-Advanced Aspects, In Tech, Germany, 2011.

30. P. B. Weisz, C. D. Prater, Adv. Catal., 6 (1954) 143.

31. W. Alharbi, E. F. Kozhevnikova, I. V. Kozhevnikov, ACS Catal., 5 (2015) 7186.

32. E. F. Kozhevnikova, I. V. Kozhevnikov, J. Catal., 224 (2004) 164.

33. J. Macht, M. Janik, M. Neurock, E. Iglesia, J. Am. Chem. Soc., 130 (2008) 10369.

34. A. Auroux, Top. Catal., 4 (1997) 71.

35. M. Brandle, J. Sauer, J. Am. Chem. Soc., 120 (1998) 1556.

36. R. P. Bell, The Proton in Chemistry, 2nd ed., Chapman and Hall, London, 1973.

37. H. G. Karge, in Handbook of Heterogeneous Catalysis, Ed. G. Ertl, H. Knözinger, F. Schüth, J. Weitkamp, Vol. 2, Wiley-VCH: Weinheim, 2008.

# Chapter 5. Dehydration of ethanol over heteropoly acid catalysts in the gas phase

## 5.1 Introduction

The dehydration of ethanol (equations 5.1 and 5.2) has long been of interest to produce ethene and diethyl ether (DEE) from non-petroleum renewable feedstock.[1] In the last decade, this reaction has attracted significant attention in the context of sustainable development.[2] Ethene is the feedstock for about 30% of all petrochemicals, and diethyl ether is a valuable chemical and a green transportation fuel alternative.[3, 4] Typically, the dehydration of ethanol is carried out in the gas phase in the presence of solid acid catalysts such as metal oxides and zeolites.[5-8]

$$CH_3CH_2OH \longrightarrow CH_2{=}CH_2 + H_2O \qquad (\mathbf{5.1})$$

$$2CH_3CH_2OH \longrightarrow (CH_3CH_2)_2O + H_2O \qquad (\mathbf{5.2})$$

DEE is the thermodynamically favoured product; it is predominantly formed at lower temperatures, whereas the selectivity to ethene increases with increasing reaction temperature at the expense of DEE.[1]

Heterogeneous acid catalysis by heteropoly acids (HPAs) has attracted much interest in both fundamental and applied research because of its potential to generate significant economic and environmental benefits. The majority of catalytic applications use the most stable and easy available Keggin HPAs comprising heteropoly anions of the formula $[XM_{12}O_{40}]^{n-}$, where X is the heteroatom ($P^{V}$, $Si^{IV}$, etc.) and M is the addendum atom ($Mo^{VI}$, $W^{VI}$, etc.). HPAs possess strong Brønsted acidity superior to that of conventional solid acid catalysts such as acidic oxides and zeolites.[9-13]

Amongst various heteropoly acids, tungsten HPAs are usually chosen as acid catalysts because of their stronger acidity and higher thermal stability compared to molybdenum HPAs.[9-13] HPAs and their acidic salts have been applied as the catalysts for ethanol dehydration and found to exhibit higher catalytic activities than the oxide and zeolite catalysts.[14-16]

The aim of this work was to investigate a wide range of HPA based catalysts in ethanol dehydration at a gas–solid interface focusing on the formation of DEE rather than ethene, which has been the target of much previous work. In particular, we looked at the effect of catalyst acid strength on the turnover rate of this reaction. Amongst the catalysts studied are $H_3PW_{12}O_{40}$ (HPW) and $H_4SiW_{12}O_{40}$ (HSiW) supported on $SiO_2$, $TiO_2$, $Nb_2O_5$ and $ZrO_2$ with sub-monolayer HPA coverage. Also we studied bulk acidic Cs salts of HPW ($Cs_{2.5}H_{0.5}PW_{12}O_{40}$ and $Cs_{2.25}H_{0.75}PW_{12}O_{40}$, thereafter abbreviated as $Cs_nH_{3-n}PW$) and the corresponding core–shell materials with the same total composition (15%HPW/$Cs_3PW_{12}O_{40}$ and 25%HPW/$Cs_3PW_{12}O_{40}$, respectively) comprising HPW supported on the neutral salt $Cs_3PW_{12}O_{40}$. It has been claimed that the core–shell catalysts are superior to the bulk Cs salts regarding their acid strength and catalytic activity.[17]

## 5.2 Mechanism of ethanol dehydration over solid acid catalysts

The dehydration of ethanol to yield ethene (equation 5.1) is suggested to occur through E2 elimination pathway (bimolecular elimination), which involves concerted cleavage of C–O and C–H bonds in alcohol using a pair of acid and base catalyst sites (**Scheme 5.1**).[18]

The formation of DEE (equation 5.2) may be represented by two different pathways termed the associative pathway and the dissociative pathway (**Scheme 5.2**), similar to the mechanism proposed for the formation of dimethyl ether from methanol.[19, 20]

Both pathways are thought to take place at Brønsted acid sites. The associative (concerted) pathway, involves adsorption of two alcohol molecules, which react and form the ether directly. The dissociative (stepwise) pathway involves initial alcohol adsorption, followed by water elimination, leading to adsorbed alkyl group and water. The alkyl group reacts with a second alcohol molecule to form the ether.

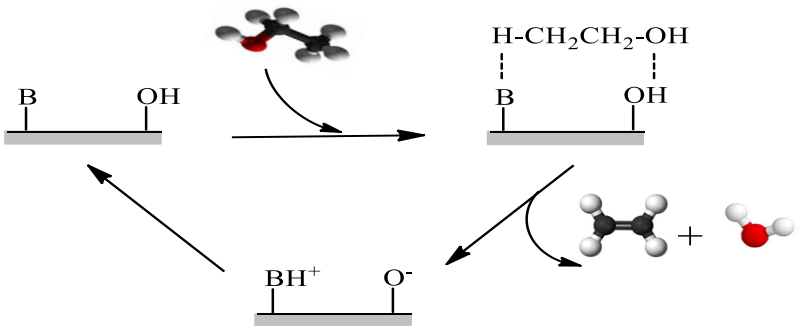


**Scheme 5.1.** E2 elimination of ethanol to form ethene at base (B) and Brønsted acid (OH) catalyst sites.

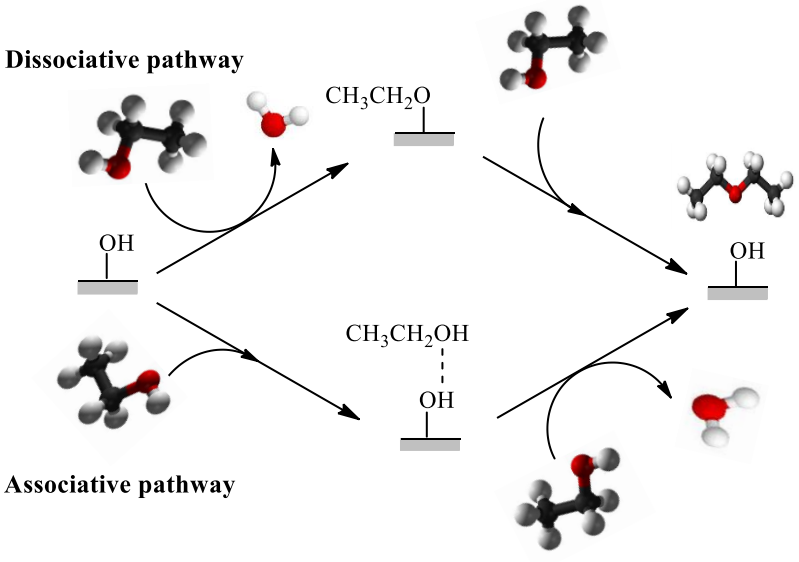


**Scheme 5.2.** Associative and dissociative pathways for ethanol-to-DEE reaction.

## 5.3 Ethanol dehydration over HPA catalysts

### 5.3.1 Measuring the reaction rate

The dehydration of ethanol was carried out under atmospheric pressure in a Pyrex fixed-bed downflow reactor (9 mm internal diameter) fitted with on-line GC analysis (Varian Star 3400 CX instrument with a 30 m×0.32 mm×0.5 μm SUPELCOWAX 10 capillary column and a flame ionisation detector) as described previously.[21-22] The temperature in the reactor was controlled by a Eurotherm controller using a thermocouple placed at the top of the catalyst bed. The gas feed containing ethanol vapour in nitrogen was obtained by passing nitrogen flow controlled by a Brooks mass flow controller through a saturator, which held liquid ethanol at a controlled temperature (±1$^{o}$C) to maintain the chosen ethanol partial pressure. Typical reaction conditions were: 0.2 g catalyst (45-180 μm particle size), 1.48 kPa EtOH partial pressure, 100-120 $^{o}$C (±0.5 $^{o}$C) temperature (90-220 $^{o}$C temperature range in light-off tests) and 20 mL min$^{-1}$ gas flow rate ($N_2$ as a carrier gas). Similar procedure was used for the dehydration of isopropanol. The configuration of catalyst bed was appropriate to allow adequate plug-flow performance. It should be noted that ethanol dehydration under the chosen conditions was a zero-order reaction, hence not affected by axial dispersion in a plug-flow reactor.[23] Before reaction, the catalysts were pre-treated in situ at the reaction temperature for 1 h in $N_2$ flow. At regular time intervals, the downstream gas flow was analysed by the on-line GC to obtain ethanol conversion and product selectivity. Typically, reactions were carried out for 3 h, during which no catalyst deactivation was observed. In individual stability tests, the reaction length was up to 20 h. The mean absolute percentage error in ethanol conversion was ≤ 5%. Reaction rates (in mol h$^{-1}$g$_{cat}^{-1}$) were calculated using the equation $r = XF/W$, where $X$ is the fractional ethanol conversion, $F$ is the molar flow rate of ethanol (mol h$^{-1}$) and $W$ is the catalyst weight (g). Typically the reaction rates were measured under differential conditions at $X \leq 0.1$ far from equilibrium. Equilibrium values of $X$ are 0.98 and 0.90 at 25 and 200 $^{o}$C, respectively.[24]

In some cases, to mantain the differential conditions, the amount of catalyst was reduced and diluted with silica to 0.2 g. Turnover frequencies (TOF) were calculated per surface Brønsted site as explained in the text.

### 5.3.2 The effect of temperature

The effect of temperature on ethanol conversion and product selectivity for ethanol dehydration over supported HPA catalysts 15%HPW/$SiO_2$ and 15%HSiW/$SiO_2$ as well as over the bulk acidic salt $Cs_{2.5}H_{0.5}PW$ is shown in **Figure 5.1**. Equilibrium conversion of ethanol for the temperature range relevant to this study was calculated using data.[24]

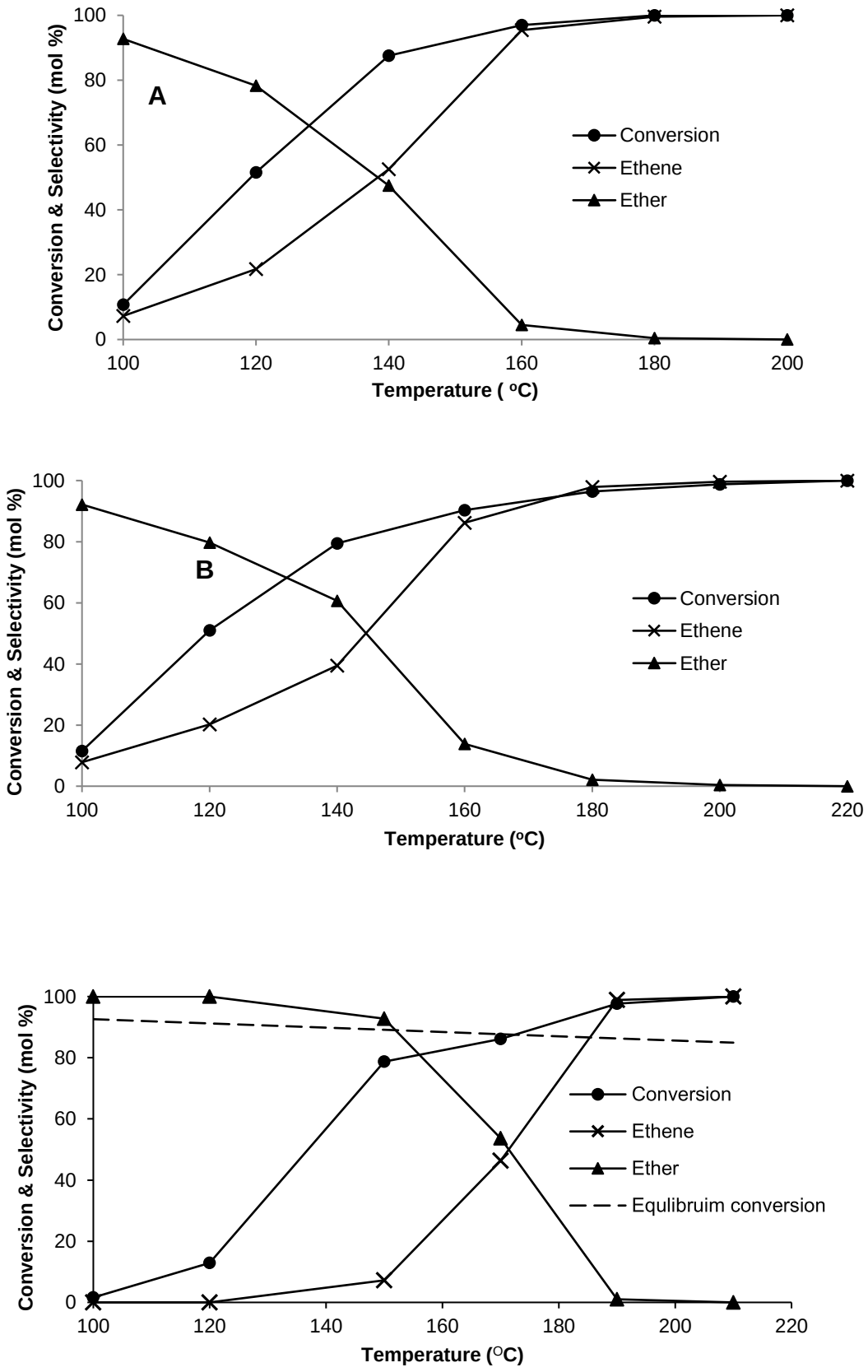


**Fig. 5.1.** Effect of temperature on ethanol dehydration over 15%HPW/$SiO_2$ (A), 15%HSiW/$SiO_2$, (B) and $Cs_{2.5}H_{0.5}PW$ (C) (0.2 g, 1.48 kPa EtOH partial pressure, $N_2$ carrier gas, 20 mL $min^{-1}$ flow rate).

With all these catalysts, the reaction yielded ethene and DEE as the only products, in agreement with previous reports.[14-16] It should be noted that these catalysts showed very good performance stability; no catalyst deactivation was observed at least for 20 h time on stream at 120 °C (**Figure 5.2**).

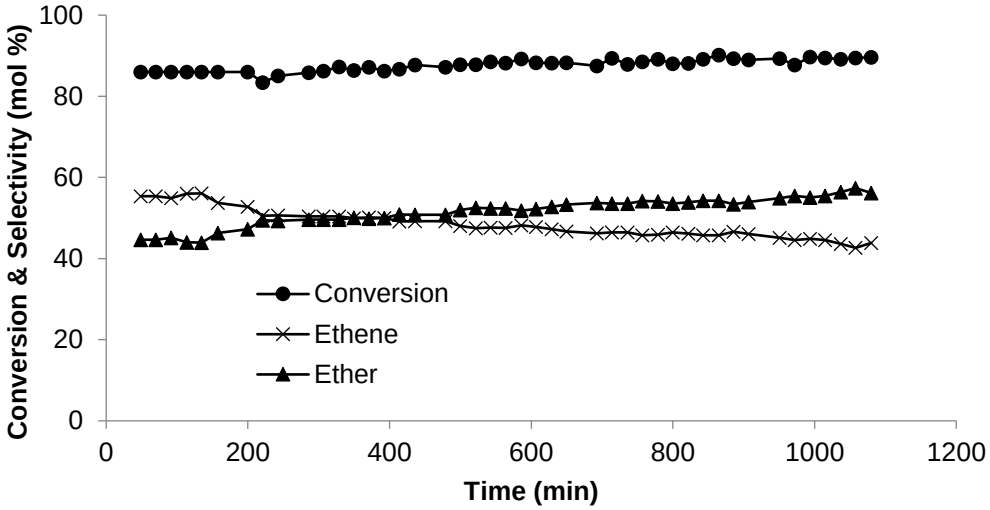


**Fig. 5.2.** Time course for ethanol dehydration over 20%HSiW/$SiO_2$ (0.2 g, 120 °C, 1.48 kPa EtOH partial pressure, $N_2$ carrier gas, 20 mL $min^{-1}$ flow rate).

The ethanol-to-DEE reaction is thermodynamically favoured at lower temperatures (the standard reaction enthalpy $\Delta H^{298}$ = -24.3 kJ $mol^{-1}$), resulting in high DEE selectivities at 90-120 °C. Equilibrium ethanol-to-DEE conversion decreases from 98 to 90% in the temperature range 25-200 °C.[24] In contrast, the ethanol-to-ethene reaction ($\Delta H^{298}$ = 45.4 kJ $mol^{-1}$) is favoured at higher temperatures hence the selectivity to ethene increases with the temperature at the expense of DEE, along with ethanol conversion, reaching 100% at around 200 °C. Despite its stronger acid strength, $Cs_{2.5}H_{0.5}PW$, with an initial enthalpy of $NH_3$ adsorption of $\Delta H_{NH3}$ = -164 kJ $mol^{-1}$, was less active than 15%HPW/$SiO_2$ and 15%HSiW/$SiO_2$ ($\Delta H_{NH3}$ = -154 kJ $mol^{-1}$ for both).

This can be explained by the lower density of surface proton sites in the Cs salt (0.076 mmol $g^{-1}$) compared to the supported 15%HPW/$SiO_2$ and 15%HSiW/$SiO_2$ catalysts (0.156 and 0.208 mmol $g^{-1}$, respectively) (see below for proton site density determination). The less active $Cs_{2.5}H_{0.5}PW$ salt, however, gave a higher DEE selectivity (90% at 50% conversion, 130 $^{o}$C) compared to ~80% selectivity for the supported HPW and HSiW at the same ethanol conversion (**Figure 5.1**).

### 5.3.3 Kinetic studies

**Figure 5.3** shows that the rate of ethanol dehydration over $Cs_{2.5}H_{0.5}PW$ did not depend on the partial pressure of ethanol in the gas feed in the range of 1.48 – 10.2 kPa. These measurements were carried out under differential conditions at ethanol conversion $X \leq 0.1$, where the reaction rate is directly proportional to $X$. Under such conditions the selectivity to DEE was 96-100%. This implies that the ethanol-to-DEE reaction is zero order in ethanol, i.e., catalyst active sites are saturated with ethanol (**Scheme 5.2**), which is typical of alcohol dehydration over solid acid catalysts in the gas phase at such alcohol pressures.[20-22] It should be noted that for the dehydration of isopropanol and 2-butanol over silica-supported HPA catalysts at lower alcohol pressures 0.05-0.5 kPa Macht *et al*.[25] have reported rate inhibition with increasing the alcohol pressure. No such effect was observed under our reaction conditions.

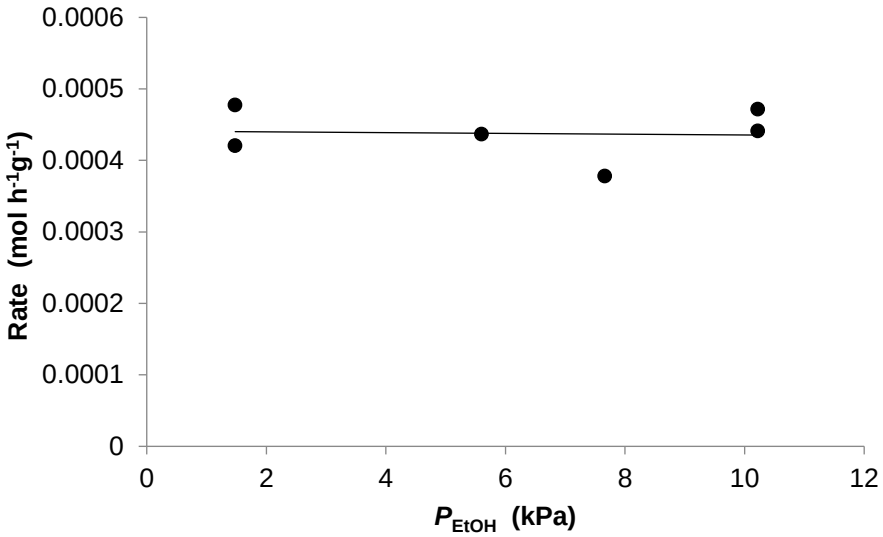


**Fig. 5.3.** Effect of ethanol partial pressure on the rate of dehydration of ethanol over $Cs_{2.5}H_{0.5}PW$ at 120°C.

Ethanol dehydration over $Cs_{2.5}H_{0.5}PW$ obeyed the Arrhenius equation in the temperature range of 90-120°C (**Figure 5.4**) with an activation energy $E_a$ = 108±2 kJ mol$^{-1}$. The same $E_a$ value was obtained when the temperature was raised and lowered. Given zero reaction order in ethanol and the high DEE selectivity, the $E_a$ value obtained can be attributed to the true activation energy for the ethanol-to-DEE reaction over $Cs_{2.5}H_{0.5}PW$. For the reaction over 15%HPW/$SiO_2$ and 15%HSiW/$SiO_2$, the activation energy was estimated to be 96 and 91 kJ mol$^{-1}$, respectively. The high $E_a$ values obtained indicate that ethanol dehydration with these catalysts is not limited by mass transport (see discussion for methanol dehydration on p.146). The absence of pore diffusion limitations was also supported by the Weisz-Prater analysis [26] of the reaction system (Weizs-Prater criterion $C_{WP} = 2 \cdot 10^{-2} < 1$ indicating no internal diffusion limitations).[27]

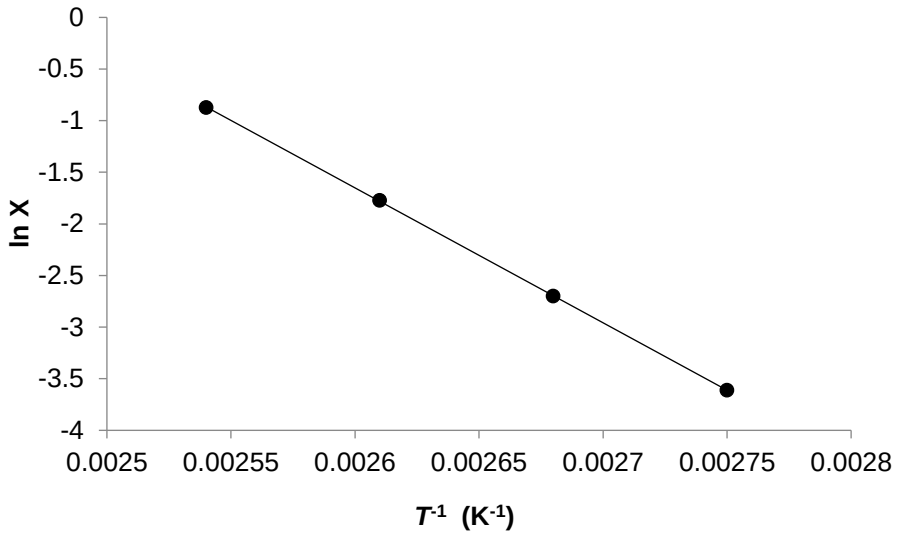


**Fig. 5.4**. Arrhenius plot for ethanol dehydration over $Cs_{2.5}H_{0.5}PW$ where *X* is the conversion of ethanol (0.2 g catalyst, 1.48 kPa ethanol partial pressure, $N_2$ carrier gas, 20 mL $min^{-1}$ flow rate).

## 5.3.4. Effect of catalyst acid strength

**Table 5.1** shows the ethanol conversion and product selectivity for the dehydration of ethanol over supported HPW and HSiW catalysts at 100 and 120 $^oC$. **Table 5.2** shows the same for bulk $Cs_nH_{3-n}PW$ salts and HPW/$Cs_3PW$ core-shell catalysts. In most cases, the selectivity to DEE was above 80%. **Tables 5.1** and **Table 5.2** also show the turnover frequencies (TOF) for ethanol dehydration over the HPA catalysts studied. The TOF values ($h^{-1}$) were calculated per a surface proton site from the values of ethanol conversion, which, due to zero reaction order in ethanol, are equivalent to the rate constants. The required densities of accessible proton sites were estimated as follows.[20-23, 27]

**Table 5.1**. *Dehydration of ethanol over supported HPA catalysts.*[a]

| Catalyst | Temperature (ºC) | Conversion (%) | TOF[b] ($h^{-1}$) | Selectivity (mol%) | |
|---|---|---|---|---|---|
| | | | | Ethene | Ether |
| 15%HSiW/$SiO_2$ | 100 | 13 | 2.2 | 9 | 91 |
| 15%HPW/$SiO_2$ | 100 | 11 | 2.5 | 8 | 92 |
| 15%HPW/$TiO_2$ | 100 | 4.8 | 1.1 | 26 | 74 |
| 15%HPW/$Nb_2O_5$ | 100 | 1.2 | 0.28 | 0 | 100 |
| 15%HPW/$ZrO_2$ | 100 | 1.5 | 0.36 | 0 | 100 |
| 5%HSiW/$SiO_2$ | 120 | 34 | 18 | 11 | 89 |
| 10%HSiW/$SiO_2$ | 120 | 42 | 11 | 14 | 86 |
| 15%HSiW/$SiO_2$ | 120 | 51 | 9.1 | 20 | 79 |
| 20%HSiW/$SiO_2$ | 120 | 76 | 10 | 33 | 66 |
| 5%HPW/$SiO_2$ | 120 | 23 | 16 | 10 | 89 |
| 10%HPW/$SiO_2$ | 120 | 45 | 16 | 17 | 82 |
| 15%HPW/$SiO_2$ | 120 | 52 | 12 | 22 | 78 |
| 20%HPW/$SiO_2$ | 120 | 60 | 11 | 38 | 62 |
| 15%HPW/$TiO_2$ | 120 | 19 | 4.5 | 32 | 68 |
| 15%HPW/$Nb_2O_5$ | 120 | 6.9 | 1.6 | 13 | 87 |
| 15%HPW/$ZrO_2$ | 120 | 7.6 | 1.8 | 12 | 88 |

[a] 0.2 g catalyst, 1.48 kPa EtOH partial pressure, $N_2$ carrier gas, 20 mL $min^{-1}$, 3 h time on stream. [b] Turnover frequency per surface proton site calculated from ethanol conversion assuming that all HPA protons were equally available for reaction.

For supported HPA catalysts, including the core-shell catalysts, which contained HPW or HSiW at sub-monolayer coverage, all HPA protons were assumed to be equally available for reaction (e.g., 0.156 and 0.208 mmol $g^{-1}$ proton density for supported 15% HPW and HSiW catalysts, respectively). This has been proved correct for silica-supported HPW by titration with $NH_3$ [28] and pyridine.[29]

For bulk Cs salts of HPW, which have been suggested to catalyse alcohol dehydration through the surface type mechanism,[9, 10, 21] the number of surface protons was calculated using a cross section of 144 Å$^2$ for Keggin unit[9, 10] and catalyst surface areas: $Cs_{2.5}H_{0.5}PW$ (132 $m^2g^{-1}$, 0.076 mmol($H^+$) $g^{-1}$) and $Cs_{2.25}H_{0.75}PW$ (128 $m^2g^{-1}$, 0.111 mmol($H^+$) $g^{-1}$).

**Table 5.2.** *Dehydration of ethanol over bulk salts $Cs_nH_{3-n}PW$ and core-shell catalysts HPW/$Cs_3PW$.*[a]

| Catalyst | Temperature (°C) | Conversion (%) | TOF[b] ($h^{-1}$) | Selectivity (mol%) | |
|---|---|---|---|---|---|
| | | | | Ethene | Ether |
| $Cs_3PW$ | 120 | 0 | 0 | 0 | 0 |
| $Cs_{2.5}H_{0.5}PW$ | 100 | 6.3 | 3.1 | 0 | 100 |
| $Cs_{2.25}H_{0.75}PW$ | 100 | 18 | 6.2 | 13 | 87 |
| 15% HPW/$Cs_3PW$ | 100 | 3.0 | 0.71 (1.5) | 0 | 100 |
| 25% HPW/$Cs_3PW$ | 100 | 15 | 2.1 (5.5) | 28 | 72 |
| $Cs_{2.5}H_{0.5}PW$ | 120 | 33 | 16 | 4 | 96 |
| $Cs_{2.25}H_{0.75}PW$ | 120 | 49 | 16 | 25 | 75 |
| 15% HPW/$Cs_3PW$ | 120 | 16 | 3.9 (8.1) | 0 | 100 |
| 25% HPW/$Cs_3PW$ | 120 | 53 | 7.6 (20) | 36 | 64 |

[a] 0.2 g catalyst, 1.48 kPa EtOH partial pressure, $N_2$ carrier gas, 20 mL $min^{-1}$, 3 h time on stream. [b] For supported HPW catalysts, turnover frequency calculated per surface proton site from ethanol conversion assuming that all HPW protons were equally available for reaction; for bulk Cs salts, TOF per surface proton site was estimated assuming a Keggin anion cross section of 144 Å$^2$ and using the surface area for fresh catalysts (Table 1). In round brackets, are TOF values for core-shell catalysts calculated assuming proton equilibration by ion migration.

.

**Figure 5.5** shows a fairly good linear relationship between the catalytic activity of HPA catalysts in ethanol dehydration, ln (TOF), and their initial enthalpy of ammonia adsorption, $\Delta H_{NH3}$. In this figure, the TOF vaues are referred to the reaction at 120 ºC and ethanol conversion range $X$ = 0.07 – 0.53. Practically the same relationship was obtained for the reaction under differential conditions ($X \leq 0.13$) at 100 ºC (**Tables 5.1-5.2**), as can be seen in **Figure 5.6**. Both supported HPA catalysts and bulk Cs salts obey this plot. This relationship implies that Brønsted acid sites play important role in ethanol-to-DEE dehydration over HPA catalysts as represented in **Scheme 5.2.** Recently, similar relationship has been reported for metanol dehydration as well as isopropanol dehydration over HPA catalysts in the gas phase.[20-21]

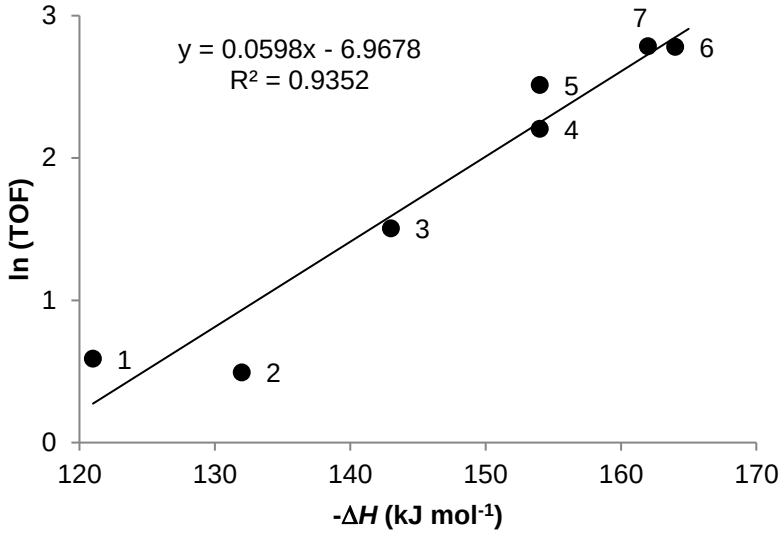


**Fig. 5.5.** Plot of ln (TOF) for ethanol dehydration (TOF in $h^{-1}$) over HPA catalysts at ethanol conversion range $X$ = 0.07 – 0.53 vs. initial heat of $NH_3$ adsorption (120 ºC, 0.2 g catalyst, 1.48 kPa ethanol partial pressure, $N_2$ carrier gas, 20 mL $min^{-1}$ flow rate; (1) 15%HPW/$ZrO_2$, (2) 15%HPW/$Nb_2O_5$, (3) 15%HPW/$TiO_2$, (4) 15%HSiW/$SiO_2$, (5) 15%HPW/$SiO_2$, (6) $Cs_{2.5}H_{0.5}PW$, (7) $Cs_{2.25}H_{0.75}PW$.

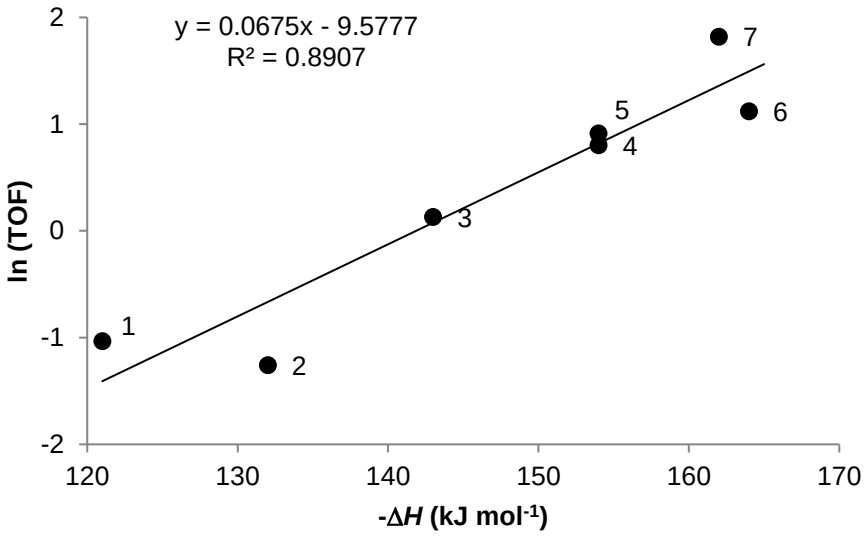


**Fig. 5.6.** Plot of ln (TOF) for ethanol dehydration (TOF in $h^{-1}$) over HPA catalysts vs. initial heat of $NH_3$ adsorption at ethanol conversion $X \leq 0.13$ (100 °C, 0.2 g catalyst, 1.48 kPa ethanol partial pressure, $N_2$ carrier gas, 20 mL $min^{-1}$ flow rate; (1) 15%HPW/$ZrO_2$, (2) 15%HPW/$Nb_2O_5$, (3) 15%HPW/$TiO_2$, (4) 15%HSiW/$SiO_2$, (5) 15%HPW/$SiO_2$, (6) $Cs_{2.5}H_{0.5}PW$, (7) $Cs_{2.25}H_{0.75}PW$.

## 5.4 Core–shell HPA catalysts

Core-shell catalysts comprising HPA (shell) supported on its insoluble neutral salt (core), such as HPW/$Cs_3PW$ and HPW/$K_3PW$, have attracted interest due to their possible advantages over the corresponding bulk acidic heteropoly salts such as $Cs_nH_{3-n}PW$ and $K_nH_{3-n}PW$.[17, 30] It is claimed that the core-shell catalysts have a larger number of accessible surface acid sites than the corresponding bulk salts of the same total composition, and these acid sites are stronger than those in the bulk salts. As a result, the core-shell HPA catalysts could have higher catalytic activities than their bulk counterparts.[17] Moreover, there is evidence that some bulk heteropoly salts, e.g., $Cs_2HPW$, are, in fact, core-shell materials.[17, 30]

### 5.4.1 Dehydration of ethanol

Recently, Matachowski *et al.*[17] have reported on the superiority of the core-shell catalyst 33%HPW/$Cs_3$PW over its bulk counterpart $Cs_2$HPW in acidity and catalytic activity in ethanol dehydration. However, in this work, the acid strength has been characterised in terms of average rather than initial enthalpies of ammonia adsorption and the catalytic activity has been represented as conversion rates per catalyst weight rather than turnover rates. It should be noted that the 33%HPW/$Cs_3$PW catalyst will have a massive bulk phase of HPW on the surface of $Cs_3$PW, which possesses much stronger proton sites than the corresponding salt $Cs_2$HPW, as can be seen from the $\Delta H_{NH3}$ values (-197 kJ $mol^{-1}$ for HPW versus -162 to -164 kJ $mol^{-1}$ for $Cs_nH_{3-n}$PW). Besides, ethanol dehydration on 33%HPW/$Cs_3$PW could proceed via bulk-type catalysis rather than surface-type catalysis, as defined by Misono *et al.*[9] This could affect the results reported by Matachowski *et al.*[17]

In our work, we looked at the core-shell catalysts with sub-monolayer coverage, namely 15%HPW/$Cs_3$PW and 25%HPW/$Cs_3$PW, where the $Cs_3$PW support had a specific surface area of 145 $m^2g^{-1}$. These catalysts were compared to their bulk counterparts, i.e., $Cs_{2.5}H_{0.5}$PW and $Cs_{2.25}H_{0.75}$PW, respectively, regarding their acid strength (in terms of the initial enthalpies of ammonia adsorption, $\Delta H_{NH3}$) and turnover rates of ethanol dehydration (TOF). The TOF values for core-shell catalysts were calculated per surface proton site assuming that all protons in the HPW shell were equally available for reaction as for other supported HPA catalysts.

The relevant $\Delta H_{NH3}$ values for 25%HPW/$Cs_3$PW and $Cs_{2.25}H_{0.75}$PW have practically the same acid strength within experimental error: -165 and -162 kJ $mol^{-1}$, respectively. Unexpectedly, the acid strength of the 15%HPW/$Cs_3$PW core-shell material (-151 kJ $mol^{-1}$) was found to be significantly lower than that of the bulk salt $Cs_{2.5}H_{0.5}$PW (-164 kJ $mol^{-1}$). These results contradict the report,[17] from which the acidity of the core-shell catalysts HPW/$Cs_3$PW could be anticipated stronger than that of the corresponding bulk salts $Cs_nH_{3-n}$PW.

The catalytic activities of these catalysts were found to be in line with their acid strengths (**Table 5.2**), hence also disagree with.[17] The activities of 25%HPW/$Cs_3PW$ and $Cs_{2.25}H_{0.75}PW$ in terms of conversion per catalyst weight were close to each other, but the TOF values for 25%HPW/$Cs_3PW$ 2-3 times lower than those for $Cs_{2.25}H_{0.75}PW$. The activity of 15%HPW/$Cs_3PW$ was 2 times lower than that of $Cs_{2.5}H_{0.5}PW$ in terms of conversion per catalyst weight and 4 times lower in terms of TOF.

It should be noted that the TOF values calculated for the core-shell catalysts assuming that all protons in the HPW shell were accessible for the reaction (**Table 5.2**) did not fit with the linear relationship in **Figure 5.5**. We also calculated another TOF values assuming that protons were fully equilibrated, which would make the core-shell catalysts equivalent to the corresponding bulk Cs salts. These TOFs, presented in **Table 5.2** in round brackets, are closer to the TOF values for the corresponding bulk Cs salts and were found to fit with the above relationship (**Figure 5.7**). This is a sound argument in favour of proton equilibration in the core-shell catalyst system. Proton equilibration might occur already upon catalyst preparation by impregnation of $Cs_3PW$ with HPW in aqueous solution. With this in mind, we also prepared core-shell catalysts by impregnation from methanol. However, these samples were no different from those prepared from aqueous solution as regards their activity in ethanol dehydration. This indicates that proton equilibration probably occurred during alcohol dehydration at elevated temperatures. In this respect, it would be interesting to test the core-shell catalysts in reactions that do not involve water such as alkane or alkene isomerization, which might benefit from the use of such catalysts.

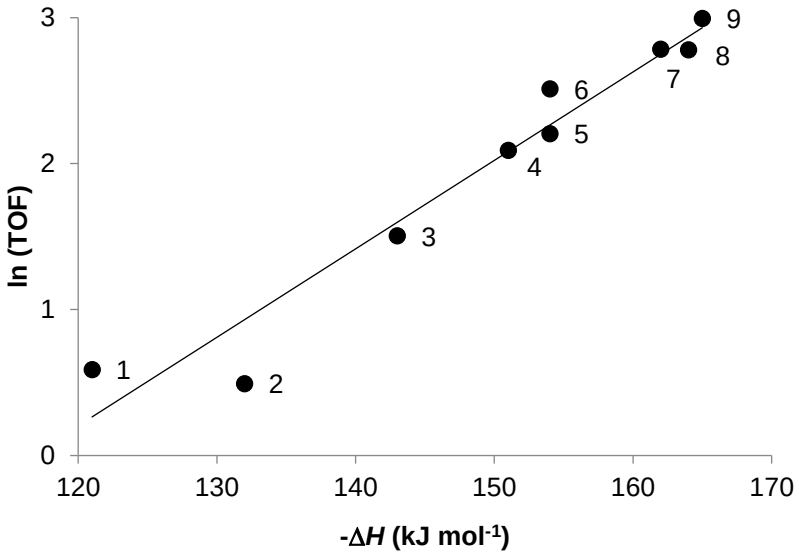


**Fig. 5.7.** Plot of ln (TOF) for ethanol dehydration (TOF in $h^{-1}$) over HPA catalysts at ethanol conversion range $X$ = 0.07 – 0.53 vs. initial heat of $NH_3$ adsorption, with core-shell catalysts included (120 °C, 0.2 g catalyst, 1.48 kPa ethanol partial pressure, $N_2$ carrier gas, 20 mL $min^{-1}$ flow rate; (1) 15%HPW/$ZrO_2$, (2) 15%HPW/$Nb_2O_5$, (3) 15%HPW/$TiO_2$, (4) 15%HPW/$Cs_3$PW, (5) 15%HSiW/$SiO_2$, (6) 15%HPW/$SiO_2$, (7) $Cs_{2.25}H_{0.75}$PW, (8) $Cs_{2.5}H_{0.5}$PW, (9) 25%HPW/$Cs_3$PW.

## 5.5.2 Dehydration of isopropanol

In addition to ethanol dehydration, we also tested the core-shell catalysts in isopropanol dehydration (**Scheme 5.3**). The dehydration of isopropanol over HPA catalysts is suggested to proceed via E1 pathway (monomolecular elimination) which breaks C-O bond in alcohol in the rate-limiting step using an acid site to form water and carbenium ion (possibly as surface alkoxonium ion)[29]; the latter undergoes proton abstraction to form propene or reacts with another alcohol molecule to form diisopropyl ether (competing $S_N1$ pathway).[21, 22, 29] Previously, the dehydration of isopropanol over HPA catalysts has been found to be zero order in alcohol in the range of isopropanol partial pressure 0.94-5.52 kPa.[22]

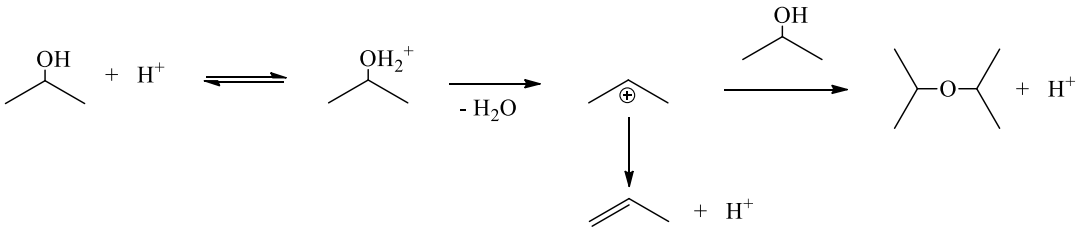

**Scheme 5.3.** Isopropanol dehydration forming propene and diisopropyl ether.

Representative results for isopropanol dehydration are shown in **Table 5.3**. It can be seen that these results are similar to those for ethanol dehydration. Again, the core-shell catalysts exhibited lower activities (TOF) than the bulk salt counterparts. Therefore, our results do not support the literature claims of superiority of core-shell catalysts over the corresponding bulk acidic heteropoly salts regarding both their acidity and catalytic activity in alcohol dehydration.

**Table 5.3.** *Dehydration of isopropanol over bulk salts $Cs_nH_{3-n}PW$ and core-shell catalysts HPW/$Cs_3$PW.*[a]

| Catalyst | Conversion (%) | TOF[b] ($h^{-1}$) | Selectivity (mol%) | |
|---|---|---|---|---|
| | | | Propene | Ether |
| $Cs_{2.5}H_{0.5}PW$ | 31 | 9.6 | 83 | 17 |
| $Cs_{2.25}H_{0.75}PW$ | 59 | 12 | 91 | 9 |
| 15% HPW/$Cs_3$PW | 15 | 2.3 | 81 | 19 |
| 25% HPW/$Cs_3$PW | 49 | 4.4 | 91 | 9 |

[a] 0.2 g catalyst, 70 °C, 0.94 kPa isopropanol partial pressure, $N_2$ carrier gas, 20 mL $min^{-1}$, 3 h time on stream. [b] TOF values calculated as in Table 5.2.

The superiority of HPA core-shell catalysts in acid strength might have been expected for large HPA loadings, with HPA crystal phase present on the core surface. For sub-monolayer HPA loadings, the acid strength of core-shell catalysts and the corresponding bulk HPA salts is likely to be similar, as indeed found for 25%HPW/$Cs_3$PW and $Cs_{2.25}H_{0.75}$PW.

In the case of 15%HPW/$Cs_3$PW and $Cs_{2.5}H_{0.5}$PW catalyst couple, with a lower HPA loading, the core-shell catalyst was found to have significantly weaker acid strength as well as lower catalytic activity than the corresponding bulk salt. This could be caused by neutralization of a part of HPW protons by the $Cs_3$PW support. It should be noted that little is known about the surface properties of the $Cs_3$PW neutral salt. It is usually prepared by adding the stoichiometric amount of $Cs_2CO_3$ to HPW in an aqueous solution. The neutralization, however, may not proceed to completion since the Keggin anion $PW_{12}O_{40}^{3-}$ undergoes decomposition upon increasing pH to form more basic lacunary polyanions. Thus, monolacunary anion $PW_{11}O_{39}^{9-}$ as a partially protonated species is formed already at pH 2.[10] Increasing the pH beyond pH 2 upon neutralization of HPW will cause further degradation. This implies that the surface of $Cs_3$PW could be quite basic rather than neutral, causing the loss in acidity of the resulting core-shell catalyst. Obviously, this will be more damaging for the catalysts with lower HPA loadings such as 15%HPW/$Cs_3$PW, with predictably smaller effect on 25%HPW/$Cs_3$PW, in agreement with the results obtained.

Therefore, the core-shell catalysts studied did not show any advantage in activity in the dehydration of alcohols that could have arisen from a higher density of accessible surface proton sites and/or stronger catalyst acidity. In fact, neither did materialize for the core-shell catalysts with sub-monolayer HPA loadings. The reason for this could be ion migration in the core-shell catalysts, which would equilibrate protons across catalyst particles. Especially, this is likely at elevated temperatures in the presence of water in the course of alcohol dehydration. Ion migration in core-shell HPW/$Cs_3$PW has been demonstrated by Misono *et al.*[31] using $^{32}$P NMR, who have found that both $Cs_{2.5}H_{0.5}$PW and 15%HPW/$Cs_3$PW have uniform proton distribution across

catalyst particles. On the other hand, Essayem *et al.*,[31] on the basis of their $^{31}$P NMR and XRD data, suggested that $Cs_nH_{3-n}PW$ salt is comprised of $Cs_3PW$ support with HPW dispersed in the pores.

## 5.5 Conclusion

In this work, we have studied the dehydration of ethanol at a gas-solid interface over a wide range of solid Brønsted acid catalysts based on Keggin-type heteropoly acids (HPAs) in a continuous flow fixed-bed reactor in the temperature range of 90-220 $^oC$ and ethanol partial pressure of 1.5-10 kPa focussing on the formation of diethyl ether (DEE), which is considered to be a green transportation fuel alternative. The catalysts under study included $H_3PW_{12}O_{40}$ (HPW) and $H_4SiW_{12}O_{40}$ (HSiW) supported on $SiO_2$, $TiO_2$, $Nb_2O_5$ and $ZrO_2$ with sub-monolayer HPA coverage. The catalysts also included bulk acidic Cs salts of HPW ($Cs_{2.5}H_{0.5}PW_{12}O_{40}$ and $Cs_{2.25}H_{0.75}PW_{12}O_{40}$) and the corresponding core-shell materials with the same total composition (15%HPW/$Cs_3PW_{12}O_{40}$ and 25%HPW/$Cs_3PW_{12}O_{40}$, respectively) comprising HPW supported on the neutral salt $Cs_3PW_{12}O_{40}$.

Under the conditions studied, the ethanol-to-DEE reaction was zero order in ethanol, which is typical for alcohol dehydration under the alcohol partial pressures used. The acid strength of catalysts has been determined by ammonia adsorption microcalorimetry in terms of the initial adsorption enthalpy. A fairly good correlation between the catalyst activity (turnover frequency) and the catalyst acid strength has been established, which demonstrates that Brønsted acid sites play important role in ethanol-to-DEE dehydration over HPA catalysts.

It has been found that the acid strength and the catalytic activity of the core-shell catalysts HPW/$Cs_3PW_{12}O_{40}$ do not exceed those of the corresponding bulk Cs salts of HPW with the same total composition. This contradicts the literature claims of the superiority of core-shell HPA catalysts over the corresponding bulk acidic heteropoly salts.[17]

## 5.6 References


1. D. Fan, D. J. Dai, H. S. Wu, Materials, 6 (2013) 101.
2. A. Corma, S. Iborra, A. Velty, Chem. Rev., 107 (2007) 2411.
3. K. Weissermel, H. J. Arpe, Industrial Organic Chemistry, 4th ed., Wiley–VCH, Weinheim, 2003.
4. T. Kito-Borsa, D. A. Pacas, S. Selim, S. W. Cowley, Ind. Eng. Chem. Res., 37 (1998) 3366.
5. S. Golay, L. Kiwi-Minster, R. Doepper, A. Renken, Chem. Eng. Sci., 54 (1999) 3593.
6. T. Zaki, J. Colloid Interface Sci., 284 (2005) 606.
7. K. Ramesh, Y. L. E. Goh, C. G. Gwie, C. Jie, T. J. White, A. Borgna, J. Porous Mater., 19 (2012) 423.
8. I. Takahara, M. Saito, M. Inaba, K. Murata, Catal. Lett., 105 (2005) 249.
9. T. Okuhara, N. Mizuno, M. Misono, Adv. Catal., 41 (1996) 113.
10. I. V. Kozhevnikov, Catalysis by Polyoxometalates, Wiley & Sons, Chippenham, 2002.
11. M. Misono, Catal. Today, 100 (2005) 95.
12. I. V. Kozhevnikov, J. Mol. Catal., A 305 (2009) 104.
13. M. N. Timofeeva, Appl. Catal., A 256 (2003) 19.
14. J. Haber, K. Pamin, L. Matachowski, B. Napruszewska, J. Poltowicz, J. Catal., 207 (2002) 296.
15. D. Varisli, T. Dogu, G. Dogu, Ind. Eng. Chem. Res., 47 (2008) 4071.
16. V. V. Bokade, G. D. Yadav, Appl. Clay Sci., 53 (2011) 263.
17. L. Matachowski, A. Drelinkiewicz, D. Mucha, J. Krys´ciak-Czerwenka, R. Rachwalik, Appl. Catal., A 469 (2014) 239.
18. H. Noller, P. Andreu, M. Hunger, Angew. Chem. Int. Ed., 10 (1971) 172.
19. P. G. Moses, J. K. Norskov, ACS Catal., 3 (2013) 735.

20. W. Alharbi, E. F. Kozhevnikova, I. V. Kozhevnikov, ACS Catal., 5 (2015) 7186.
21. A. M. Alsalme, P. V. Wiper, Y. Z. Khimyak, E. F. Kozhevnikova, I. V. Kozhevnikov, J. Catal., 276 (2010) 181.
22. G. C. Bond, S. J. Frodsham, P. Jubb, E. F. Kozhevnikova, I. V. Kozhevnikov, J. Catal., 293 (2012) 158.
23. F. Kapteijn, J. A. Moulijn, in: G. Ertl, H. Knozinger, F. Schuth, J. Weitkamp (Eds.), Handbook of Heterogeneous Catalysis, vol. 4, Wiley-VCH, 2008.
24. J. E. Connett, J. Chem. Termodynamics 4 (1972) 135.
25. J. Macht, M. Janik, M. Neurock, E. Iglesia, J. Am. Chem. Soc. 130 (2008) 10369.
26. P. B. Weisz, C. D. Prater, Adv. Catal., 6 (1954) 143.
27. W. Alharbi, E. Brown, E. F. Kozhevnikova, I. V. Kozhevnikov, J. Catal., 319 (2014) 174.
28. E. F. Kozhevnikova, I. V. Kozhevnikov, J. Catal., 224 (2004) 164.
29. J. Macht, M. Janik, M. Neurock, E. Iglesia, J. Am. Chem. Soc., 130 (2008) 10369.
30. L. Matachowski, A. Drelinkiewicz, E. Lalik, M. Ruggiero-Mikołajczyk, D. Mucha, J. Krys´ciak-Czerwenka, Appl. Catal., A 469 (2014) 290.
31. N. Mizuno, M. Misono, Chem. Rev., 98 (1998) 199.
32. N. Essayem, G. Coudurier, M. Fournier, J. Vedrine, Catal. Lett., 34 (1995) 223.

# Chapter 6. General conclusions and future look

## 6.1. General summary

At the turn of the 19th century, fossil fuels were in abundant supply to satisfy the world's energy requirements. However, growing energy costs, adverse environmental impacts and decreasing supplies of fossil fuels have encouraged the investigation and development of sustainable materials originated from renewable sources such as biomass that can be used as clean alternative fuels.

Biofuels, such as bioalcohols and biodiesel, have been recommended as alternatives for internal combustion engines for vehicles. In particular, biodiesel has received much attention in recent years as a replacement for diesel fuel due to increased health and environmental concerns regarding the effects of diesel engine particulate and $NO_x$ emissions.

Production of ethers by intermolecular dehydration of primary alcohols such as methanol and ethanol has attracted considerable attention in recent years. Dimethyl ether (DME) and diethyl ether (DEE) can be used as an alternative to diesel fuel or diesel fuel additives to reduce $NO_x$, $SO_x$ and particulate matter emissions. The formation of DME and DEE is thermodynamically favoured at lower temperatures.

Mechanism of methanol-to-DME dehydration is still debated. Formation of DME from methanol may be represented by two different pathways termed the associative pathway and the dissociative pathway. Both pathways are thought to take place at Brønsted acid sites. The formation of DEE may be represented by two different pathways similar to the mechanism proposed for the formation of dimethyl ether from methanol.

Keggin-type HPAs comprising heteropoly anions of the formula $[XW_{12}O_{40}]^{n-}$, where X is the heteroatom ($P^{V}$, $Si^{IV}$, etc.), possess very strong Brønsted acidity. In the last three decades, catalysis by HPAs has attracted much interest because of its potential to generate economic and environmental benefits; several large-scale chemical processes based on HPA catalysis have been commercialized.

The aim of this thesis was to investigate a wide range of HPA catalysts for the dehydration of methanol and ethanol to produce the corresponding ethers at a gas-solid interface. The main outcomes of this project can be summarized as follows:

1. The methanol-to-DME dehydration has been studied over a wide range of bulk and supported Brønsted acid catalysts based on tungsten Keggin heteropoly acids (HPA) and compared with the reaction over HZSM-5 zeolites (Si/Al = 10−120). Turnover rates for all these catalysts have been measured under zero-order reaction conditions. The HPA catalysts have been demonstrated to have much higher catalytic activities than the HZSM-5 zeolites. A good correlation between the turnover rates and catalyst acid strengths represented by the initial enthalpies of ammonia adsorption has been established. This correlation holds for all the HPA, and HZSM-5 catalysts studied, which indicates that the methanol-to-DME dehydration with both HPA and HZSM-5 catalysts occurs via the same (or similar) mechanism, either associative or dissociative. The turnover rate of methanol dehydration for both catalysts is primarily determined by the strength of catalyst acid sites, regardless of the catalyst pore geometry.

The activity-acid strength relation may be used to predict the activity of other Brønsted acid catalysts in methanol-to-DME dehydration from their $\Delta H_{NH3}$ values and vice versa.

2. The dehydration of ethanol at a gas-solid interface was also studied over a wide range of solid Brønsted acid catalysts based on Keggin-type heteropoly acids (HPAs) in a continuous flow fixed-bed reactor in the temperature range of 90-220 $^{o}$C. The catalysts under study included

$H_3PW_{12}O_{40}$ (HPW), and $H_4SiW_{12}O_{40}$ (HSiW) supported on $SiO_2$, $TiO_2$, $Nb_2O_5$ and $ZrO_2$ with sub-monolayer HPA coverage. The catalysts also included bulk acidic Cs salts of HPW ($Cs_{2.5}H_{0.5}PW_{12}O_{40}$ and $Cs_{2.25}H_{0.75}PW_{12}O_{40}$) and the corresponding core-shell materials with the same total composition (15%HPW/$Cs_3PW_{12}O_{40}$ and 25%HPW/$Cs_3PW_{12}O_{40}$, respectively) comprising HPW supported on the neutral salt $Cs_3PW_{12}O_{40}$. Under the conditions studied, the ethanol-to-DEE reaction was zero order in ethanol, which is typical for alcohol dehydration under the alcohol partial pressures used. The acid strength of catalysts has been determined by ammonia adsorption microcalorimetry regarding the initial adsorption enthalpy. A fairly good correlation between the catalyst activity (turnover frequency) and the catalyst acid strength has been established, which demonstrates that Brønsted acid sites play an important role in ethanol-to-DEE dehydration over HPA catalysts. It has been found that the acid strength and the catalytic activity of the core-shell catalysts HPW/$Cs_3PW_{12}O_{40}$ do not exceed those of the corresponding bulk Cs salts of HPW with the same total composition. This contradicts the literature claims of the superiority of core-shell HPA catalysts over the corresponding bulk acidic heteropoly salts.

## 6.2 Guidelines for future work

Some avenues for future work have arisen during the course our studies. These are outlined below:

1- The turnover rate of methanol dehydration for both catalysts HPAs and HZSM-5 zeolites is primarily determined by the strength of catalyst acid sites, regardless of the catalyst pore geometry. Evidence to the contrary claimed by Jones *et al.* has come from the rate/acid strength correlation, where the acid strength of silica-supported HPA catalysts was represented by deprotonation energies derived from DFT calculations. The latter probably did not take into account the effect of support on the HPA acid strength, which is evident from the experimental $\Delta H_{NH3}$ values. Therefore, the present study could serve as the basis for further investigations into the mechanism of methanol-to-DME dehydration.

2- The core-shell catalysts studied did not show any advantage in activity in the dehydration of alcohols that could have arisen from a higher density of accessible surface proton sites and/or stronger catalyst acidity. In fact, neither did materialize for the core-shell catalysts with sub-monolayer HPA loadings. The reason for this could be ion migration in the core-shell catalysts, which would equilibrate protons across catalyst particles. Especially, this is likely at elevated temperatures in the presence of water in the course of alcohol dehydration. In this respect, it would be interesting to test the core-shell catalysts in reactions that do not involve water such as alkane or alkene isomerization, which might benefit from the use of such catalysts.

## 6.3 References

(1) I. V. Kozhevnikov, Catalysis by Polyoxometalates; Wiley & Sons: Chichester, England, 2002.

(2) W. Alharbi, E. Brown, E. F. Kozhevnikova, I. V. Kozhevnikov, J. Catal., 319 (2014) 174.

(3) W. Alharbi, E. F. Kozhevnikova, I. V. Kozhevnikov, ACS Catal., 5 (2015) 7186.